Departament of Energy Tehnology-Pontoppidanstræde 101
Aalborg University, Denmark

CONTROL OF VSC-BASED HVDC TRANSMISSION SYSTEM FOR OFFSHORE WIND POWER PLANTS

Master Thesis

Conducted by group WPS 4 - 1050
Spring Semester, 2010

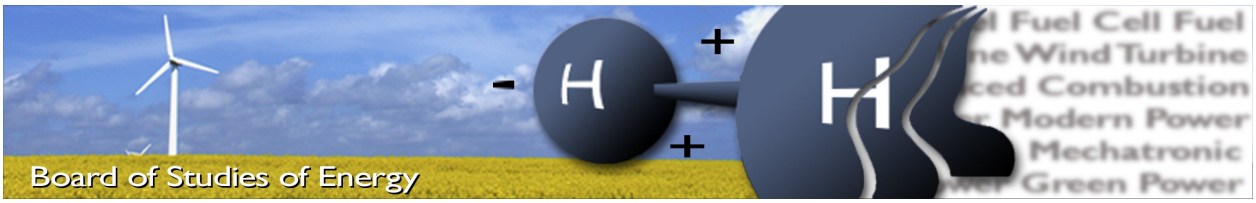

Title:	Control of VSC-based HVDC transmission system for offshore wind power plants
Semester:	4^{th}
Semester theme:	Master Thesis
Project period:	08.02.2010 to 02.06.2010
ECTS:	30
Supervisor:	Remus Teodorescu Pedro Rodriguez Rodrigo da Silva
Project group:	WPS4-1050

Ana - Irina Stan

Daniel - Ioan Stroe

SYNOPSIS:

In a world confronting with an increasing demand of power, the large offshore wind power plants represent promising alternative sources of energy. Among the available solutions, the VSC-based HVDC transmission systems represent at this moment the most feasible and competitive solution for grid-integration of this large offshore amount of power.

Throughout this thesis the modeling and the control of the VSC-based HVDC system are investigated and described. Two different control methods capable of controlling such systems are proposed. Both developed control strategies are implemented in the *dq* synchronous reference frame. In order to analyze both steady state and dynamic behavior of the developed VSC-based HVDC transmission system several study cases are carried out using MATLAB/Simulink.

Moreover, the results obtained from simulations are validated using a small-scale laboratory setup (2.2 kW) controlled through a dSPACE platform.

Copies:	4
Pages, total:	93
Appendix:	2
Supplements:	4 CDs

By signing this document, each member of the group confirms that all participated in the project work and thereby all members are collectively liable for the content of the report.

Preface

The present Master Thesis is conducted at the Departament of Energy Technology, Aalborg University. It is written by group WPS4-1050 during the period 8^{th} of February - 2^{nd} of June 2010. The thesis theme with the title *"Control of VSC-based HVDC Transmission System For Offshore Wind Power Plants"* was chosen from the Vestas Student Project Catalogue.

Reading Instructions

The references are shown in form of a number placed into square brackets. Detailed information about literature is presented in Bibliography. The format of equations is (X.Y), where X is number of chapter and Y is number of equation. The figures are numbered Figure X.Y, where X is the number of chapter and Y is number of figure.

In this thesis the chapters are consecutive numbered whereas the appendixes are labeled with letters. All appendixes are assigned with capital letters and put in an alphabetical order.

The enclosed CD-ROM contains the thesis report written in LATEX, Adobe PDF formats, source codes, documents used throughout the thesis and Simulink Models.

Acknoledgements

The authors are especially grateful to their supervisors Remus Teodorescu, Pedro Rodriguez and Rodrigo da Silva which with their patience and generosity devoted valuable time provided great help to the development of this thesis. The authors are also grateful to their Vestas industrial contact Florin Lungeanu for his valuable comments and suggestions provided during the development of this thesis.

Contents

Chapter 1

Introduction

1.1 Backgroud of HVDC Transmission

At the beginning of the 1970s, once with the first oil crisis, the interest on the renewable energy sources had emerged. Thus, the wind power industry, one of the most powerful and successful industry in the last four decades, had appeared. Since then, the development in this industry is continuous and at a high rate, fact which can be observed from Figure 1.1 which presents the development of the wind turbines during last three decades.

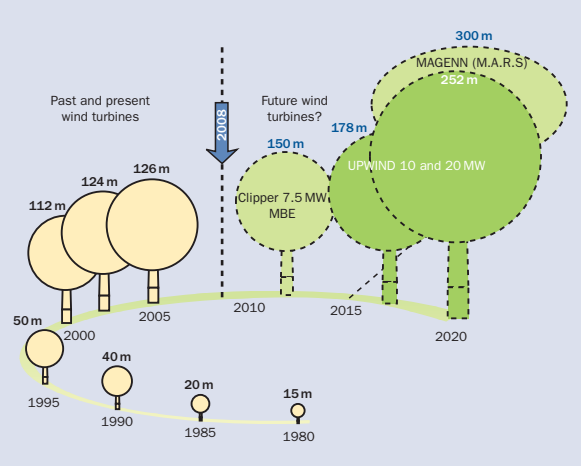

Figure 1.1: *Growth in size of commercial wind turbine designs [1]*

The fast growth in everything which means wind power is possible due to several facts, such as: reticence in using fossil fuels (from both environmental issues and high prices point of view) and development of power electronics etc. Figure 1.2 and Figure 1.3 are presenting the annual wind power installation in the European Union during the last fifteen years and the cumulative wind power installations in the European Union, for the same period, respectively.

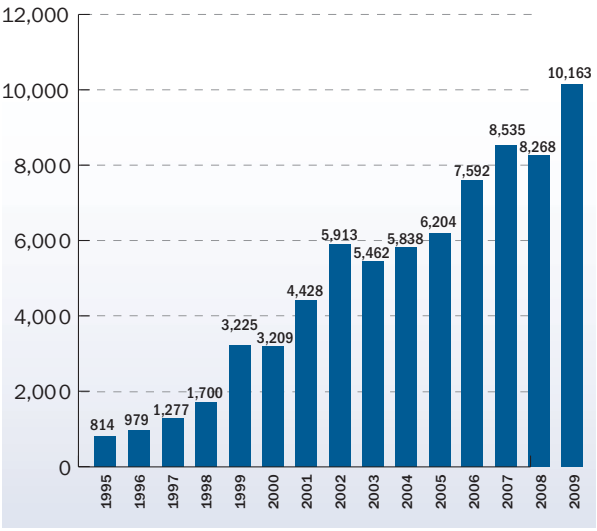

Figure 1.2: *Annual wind power installation in EU (MW) [2]*

According to Figure 1.2 the wind energy sector continued its market growth in the EU at an increased rate of 23% compared to year 2008 installations. From the total 10163 MW installed in EU, 9581 MW was installed onshore (21% more compared to the previous year), while 582 MW was installed offshore (56% more compared to the previous year) [2]. Furthermore, as it may be observed in Figure 1.2, the annual installations in The European Union have increased steadily during the last fifteen years from only 472 MW wind power installed in 1994 to more than 10 GW in 2009.

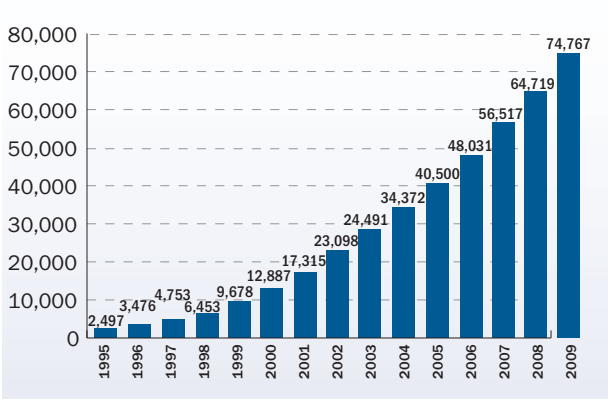

Figure 1.3: *Cumulative wind power installations in EU (MW) [2]*

Figure 1.3 presents the cumulative wind power installations in the European Union in the last fifteen years, achieving at the end of 2009 a total installed capacity of 74767 MW. The EU leading country, concerning the installed capacity is Germany, followed by Spain and Italy.

As it is well known, the offshore wind power is very important to the Europe future, and so, the present trend in the wind power industry is to develop its offshore sector. According to the European Wind Energy Association (EWEA), the total offshore wind turbine capacity

installed until the end of 2009 was 2056 MW. During the year 2009, eight new offshore wind farms were commissioned, consisting of 199 wind turbines [3]. The expectations for the year 2010 are even bigger than the achievements of the year 2009 in which concerns the development of the offshore wind energy sector. Thus, according to [3], EWEA expects the finalizing of ten offshore wind farms in Europe, during the year 2010, which will increase the total installed capacity with more than 1000 MW - fact which is synonymous to a market growth of 75% compared to 2009.

The present distribution of the onshore and offshore wind power production as well as a prediction, over the next twenty years, concerning the same wind energy sectors is presented in Figure 1.4.

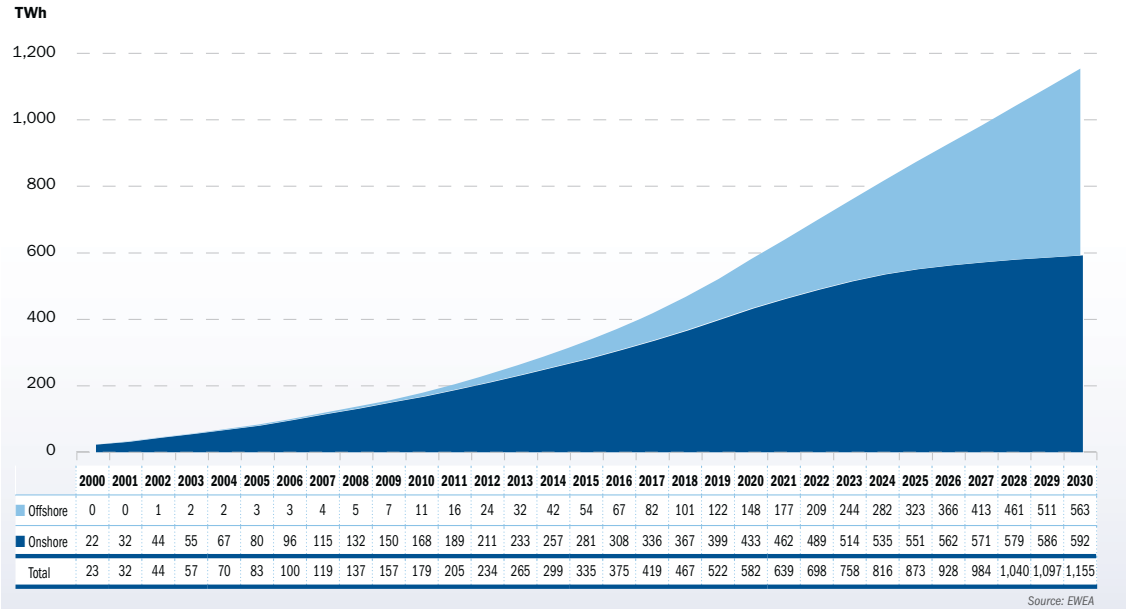

	2000	2001	2002	2003	2004	2005	2006	2007	2008	2009	2010	2011	2012	2013	2014	2015	2016	2017	2018	2019	2020	2021	2022	2023	2024	2025	2026	2027	2028	2029	2030
Offshore	0	0	1	2	2	3	3	4	5	7	11	16	24	32	42	54	67	82	101	122	148	177	209	244	282	323	366	413	461	511	563
Onshore	22	32	44	55	67	80	96	115	132	150	168	189	211	233	257	281	308	336	367	399	433	462	489	514	535	551	562	571	579	586	592
Total	23	32	44	57	70	83	100	119	137	157	179	205	234	265	299	335	375	419	467	522	582	639	698	758	816	873	928	984	1,040	1,097	1,155

Figure 1.4: *Power Production from Onshore and Offshore Wind in the EU (2000-2030) [4]*

According to [4], from the beginning of 2020, most of the European Union renewable power will be produced by onshore wind farms, while the next decade will be dedicated to the large-scale exploitation of the largest energy resource, the offshore wind power.

The offshore wind industry will overtake the onshore wind industry (as may be observed in Figure 1.4) mainly due to two aspects. Firstly, the "offshore wind" is characterized by average annual wind speeds bigger than the "onshore wind" and secondly, the onshore sites which are available to be used for wind farms will slowly decreasing. Thus, in the next years, the trend in the wind power industry will be to move from onshore to offshore.

Until now, the offshore sites which were preferred to be used for wind farms were the ones close to the shore and with relative small water depths. But, there are several aspects which burden the use of these sites: the near-shore area is often used for maritime traffic, recreational activities and/or fishing. Moreover the placement of a wind farm close to the shore will have a bad impact from the noise disturbances and visibility point of view [5]. Based on these presented facts, one of the trends concerning offshore wind farms is to increase the distance from the wind farm to the shore.

A consequence of this trend is that the generated power in offshore wind farms has to be

transported over very long distances to make a connection with the main supply grid. The solution which overcomes this problem is the use of the High Voltage Direct Current (HVDC) transmission systems which are more feasible and also more competitive than the traditional High Voltage Alternative Current (HVAC) transmission systems. One of the most important advantages of HVDC transmission technology over the HVAC transmission technology is that the first one is suitable for long distances (even 500 - 600 km) with minimal losses. The second big advantage concerns the Right-of-Way (RoW); often it is more easy to obtain RoW permission for submarine DC cables because of the reduced environmental impacts [5], [6]. Furthermore, in the case of VSC-based HVDC transmission system, the voltage source converter substations can be used to stabilize the AC networks in their connection points and also it can be used to provide black start and may support the system recovery in case of a failure [5], [6].

1.2 Problem Formulation

Nowadays, the energy demand is growing at a high rate and the renewable energy sources represent a reliable and cost effective alternative to the old-fashioned methods (fossil-fuels, uranium etc). Among all these renewable energy sources the wind represents one of the best developed and researched sectors. At the moment the onshore wind power industry is more developed than the offshore sector but as presented in the previous chapter the trend is to go offshore. Basically due to the increase of size, noise, visual pollution but also thanks to higher values of wind speed, the offshore wind applications are winning more and more terrain over the onshore wind farms. But placing wind farms offshore rises a lot o challenges related to construction, installation and nevertheless with the energy transmission. The last case requires a great effort in order to make the offshore wind farm viable, especially for long distances between the wind farm and the shore.

The solution which can solve the above presented problem is the use of HVDC transmission systems. The main advantages of these transmission systems are related with the transmission losses as well as with the costs which are lower than in the case of the traditional HVAC transmission systems.

At the beginning, HVDC transmission systems were based on line commuted converters (LCC). So, using this configuration (LCC-based HVDC), large amount of power could be process, but, however full controllability of the system was not achieved and also high harmonic content was present. Once with the development of power electronics devices, the use of VSCs in high voltage applications became possible. Thus, the use of VSC-based HVDC configuration became more suitable for long distances power transmission since it remotes the drawbacks of the LCC-based HVDC transmission systems. The scheme of such a transmission system is presented in Figure 1.5 and it consists mainly of two voltage source converters connected through a DC transmission line; moreover each converter is able to control the AC voltage in each bus and the DC link voltage as well as the active and reactive power in the system.

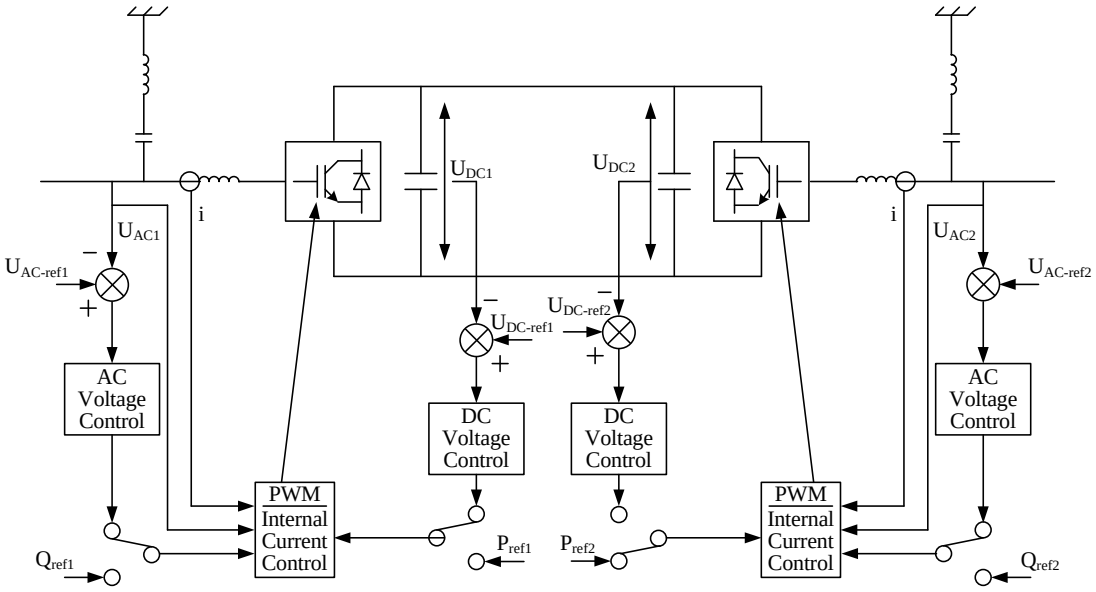

Figure 1.5: *VSC-based HVDC transmission system*

The aim of this thesis is to develop good understanding about the behavior and the control strategies regarding VSC-based HVDC transmission and its applications in the renewable energy systems.

1.3 Objectives

The objective of the present thesis is to model and analyze the behavior a VSC-based HVDC transmission system for offshore wind farms, while for verification a small-scale laboratory setup will be used. The main goals of the thesis are summarized below:

- good understanding of the VSC-based HVDC transmission system concept and of its behavior;
- modeling of the VSC-based HVDC transmission system using MATLAB/Simulink package;
- implementation of different control strategies for the VSC-based HVDC transmission system;
- analysis of the developed system behavior under different conditions;
- laboratory validation of the developed MATLAB/Simulink model using a small-scale setup and a dSPACE platform.

1.4 Limitations

The most important limitations encountered during the development of this thesis are summarized and presented below:

- Due to the unavailability of data for a real VSC-based HVDC transmission system the simulations (study-cases) are carried out for the data available in the laboratory:
  - Nominal power: 2.2 kW;
  - Nominal current: 4.3 A;
  - Grid voltage: 230 V;
  - Dc link voltage: 650 V;
  - Filter parameters: $L_f = 6.9$ mH; $C_f = 4.7$ μH; $L_{trafo} = 2$ mH;
- No model for a wind power plant was developed since its implementation on the laboratory setup cannot be achieved; the standard setup is composed of two inverters, which in this case are emulating the VSC-HVDC transmission, no inverter being available to emulate the WPP;
- Due to the above discussed limitation, the behavior of the VSC-based HVDC transmission system could not be analyzed in the laboratory for the second discussed control strategy (Strategy 2).

1.5 Thesis Outline

This thesis studies the control of voltage source converter based HVDC power transmission and the present report is strutured in seven chapters.

The first chapter may be seen as an introduction to the studied subject, containing a short background,the problem formulation and the objectives of the current thesis. The limitation of this thesis are also presented in this chapter.

The second chapter represents an overview of VSC-based HVDC transmission system. Firstly, a comparaison between HVAC and HVDC transmission is presented. The applications and the configuration of HVDC system are also discussed. After that, the advantages, the applications and the configurations of VSC-based HVDC transmission system are briefly presented. This chapter ends with an overview about Danish grid code requirements.

The third chapter deals with the modeling of the system. Each component is separately explained by presenting its role in the system.

The design of the control strategies for the VSC-based HVDC power transmission are investigated in Chapter 4. The PLL technique used to synchronize the developed system with the grid voltages is also presented in this section. This chapter also containes the design of the current controller, the DC voltage controller, the active and reactive power controllers and the AC voltage controller. The tuning process of these controllers was realized using SISOtool provided by MATLAB/Simulink.

In the fifth chapter several study cases are carried out in order to analyze and to prove the behavior of the developed VSC-based HVDC transmission system model.

The sixth chapter presents the laboratory implementation of the developed control strategies, in order to validate the simulation results.

Finally, the conclusions of the thesis and also ideas for the future work are pointed out in Chapter 7.

Chapter 2

Overview of VSC-Based HVDC Transmission System

This chapter contains an overview of the VSC-based HVDC transmission systems. Firstly, a comparison between HVDC and HVAC transmission systems is presented. Furthermore, several basic applications were the HVDC transmission systems are suitable are briefly exposed. The chapter will continue with a presentation of the VSC-based HVDC transmission systems. The advantages of such systems, their areas of application and their configurations are also discussed. In the end of this chapter several grid codes requirements provided by the Danish TSO are briefly stated.

2.1 Introduction to HVDC Transmission System

The HVDC transmission system is a high power electronics technology used in electric power systems mainly due to its capability of transmitting large amount of power over long distances [7], [8]. Overhead lines or underground/submarine cables can be used as transmission path.

The High Voltage Direct Current (HVDC) technology was used for the first time in 1954 in the under-sea cable interconnection between the island of Gotland (Sweden) and Sweden. For this transmission, thyristors with a rating of 50 kV and 100 A were used.

From its beginnings until the mid 1970s, the HVDC transmissions were based on mercury arc valves. After that, for the next 25 years, line commutated converters - using thyristors as based component - were used in the HVDC transmission systems. Once with the development of the high power switching devices and their availability al low prices, the LCCs were replaced by the self commutated converters and now the voltage source converters are more and more used for HVDC transmissions [7].

2.1.1 Comparison of HVAC and HVDC Transmissions

The HVDC transmissions can be compared with the HVAC transmission basically from two points of view: from the transmission costs point of view and from the technical point of view respectively.

Analyzing the two systems regarding the transmission costs, the next advantages of HVDC transmission systems over the HVAC transmission systems can be found [7]:

- considering similar insulating requirements for peak voltage levels, a DC line/cable will carry the same amount of power with two conductors as an AC line/cable with three conductors; thus, for the same power level, an HVDC transmission system will require smaller Right-of-Way, simpler towers and also the conductor and insulator costs will be reduced, in comparison with a classical HVAC transmission;
- the power transmission losses (conductor losses) are reduced by about two-thirds when the DC option is used instead of the AC one;
- furthermore, when a HVDC transmission is used, the absence of the skin effect can be noticed and also the dielectric and corona losses are kept at low level, thus the efficiency of the transmission is increased;
- however, the disadvantage of the HVDC transmissions regarding the costs comes from use of the converters and filters.

As a conclusion it can be said that the HVAC transmissions are more economical than HVDC transmissions when used for small distances. Once the breakeven distance is reached the DC alternative becomes more economical fact which may be observed from Figure 2.1

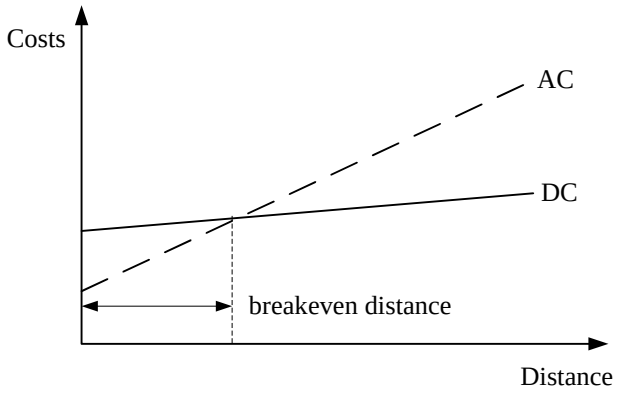

Figure 2.1: *Comparison of AC/DC lines - breakeven distance*

In the case of the overhead lines the breakeven distance can vary between 400 to 700 km, depending on the per unit line costs while, if a cable system is used the breakeven distance vary between 25 and 50 km [7]. The typical breakeven distance for overhead lines is 500 km [9].

Analyzing the two transmission systems, from the technical point of view, the HVDC transmissions overcome some of the problems which are usually associated with the AC transmissions. Thus, the stability limits are overcome when an HVDC transmission is used due to the fact that the power carrying ability of DC lines is not affected by the transmission distance. In the case of the HVAC transmission the power transfer in the AC lines is dependent on the phase angle which increases with the distance and thus the power transfer is limited.

The second problem which is solved by using the DC transmission instead of the AC transmission is the line charging. In the case of an HVAC transmission, line compensation (using STATCOMs, SVCs etc) is used in order to solve the line charging issue, while in the

case of DC lines such compensation is not required [7], [9]. Due to this issue, in the case of HVAC transmission the breakeven distance is reduced to 50 km.

Moreover, asynchronous interconnection of two AC power systems can be realized using the HVDC technology.

On the other hand the early use of HVDC transmission systems was limited due to several factors such as: high cost of converters, generation of harmonics, complexity of controls, inability to use transformer to alter voltage levels etc [7]. However, over the time many of these above presented issues were solved except the inability to use transformer to alter voltage levels.

As a conclusion to this comparison it can be said that the HVDC transmission technology is attractive and advantageous for long power transmissions, bulk power delivery, long submarine power crossing and also asynchronous interconnections [9], [10].

2.1.2 Applications of HVDC Transmissions

The HVDC transmissions are basically used in one of the following four applications:

- underground/submarine cable transmissions

  In the case of underground or submarine HVDC cables there is no physical restriction concerning the distance, the power level and also there are considerable savings in installed cable costs. Furthermore, in the case of the underground cables, these ones can be used on shared Right-of-Way with other utilities [9], [10].

  Some examples in this type of application are: Gotland project (1954), Sardinia (1967) and more recent the 180 MW Directlink connection in Australia (2000).

- long distance bulk power transmissions

  The HVDC transmission systems provide an economical alternative to AC transmission systems regarding the bulk power delivery from remote locations such as hydroelectric developments or large scale wind farms whenever the breakeven distance is exceeded [7], [10]. As presented above, a higher power transfer is possible over long distances using fewer lines with HVDC technology than with the AC technology.

- asynchronous connections of AC power systems

  The HVDC transmissions systems offer a reliable and economical way of interconnection between two AC asynchronous networks. Usually, these interconnections are realized using back-to-back converters with no transmission line [9], [10].

  Many examples of asynchronous interconnections can be found in North America, as in the case of Electric Reliability Council of Texas (ERCOT) and its neighbors [10].

- stabilization of power flows in integrated power systems

  According to [7], due to the fast controllability of dc power, strategically placed DC lines can solve issues like power flow in AC ties which can be uncontrollable and can lead to overloads and stability problems.

  One example of using HVDC transmission systems in such application is the IPP link in USA [7].

- offshore transmission

  Due to their advantages, such as: self-commutation, black-start capability and dynamic voltage control, VSC-based HVDC transmissions can be used to serve isolated loads on islands or offshore platforms over [10]. Moreover, VSC-based HVDC transmission systems can provide reactive power support to wind farms as well as interconnection point.

2.2 HVDC System Configuration

Based on the functions and the locations of the converter station, four main HVDC system configurations are used in power system transmissions. These four HVDC system configurations can be used for both VSCs and CSCs converter topologies [11].

Monopolar HVDC System

In this configuration, two converters separated by a single pole line are used. Positive or negative DC voltage can be used, but in the case of using negative polarity the corona effects in the DC line are less [7]. Depending on the application, in the case of the monopolar configuration, ground or a metallic conductor can be used as return path, as illustrated in Figure 2.2.

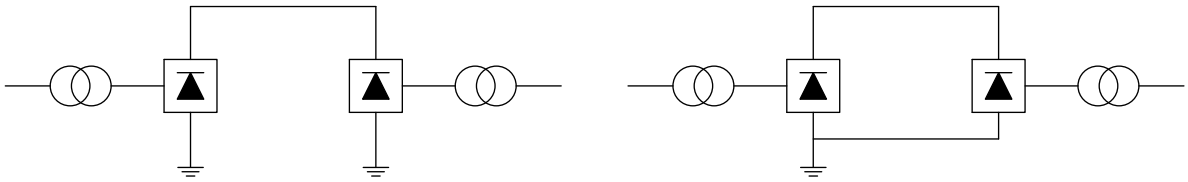

(a) with ground return (b) with metallic return

Figure 2.2: *Monopolar HVDC system*

This configuration is usually preferred in the case of cable transmissions with submarine connections [11].

Bipolar HVDC System

In this case, the configuration uses two conductors, one positive and the other negative. The connection between the two sets of converter is grounded at one or at both ends [7]. Basically the bipolar system consists of two monopolar systems. The advantage of this configuration is given by the fact that one of the poles can continue to transmit power in case the other one is out of service [7], [11]. Thus, the two poles may be used independently, if both neutral points are grounded [8]. The bipolar HVDC system configuration is illustrated in Figure 2.3.

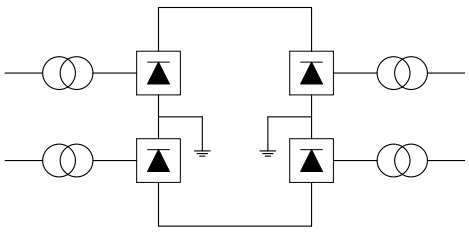

Figure 2.3: *Bipolar HVDC system*

Theoretically the ground current is zero in the case of this configuration since both poles operate with equal current [7], [11]. Based on the above presented things, this is the most common configuration for modern HVDC transmission lines [10], [11].

Back-to-back HVDC System

In this configuration, the two converters stations are placed at the same site and there is no transmission of power with a DC link over a long distance [11]. The block diagram of a back-to-back system is presented in Figure 2.4.

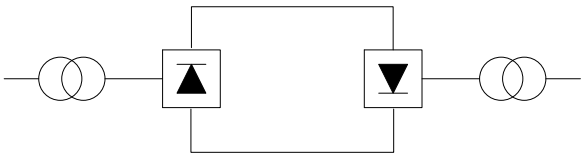

Figure 2.4: *Back-to-back HVDC System*

Such a back-to-back HVDC system is used two interconnect two AC systems which may have different frequencies (asynchronous interconnection) [10].

Multi-terminal HVDC System

A multi-terminal HVDC transmission system consists of three or more converter substations, some of them working as inverters while the other ones as rectifiers [12]. Depending on the positioning of the converter substations, two basic arrangements of the multi-terminal HVDC system can be obtained: series multi-terminal HVDC system and parallel multi-terminal HVDC system. These two arrangements are presented below.

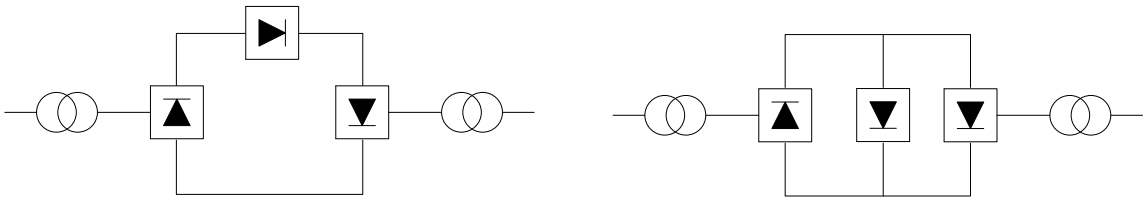

(a) Series arrangement

(b) Parallel arrangement

Figure 2.5: *Multi-terminal HVDC system*

A combination of series and parallel connections of the converters forms a hybrid multi-terminal HVDC transmission system.

Due to the high number of converter stations used in such a transmission system, the use of this configuration is not justified from the economical point o view.

2.3 VSC Based HVDC Transmission System

The HVDC transmission technology can be realized by using current source converters (CSCs) commutated thyristor switches, known as traditional HVDC or classic HVDC, or by using voltage source converters (VSC-based HVDC). Due to the rapid development of power electronic devices with turn-off capability and of DSPs, which are generating the appropriate firing patterns, the VSC are getting more and more attractive for HVDC transmission [7]. A detailed comparison between CSCs and VSCs may be found in [7].

Usually, the VSCs are using insulated gate bipolar transistor (IGBT) valves and pulse width modulation (PWM) for creating the desired voltage wave form.

The first HVDC transmission using VSC was installed in 1997 in Gotland (Sweden) [13].

On the market, mainly two manufacture refer to the technology of DC transmission using VSC; these are: ABB under the name HVDC Light® [14], with a power rating from tenths of megawatts up to over 1000 MW, and the second manufacturer is Siemens under the name HVDC Plus ("Plus" - Power Link Universal Systems) [15].

2.3.1 Advantages and Applications for VSC-based HVDC

By analyzing the operation of both classic HVDC technology and VSC-based HVDC technology, the main difference between these two technologies can be highlighted: the controllability. Thus, the controllability in the case of VSC-based HVDC technology is higher compared with the one of the earlier developed technology. Thereby, if VSCs are used instead of line-commutated CSCs several advantages can be stated, some of them being presented below:

- VSC converter technology provides rapid and independent control of active and reactive power without needing extra compensating equipment; the reactive power can be controlled at both terminals independently of the DC transmission voltage level [7], [9], [10], [11];
- the commutation failures due to disturbances in the AC network can be reduced or even avoided if VSC-HVDC technology is used [5], [11];
- the VSC-HVDC system can be connected to a "weak" AC network or to a network where no generation source is available (the VSC can work independently of any AC source), so the short circuit level is low [5], [11];
- self (forced) commutation with voltage source converters permits black start, which means that the VSC is used to synthesize a balanced set of three phase voltages as a virtual synchronous generator [9], [10];
- due to its modular, compact and standardized construction, the converter can be easily and rapidly installed/commissioned at the desired site [7];

- in comparison with the classic HVDC transmission, the VSCs don not have any reactive power demand and moreover, they can control their reactive power to regulate the AC system voltage like a generator [10].

However, the VSC-based HVDC technology has some drawbacks, which include potentially high power losses and high cost (caused by the converter stations) compared with traditional HVDC technology.

Because of its advantages, some of them presented above, the VSC-based HVDC transmission suits very well in certain application. An enumeration of these applications is presented below:

- Power supply to insular loads

  Due to some of its advantages such as: dynamic voltage control, black start capability or forced-commutation the VSC-HVDC transmission is capable to supply remote locations (i.e. islands) using submarine cables and without any need of running expensive local generation [7], [9]. An example of this application is the Gotland Island System.

- Offshore applications

  The VSC-based HVDC technology represents a very suitable way of transmitting power from wind farms to the main AC grid. The ability of controlling reactive power as well as the AC voltage and its contribution to the grid stability makes the VSC-HVDC technology very popular for such applications. Moreover, the technology is flexible and new units can be easily added if the expand of the WF is desired [7].

  The VSC-HVDC transmission is a compact transmission and can feed production or transportation loads on offshore oil or gas platforms from shore [9].

- Underground/underwater cables

  The use of HVDC cable systems is not constraint by any distance limitations as in the case of AC cable systems. Moreover, the losses are reduced when an HVDC cable system is used. The XLPE (Cross Linked Poly-Ethylene) extruded HVDC cables can overcome RoW constrains and the power transfer capacity is increased at the same time [7], [9].

- Urban Infeed

  Mainly due to RoW constraints and land use constraints, the compact VSC-based HVDC technology represents a feasible solution to feed the city centers. Thus, the underground transmission circuits are placed on already existing dual-use RoWs in order to bring in power as well as to provide voltage support [9], [11]. This process is realized without compromising reliability and it is an economical way of power supply.

Other applications, in which the use of VSC-based HVDC transmission systems is suitable, such as: asynchronous interconnection, multiterminal systems etc are presented in detail in [5], [9], [11].

2.3.2 VSC-based HVDC Transmission System Configurations

The typical configuration of VSC-based HVDC transmission system is presented in Figure 2.6.

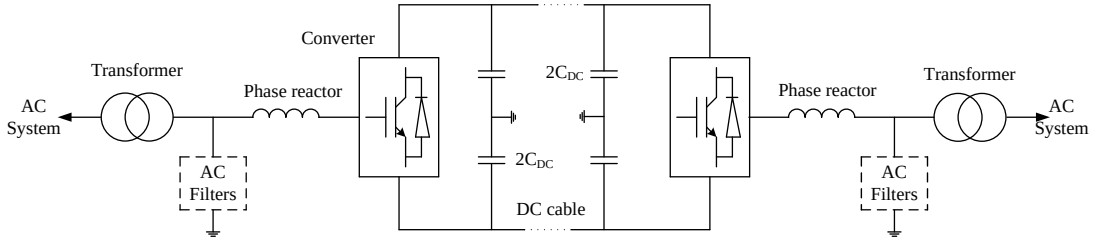

Figure 2.6: *Typical VSC-HVDC system [16]*

Such a transmission system consists of: two voltage source converters, transformers, phase reactors, AC filters, DC-link capacitors and DC cables. In the upcoming paragraphs each of these components will be briefly discussed.

Voltage Source Converter

The two VSCs may be seen as the core of this transmission system topology. One of the VSCs works as rectifier, while the other one works as an inverter, and both of them are based on IGBT power semiconductors. The two VSC stations are connected through a DC transmission line or an overhead line.

Mainly, two basic configurations of VSCs are used on HVDC transmission system. These are the two-level VSC converter, presented in Figure 2.7(a), and the three-level VSC converter, which is presented in Figure 2.7(b).

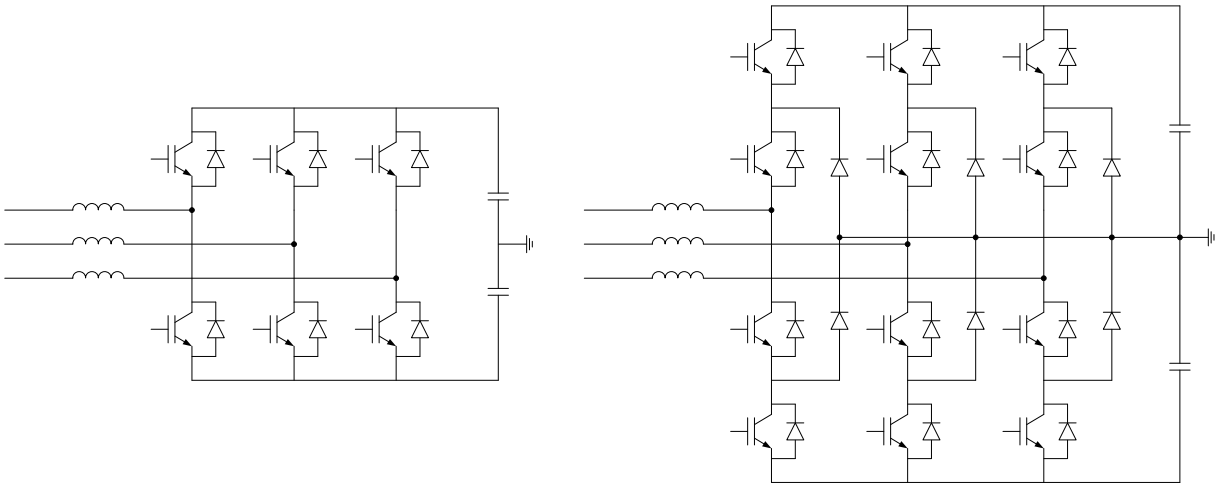

(a) Two-level VSC

(b) Three-level VSC

Figure 2.7: *The topology of the VSC*

The two-level VSC, also known as the three phase, two level, six-pulses bridge, is the simplest configuration suitable for HVDC transmission. Such a converter consists of six valves (each valve consist of an IGBT and an anti-parallel diode) and is capable of generating two voltage levels $-0.5 \cdot U_{DCn}$ and $+0.5 \cdot U_{DCn}$.

In high power applications, the three-level VSC configuration (see Figure 2.7(b)), represents a reliable alternative to the two-level VSC configuration, because the phase potentials can be modulated between three levels, $-0.5 \cdot U_{DCn}$, 0 and $+0.5 \cdot U_{DCn}$. In this configuration, one arm of the converter consists of four valves.

Transformer

As it can be observed in Figure 2.6, the transformers are used to interconnect the VSC with the AC network. The main function of the transformers is to adapt the voltage level of the AC network to a voltage level suitable to the converter. This voltage level can be controlled using a tap changer, which will maximize the reactive power flow.

Phase Reactor

The phase reactors, known also as converter reactors, are used to continuously control the active and reactive power flow. According to [14], the phase reactors have three main functions:

- the first one is to provide low-pass filtering of the PWM pattern in order to provide the desired fundamental frequency voltage;
- the second function is to provide active and reactive power control; the active and reactive power flow between the AC and the DC side is defined by the fundamental frequency voltage across the reactors [14];
- the last function is to limit the short-circuit currents.

Typically, the short-circuit voltage of the phase reactor is 15%.

AC Filter

The main goal of the AC filters is to eliminate the harmonic content - which was created by using the PWM technique - of the output AC voltage. Otherwise, if these harmonic components are not eliminated or reduced, malfunctioning in the AC grid will appear.

Typical requirements for AC filters are: individual harmonic distortion level ($D_h \approx 1\%$), total harmonic distortion (THD) level may vary between 1.5% and 2.5% and telephone influence factor (TIF) between 40 and 50 [14].

Depending on the desired filter performances or requirements, the filter configuration is varying from application to application. In a typical HVDC Light scheme, the AC filter consists of two or three grounded /ungrounded tuned filter branches [14].

DC-link Capacitor

As presented in Figure 2.6, on the DC side, there are two capacitor stacks of the same power rating. The main goal of the DC-link capacitor is to provide a low-inductance path for the

turned-off current [14]. Moreover, the DC capacitor serves as an energy store and it reduces the harmonics ripple on the DC voltage.

Depending on the size of the DC side capacitor, DC voltage variations caused by disturbances in the system (e.g. AC faults) can be limited [14].

DC Cable

Mainly, three types of DC cables are suitable for HVDC transmission systems. These are: the self contained fluid filled(oil filled, gas pressurized) cables, the solid cables and XLPE polymer extruded cables. Lately, the last mentioned type seems to be the the preferred choice for VSC-based HVDC transmission system, because of their mechanical strength, flexibility and low weight [17].

2.3.3 HVDC Light Technology - BORWIN (Borkum 2) Offshore Wind Farm

The BORWIN (Borkum 2) offshore wind farm is situated 128 km off the North Sea Cost and is the largest and most remote offshore wind farm in the world [18]. Furthermore, for the case of BORWIN it is for the first time when wind power generated at such a distance is connected to the AC grid through high voltage direct current transmission [19]. The connection with the grid is realized through a 400 MW HVDC Light transmission system, developed by ABB.

The HVDC Light Cable technology has a series of advantages (over the HVAC technology) for connecting the offshore wind power plants to the onshore grid, such as: their reduced weight and dimensions, resulting in a higher power density [18]. Moreover, the HVDC Light cables operate at higher electric field stress and in comparison with the traditional HVAC cables, they have to be dimensioned only for their ohmic conductor losses [18] and [19].

In Figure 2.8, the Borkum 2 wind farm and its grid connection through HVDC transmission is presented.

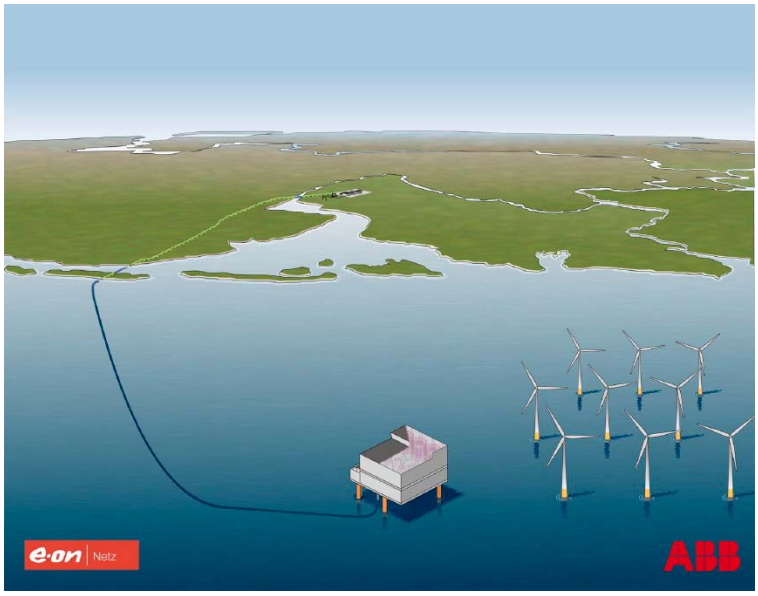

Figure 2.8: *The Borkum 2 wind farm cluster situated 128 km from shore [20]*

The discussed system is a self-commutated HVDC which is based on IGBTs and uses lightweight eco-friendly polymer cables [19]. Because of the independent control of active power flow and reactive power flow, with total control of power from zero to rated power without filter switching, a reliable and smooth operation of the wind power plant is achieved [20].

The main data of the BORWIN transmission system are presented in the following:

- Power rating: 400 MW;
- AC voltage: 170 kV (offshore) and 380 kV (onshore)
- DC Voltage: $\pm$150 kV
- Land cable length: 2×75 km;
- Sea cable length: 2×128 km;

In conclusion it must be specified that, according to [19], by using the above presented HVDC system the transmission losses are decreased with 25%.

2.4 Grid Code Requirements

The Danish Transmission System Operator (TSO), Energinet, provides grid code requirements for connecting wind turbines and/or wind farms to the national grids. These grid code requirements are classified in two categories: for voltage levels above 100 kV and below 100 kV. Due to the fact that nowadays more interest is given to the installation on large wind farms than to the installation of individual wind turbines, in this section only the Danish grid code requirements for grid voltage levels above 100 kV are considered [21].

Active Power Regulation

In [21], the next regulation techniques have been defined, regarding the active power requirements. Furthermore, in order to avoid unintended interferences between these techniques, the following priority order shall be respected:

- System protection - this is a protective function for downward regulation of the power generated by the wind power plant to a level that is acceptable to the power system.
- Frequency control - when frequency deviations occur in the power systems, the WPP must contribute at the restoration of the normal frequency (50 Hz) by controlling actively the power production. In Figure 2.9 two methods of frequency control are presented.

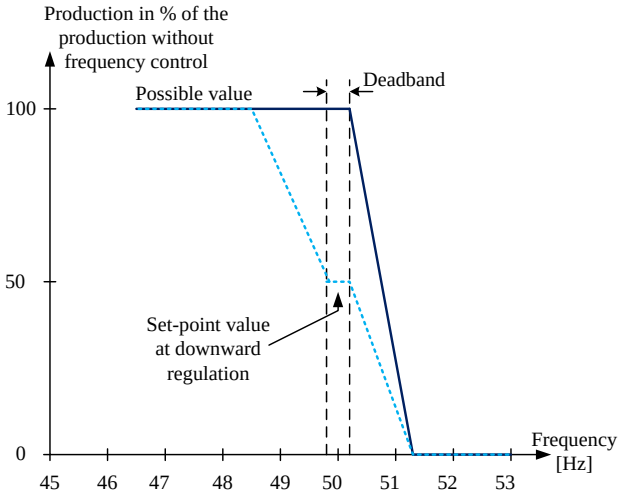

Figure 2.9: *Frequency regulation with and without previous downward regulation [21]*

In the first case (full-drawn line) the frequency control only regulates downward the power production, while in the second case (dotted line), the frequency control can also make an upward regulation because of the previous downward regulation [21].

- Stop regulation - if the wind speed increases, the wind farm must be able to maintain the current power production (see Figure 2.10)

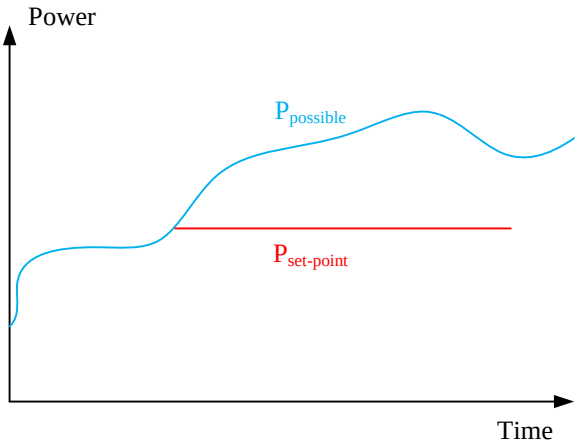

Figure 2.10: *Stop regulation*

- Balance regulation - this technique must be implemented as a rapid power regulation which ensures upward and/or downward regulation of the wind farm production when required [21].
- Power gradient constraint - this method prevents the fast increasing of power generated by the wind farm when the wind speed increases or when the wind farm is started in high winds (see Figure 2.11).

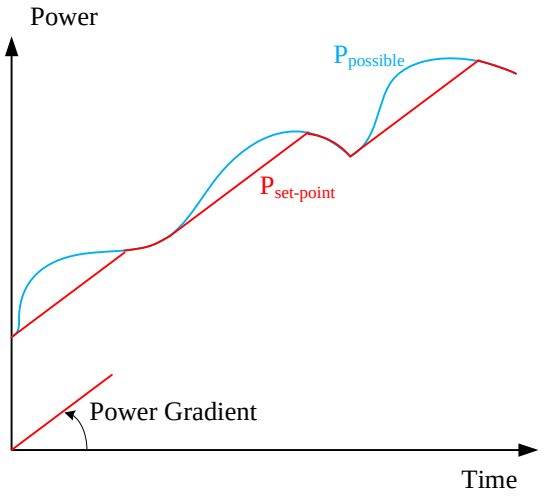

Figure 2.11: *Power gradient constraint*

- Absolute production constraint - limits the power production at a previously set maximum reference point (see Figure 2.12).

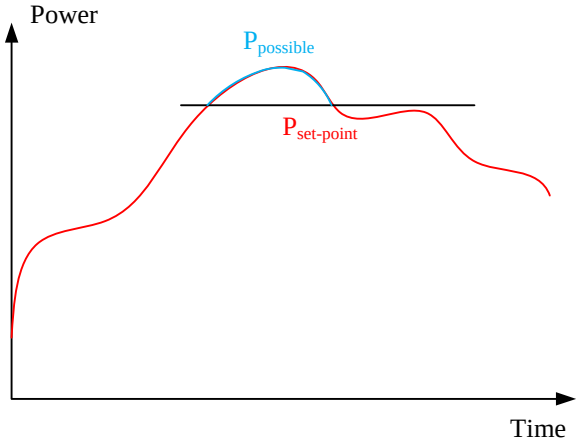

Figure 2.12: *Absolute production constraint*

- Delta production constraint - using this technique power reserves are allocated by limiting the current power production to a value below the actual possible power production.

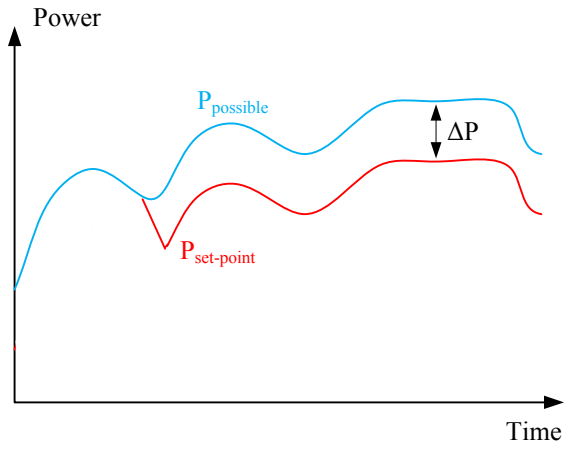

Figure 2.13: *Delta production constraint*

Reactive Power Regulation

According to [21], the wind farms must be equipped with reactive power compensation which ensures that the mean value of the reactive power over 10 seconds (at the PCC) is kept inside the control band presented in Figure 2.14.

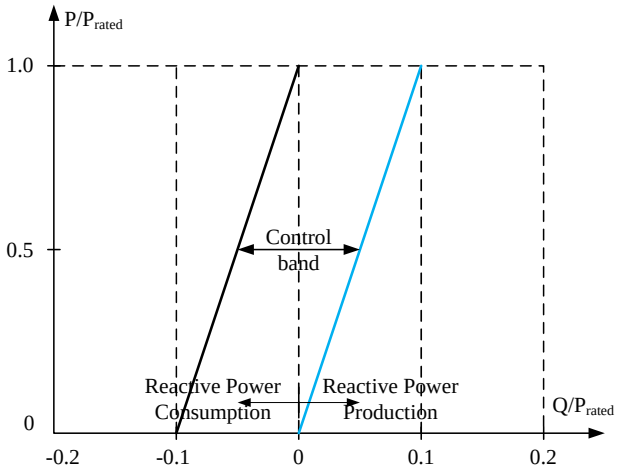

Figure 2.14: *Control band for the real power control method at PCC*

Furthermore, in the Danish grid codes it is stated that the owner of the wind farm must supply a P-Q diagram which shows the reactive power regulation capability at PCC.

In [21], three type of regulation are mentioned: MVAR regulation, voltage regulation and reactive regulation according to minimum requirements.

Reactive regulation shall be done for the total wind farm by the farm controller function [21].

Voltage Quality

Other important requirements imposed usually by TSOs concern the voltage quality aspects. In this case, requirements from three main topics have to be fulfilled:

- Rapid voltage changes

A rapid voltage change can be defined as a single rapid change of the RMS value of the voltage and it may occur in the wind farms due to the breaker switching [21].

- Voltage fluctuations and flicker

According to [21], the flicker contribution, P_{st} and P_{lt}, does not have to exceed some well established limits:

$$P_{st} < 0.3 \tag{2.1}$$

$$P_{lt} < 0.2 \tag{2.2}$$

The flicker coefficient P_{st} is determined as a weighted average of the flicker contribution during ten minutes, while the coefficient P_{lt} is determined as a weighted average of the flicker contribution during two hours [21]. Both coefficients are defined in IEC/TR $61000 - 3 - 7$ [22].

In [21], two main requirements regarding harmonics are stated. The harmonic disturbance for each individual harmonic, given by relation (2.3), shall be lower than 1 per cent for $1 < n < 51$ at PCC. The second requirement concerns the total harmonic distortion (THD) coefficient, given by (2.4), which must be smaller than 1.5 per cent.

$$D_n = \frac{U_n}{U_l} \times 100\% \tag{2.3}$$

$$THD = 100\sqrt{\sum_{n=2}^{50}(\frac{U_n}{U_l})^2}\ \% \tag{2.4}$$

Operation during grid disturbances

A description of the situations for which the wind farms shall be disconnected and another description for the situations in which the wind farms must not trip is presented in [21].

Tests on the wind turbines shall be performed using the voltage profile presented in Figure 2.15.

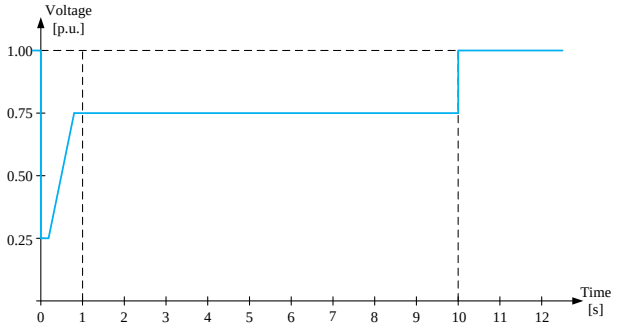

Figure 2.15: *Voltage profile for simulation of symmetric three phase faults [21]*

According to [21], the requirements (concerning operation during grid disturbances) which must be fulfilled by the wind farm for a proper working are:

- the WF must produce the rated power in the first 10 seconds after the voltage is above 0.9 p.u.;
- the reactive power exchange with the grid must meet the requirements in the first 10 seconds after the voltage is above 0.9 p.u.;
- the WF's regulation of the reactive power must change from normal regulation to maximum voltage support during the voltage dip.

2.5 Summary

The purpose of this chapter was to introduce the reader to the various aspects concerning HVDC transmission systems in general and VSC-based HVDC transmission systems in particular.

Thereby, the first part of this section was dedicated to the introduction to the HVDC transmission systems. In order to show why the HVDC transmission technology is more and more used in different applications, a comparison between HVAC transmissions and HVDC transmissions was presented and the advantages of the first technology were highlighted. These advantages make the HVDC transmission systems suitable for several applications, such as: long distance bulk power transmissions, asynchronous connection of AC power systems etc.

The second topic discussed in this chapter was about basic HVDC system configurations. The four main configurations: monopolar, bipolar, back-to-back and multi-terminal were briefly explained.

The VSC-based HVDC transmission system technology was the next topic discussed. Advantages of this topology over the classic HVDC transmission topology were presented and also some fields of application of these new power transmission systems were enumerated (e.g. power supply to insular loads, offshore applications etc). The basic configuration of a typical VSC-based HVDC system was presented and a short description of each components was given.

The chapter ends with the presentation of several Danish grid requirements which have to be fulfilled by wind farms.

Chapter 3

System Modeling

In this chapter the mathematical modeling of the main components (VSC, filter and grid) of the VSC-based HVDC system will be described. The modeling of the components will be realized in the dq synchronous reference frame since the control will be implemented in the same reference frame.

3.1 Voltage Source Converter Model

The main circuit of a three-phase AC-DC voltage source converter is shown in Figure 3.1.

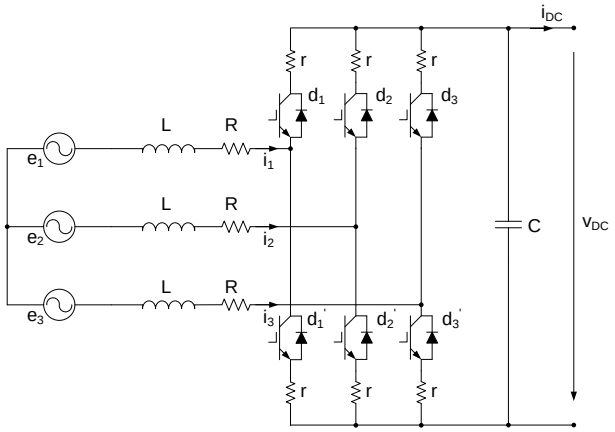

Figure 3.1: *Circuit diagram of a three-phase VSC*

The three-phase mathematical model for a VSC similar to the one presented above was presented in [23] and [24]. If a balanced three-phase system with neutral connection is assumed and neglecting the resistance r of the switches [24], the voltage source converter can be modeled by using equations (3.1) - (3.3):

$$C\frac{dv_{DC}}{dt} = \sum_{k=1}^{3} i_k d_k - i_{DC} \tag{3.1}$$

$$L\frac{di_k}{dt} + Ri_k = e_k - v_{DC}(d_k - \frac{1}{3}\sum_{n=1}^{3} d_n) \tag{3.2}$$

$$\sum_{k=1}^{3} e_k = \sum_{k=1}^{3} i_k = 0 \tag{3.3}$$

where,

- k - represents the index for the three-phase;
- d_k - represents the duty cycle;
- e_k - represents the phase voltage;
- i_k - represents the phase current;
- v_{DC} - represents the DC-link voltage;
- i_{DC} - represents the DC current;
- r - represents the resistance of the switch;
- L - represents the inductance of the phase reactor;
- R - represents the resistance of the phase reactor.

Thus, using equations (3.1) and (3.2), the block diagram of a three-phase VSC can be obtained:

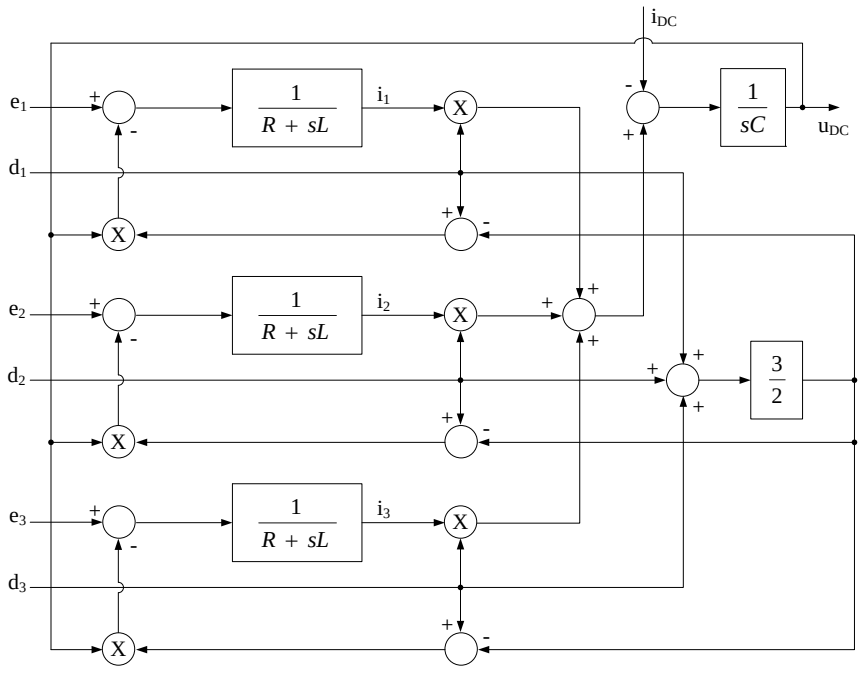

Figure 3.2: *The block diagram of a three-phase VSC*

Based on the three-phase mathematical model of the voltage source converter, the converter's model in the *dq* synchronous reference frame can be derived. The model of the VSC in the *dq* reference frame will be implemented in Simulink and used for further study-cases

analysis. In order to achieve the mathematical model of the VSC in the *dq* synchronous reference frame, the orientation of the *dq* system, in the complex plane, in respect to the three-phase system, is considered as presented in Figure 3.3.

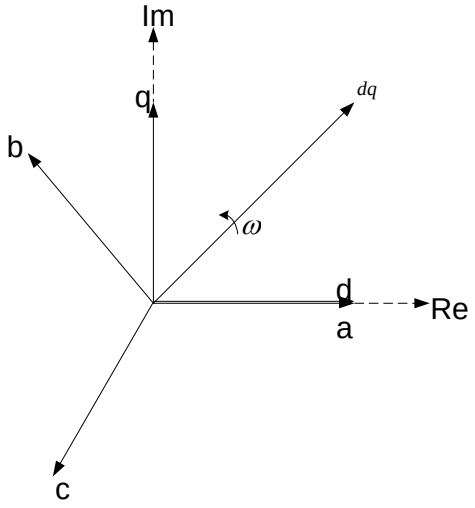

Figure 3.3: *Orientation of the dq and three phase systems in the complex plane*

Thus, starting from the three-phase mathematical model of the VSC given by equations (3.1) - (3.3) and taking into account of the system's orientation (see Figure 3.3) and of the Clarke and Park transformations, the *dq* mathematical model of the VSC was derived:

$$C\frac{dv_{DC}}{dt} = \frac{3}{2}Ri_{dq}d_{dq} - i_{DC} \tag{3.4}$$

$$L\frac{di_{dq}}{dt} + j\omega Li_{dq} + Ri_{dq} = e_{dq} - v_{DC}d_{dq} \tag{3.5}$$

By separating equations (3.4) and (3.5) into d and q components the desired model of the converter was obtained and is given by:

$$C\frac{dv_{DC}}{dt} = \frac{3}{2}(i_q d_q + i_d d_d) \tag{3.6}$$

$$L\frac{di_q}{dt} - \omega Li_d + Ri_d = e_q - v_{DC}d_q \tag{3.7}$$

$$L\frac{di_d}{dt} - \omega Li_q + Ri_d = e_d - v_{DC}d_d \tag{3.8}$$

Using equations (3.6) - (3.8) the block diagram for the VSC, in the synchronous reference frame, can be obtained and it is shown in Figure 3.4.

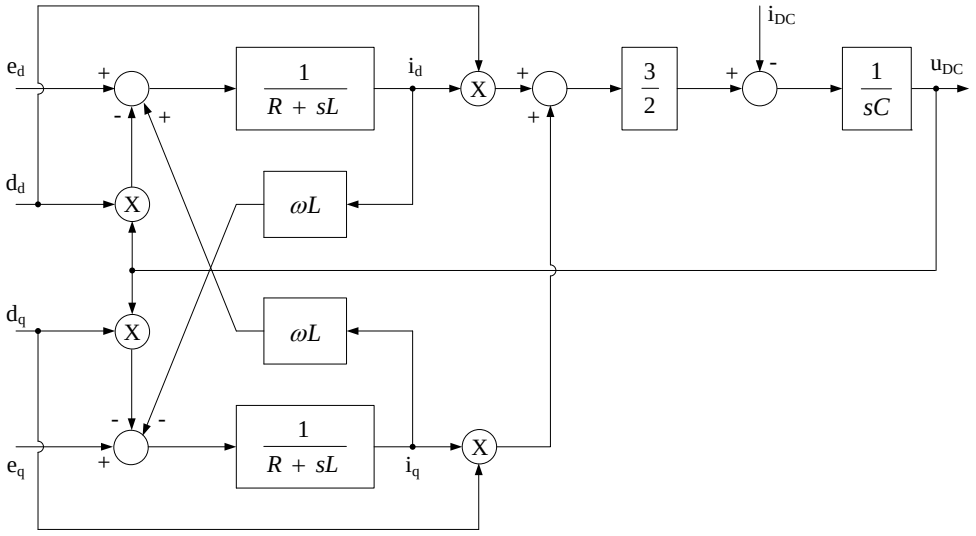

Figure 3.4: *The model of a three-phase VSC in dq synchronous reference frame*

3.2 Filter Model

The electrical circuit of a three-phase C filter which is to be modeled in this section is shown in Figure 3.5.

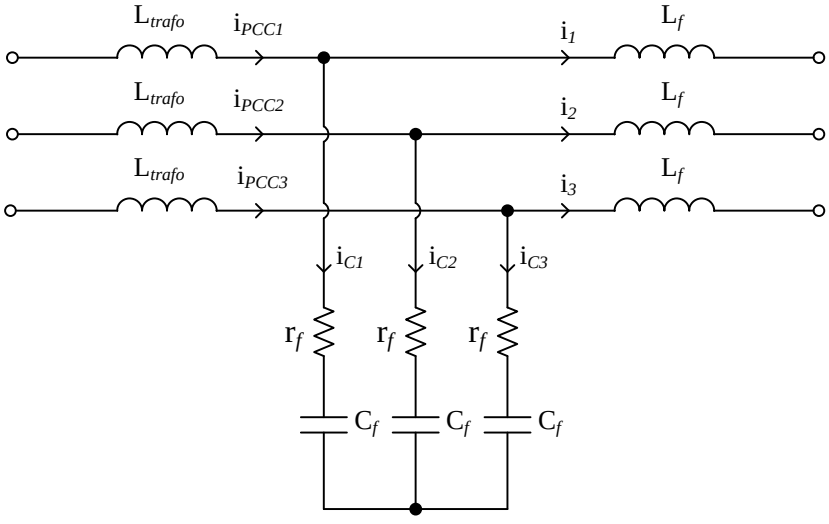

Figure 3.5: *Circuit diagram of a C filter*

The three-phase mathematical model for a C filter similar to the one presented above is discussed in detail in [25]. If the resistance r_f of the capacitor is neglected, the filter can be modeled by using equations (3.9), (3.10):

$$C_f \frac{de_k}{dt} = i_{c_k} \tag{3.9}$$

$$i_{c_k} = i_{PCC_k} - i_k \tag{3.10}$$

Where,

- k - represents the index for the three-phase;
- e_k - represents the phase voltage;
- i_k - represents the current across filter capacitance;
- i_{PCC_k} - represents the phase current at PCC;
- i_{c_k} - represents the current flowing in the capacitor;
- C_f - represents the filter's capacitor;
- r_f - represents the internal resistance of the capacitor.

Based on the three-phase mathematical model of the filter, the filter's model in the dq synchronous reference frame can be derived. Thus, starting from the three-phase mathematical model of the filter given by (3.9) and (3.10) and taking into account the system's orientation (see Figure 3.3), Clarke and Park transformation, respectively, the dq model of the filter was derived:

$$C_f \frac{de_{dq}}{dt} = i_{c_{dq}} \tag{3.11}$$

$$i_{c_{dq}} = i_{PCC_{dq}} - i_{dq} \tag{3.12}$$

By separating equations (3.11) and (3.12) into the d and q components, the desired model of the filter was obtained and is given by:

$$C_f \frac{de_d}{dt} = \omega C_f e_q + i_{c_d} \tag{3.13}$$

$$C_f \frac{de_q}{dt} = \omega C_f e_d + i_{c_q} \tag{3.14}$$

$$i_{c_d} = i_{PCC_d} - i_d \tag{3.15}$$

$$i_{c_q} = i_{PCC_q} - i_q \tag{3.16}$$

Using equations (3.13) - (3.16) the block diagram for the C filter, developed in the synchronous reference frame, can be obtained and it is illustrated in Figure 3.6.

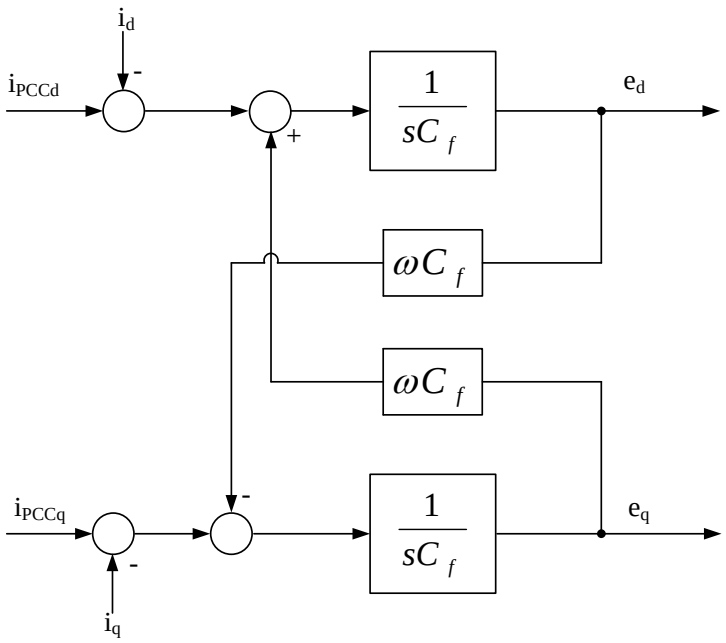

Figure 3.6: *The model of the three-phase C filter in dq synchronous reference frame*

3.3 Grid Model

Usually, a grid model can be developed by using the Thevenin equivalent circuit [26]. The equivalent circuit per phase for the grid model is presented in Figure 3.7, where by an (R-L) equivalent impedance the distribution lines are emulated.

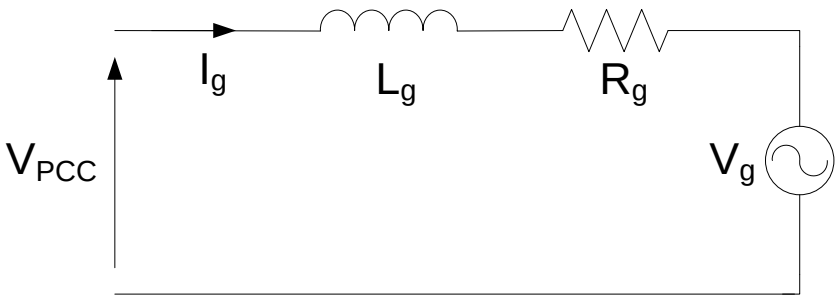

Figure 3.7: *Thevenin equivalent circuit*

For each of the three phases, the voltage equation can be written as follows:

$$V_g = R_g I_g + L_g \frac{di_g}{dt} + V_{PCC} \tag{3.17}$$

where,

- V_g - represents the grid voltage;
- V_{PCC} - represents the voltage at the PCC.

However, for simplicity, the grid can be represented as an ideal symmetrical three-phase voltage source [27], as shown in Figure 3.8.

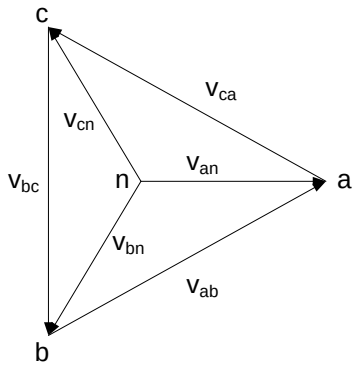

Figure 3.8: *Symmetrical three-phase system*

The three-phase voltages of the symmetrical system are defined as:

$$v_{an} = V \cos \omega t \tag{3.18}$$

$$v_{bn} = V \cos(\omega t - \frac{2\pi}{3}) \tag{3.19}$$

$$v_{cn} = V \cos(\omega t + \frac{2\pi}{3}) \tag{3.20}$$

where,

- V - represents the amplitude of the phase voltage;
- ω - represents the angular frequency.

Furthermore, the line-to-line voltages are defined as:

$$v_{ab} = v_{an} - v_{bn} \tag{3.21}$$

$$v_{bc} = v_{bn} - v_{cn} \tag{3.22}$$

$$v_{ca} = v_{cn} - v_{an} \tag{3.23}$$

Also, the three phase currents of the symmetrical system can be defined as:

$$i_a = I \cos \omega t \tag{3.24}$$

$$i_b = I \cos(\omega t - \frac{2\pi}{3} + \varphi) \tag{3.25}$$

$$i_c = I \cos(\omega t + \frac{2\pi}{3} + \varphi) \tag{3.26}$$

where,

- I - represents the amplitude of the phase currents;
- φ - represents the phase shift angle between the voltage and current.

3.4 Summary

In this chapter the mathematical models of the main components of the VSC-based HVDC transmission system were presented. Due to the fact that the control of the system will be implemented in the dq synchronous reference frame, the models of the voltage source converter and of the filter were developed in the same reference frame.

For simplicity, the AC grid was represented as an ideal three-phase voltage source.

Chapter 4

System Control Design

This chapter presents the design of the control strategies for the VSC-based HVDC transmission system. Firstly a brief presentation of the control strategies suitable for such an application will be realized. The chapter will continue with the individual presentation of all the control loops which will be used for simulating the VSC-HVDC system. The tuning process of these controllers will be also described. The PLL method to synchronize the system with the grid is going to be also introduced in this chapter.

4.1 Introduction

In the case of VSC-based HVDC transmission systems the transfer of power is controlled in the same way as in the case of a classical HVDC transmission. The inverter side controls the active power, while the rectifier side controls the DC voltage [8].

If the power transmission is considered between two AC grids, the power flow can be bidirectional. But, if the VSC-based HVDC system is used to deliver power from an offshore wind power plant (WPP), the active power flow is unidirectional (the offshore side is delivering active power to the onshore side and not vice-versa).

As presented in Chapter 2, one of the advantages of VSC-HVDC using PWM technology is that it makes possible to independently control the active power and the reactive power [22]. Thus, the reactive power may be controlled separately in each converter. The active power flow can be controlled by means of the DC voltage on the DC side or by variation of frequency on the AC side [8]. Moreover, the active power flow can be set manually.

In conclusion, when using VSC-based HVDC technology the active and reactive power, as well as the AC and DC voltage and the frequency can be controlled, fact which is presented in Figure 4.1.

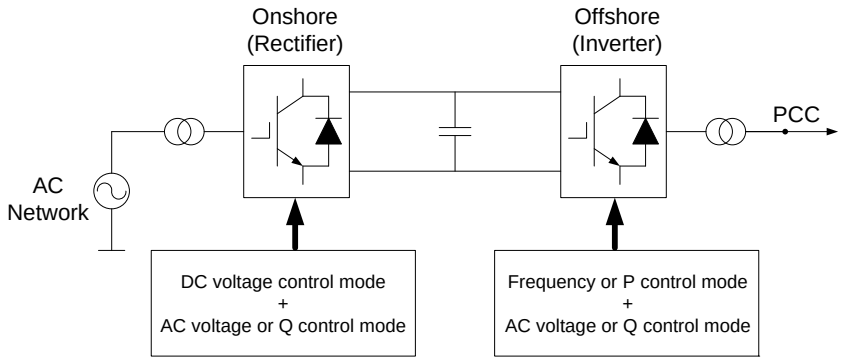

Figure 4.1: *Overall control system of the VSC-based HVDC (based on [16])*

In the case of a VSC-based HVDC transmission between an offshore WPP and an AC network, the offshore VSC controller maintains the offshore AC voltage and frequency, while the onshore VSC controller regulates the DC voltage and the reactive power (or AC terminal voltage) [28].

The control system of the VSC-based HVDC is realized by using a fast inner current control loop and several outer control loops, depending on the application [8], [29].

The control system of the VSC-HVDC systems has at its base level a fast inner current control loop controlling the AC currents. The AC current references are provided by the outer controllers [29]. The slower outer controllers include the DC voltage controller, the AC voltage controller, the active power controller, the reactive power controller and the frequency controller. Thus, the reference of the active current can be obtained from the DC voltage controller, from the active power controller or from the frequency controller. On the other hand, the reference of the reactive current can be derived from the reactive power controller or from the AC voltage controller [8].

According to [28], in the case when the VSC-HVDC technology is used for transmitting power from an offshore terminal to an onshore terminal the reference values for the current controllers are obtained as follows: on the offshore side, the AC voltage controllers are providing reference values for both active and reactive current while on the onshore side, the DC voltage controller provides the reference value for the active current and the reactive power controller or the AC voltage controller for the reactive current.

As it obviously is, not all the controllers can be used at the same time [8] and [29]. The choice of the different kinds of outer controllers is made depending on the application.

The overall control structure of the VSC-based HVDC transmission system considered in this project is shown in Figure 4.2.

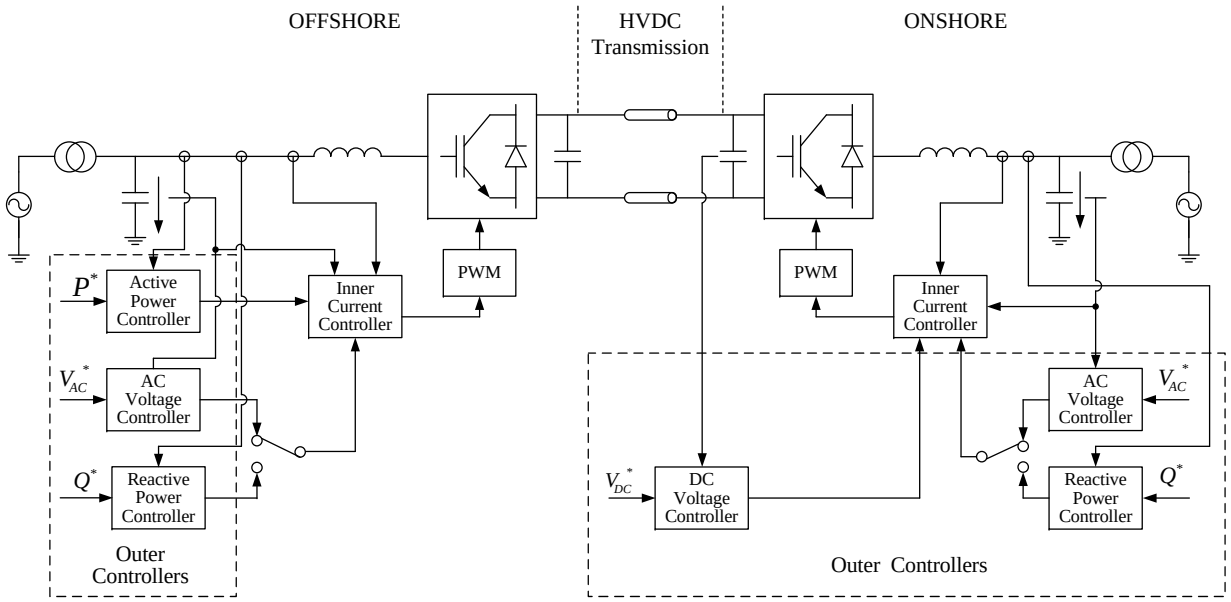

Figure 4.2: *Overall control structure of the VSC-HVDC transmission system*

The inner current controller as well as all the outer controllers will be described in detail on the following.

4.2 Phase Locked Loop

The grid synchronization is a very important and necessary feature of grid side converter control. The synchronization algorithm is able to detect the phase angle of grid voltage in order to synchronize the delivered power. Moreover, the phase angle plays an important role in control, being used in different transformation modules, as Park's transformation.

There are several methods capable to detect the phase angle: the zero crossing detection, the filtering of grid voltages and the phase locked loop (PLL) technique [30].

In this project, the last mentioned algorithm is implemented in order to synchronize the delivered power.

PLL is a phase tracking algorithm, which is able to provide an output synchronized with its reference input in both frequency and phase [30]. The purposed of this method is to synchronize the inverter output current with the grid voltage, in order to obtain a unitary power factor.

The block diagram of the PLL algorithm implemented in the synchronous reference frame is presented in Figure 4.3.

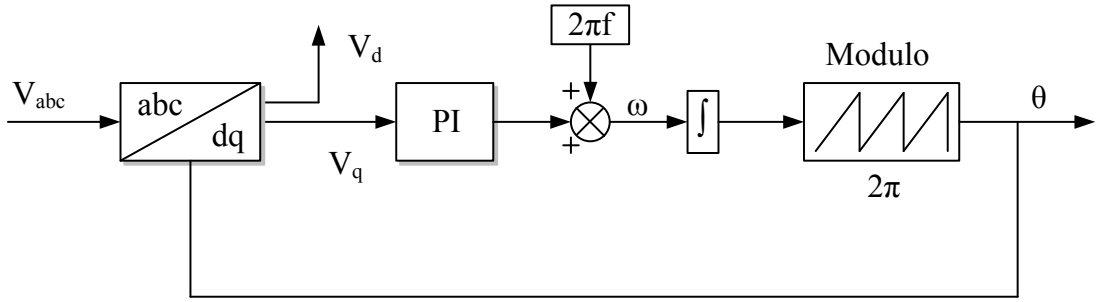

Figure 4.3: *Block diagram of PLL*

The inputs of the PLL model are the three phase voltages measured on the grid side and the output is the tracked phase angle. The PLL model is implemented in *dq* synchronous reference frame, which means that a Park transformation is needed. The phase locking of this system is realized by controlling the *q*-axis voltage to zero. Normally, a PI controller is used for this purpose. By integrating the sum between the PI output and the reference frequency the phase angle is obtained.

The transfer function of the *dq* PLL system is given by [30]:

$$H(s) = \frac{k_p \cdot s + \frac{k_p}{T_i}}{s^2 + k_p \cdot s + \frac{k_p}{T_i}} \tag{4.1}$$

As it can be observed, this equation is similar to the second order transfer function having a zero that is shown in the following expression:

$$G(s) = \frac{2\zeta\omega_n \cdot s + \omega_n^2}{s^2 + 2\zeta\omega_n \cdot s + \omega_n^2} \tag{4.2}$$

By comparing (4.1) and (4.2), the gain of the controller can be obtained. In order to calculate the parameters of the controller, a settling time T_{set} of 0.04 s and a damping factor $\zeta = \frac{1}{\sqrt{2}}$ are chosen.

The PI parameters can be calculated as:

$$k_p = 2\zeta\omega_n = \frac{9.2}{T_{set}} \tag{4.3}$$

$$T_i = \frac{T_{set}\zeta^2}{2.3} \tag{4.4}$$

Where the natural frequency, ω_n, is given by:

$$\omega_n = \frac{4.6}{\zeta T_{set}} \tag{4.5}$$

The grid phase angle obtained with the described PLL algorithm is shown in Figure 4.4.

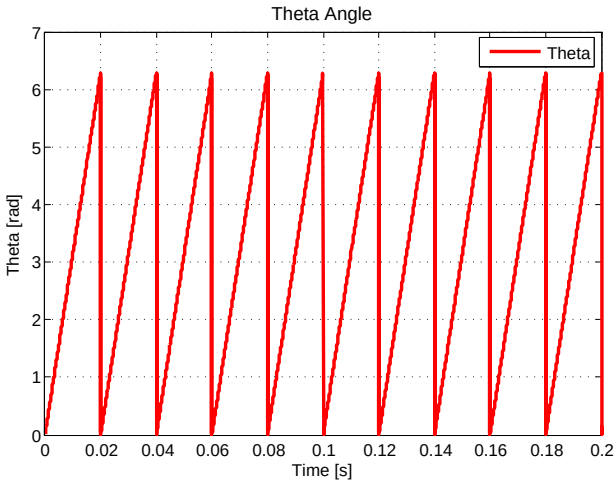

Figure 4.4: *Phase angle of the grid voltage*

4.3 Current Control Loop

The inner current controller is implemented in the *dq* synchronous reference frame [29], [31], [32]. Usually, the *dq*-control structures are associated with PI controllers due to their good behavior when regulating DC variables [32]. However, according to [31], the PI current controllers have no satisfactory tracking performances when they have to regulate coupled systems like the one described by equations (3.7) and (3.8). Therefore, in order to improve the performances of the PI current controllers in such systems, cross-coupling terms and voltage feed forward is usually used [31], [32], [33].

The structure of the inner current controller implemented in the synchronous reference frame is presented in Figure 4.5.

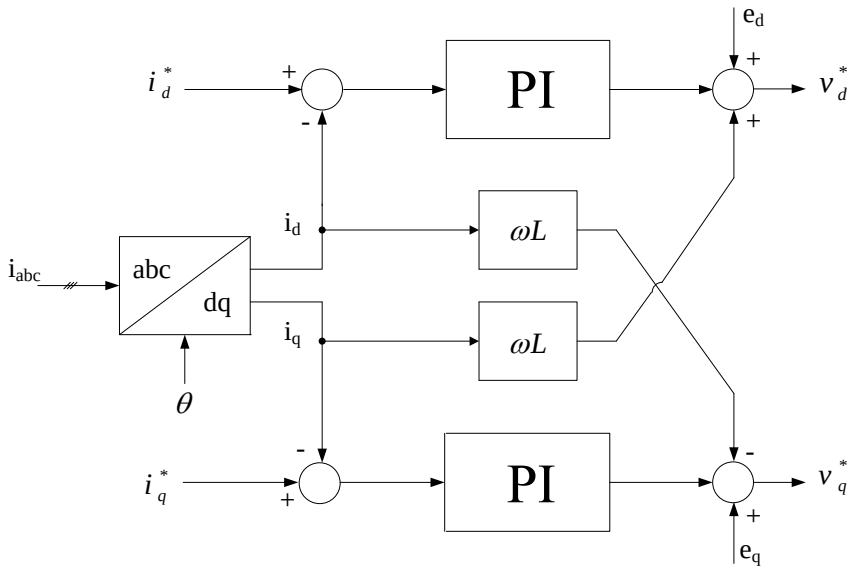

Figure 4.5: *The structure of the inner current controller implemented in synchronous reference frame*

Tuning of the Current Controller

The inner current control loops for both d and q components of the current have the same dynamics. Thus, the tuning of the current controllers is realized only for the d-axis, while the parameters of the q-axis current controller are considered the same with the one for the d-axis.

The current control diagram is presented in Figure 4.6. As it can be observed the decoupling between the d-axis and the q-axis as well as the voltage feed forward have been neglected as they were considered disturbances in the system.

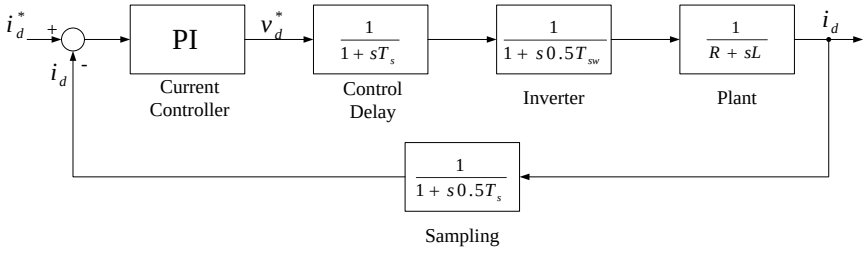

Figure 4.6: *Block diagram of the current control loop*

The blocks presented in Figure 4.6 are described below:

- the current controller block used for regulating the current is a PI controller with the transfer function given by:

$$G_{PIc} = k_{pc} + \frac{k_{ic}}{s} \tag{4.6}$$

Where, k_{pc} represents the proportional gain and k_{ic} represents the integral gain of the current controller;

- the control delay block emulates the delay introduced by the digital calculation; its transfer function is given by (4.7) and it has the form of a first order transfer function with the time constant $T_s = 1/f_s$.

$$G_{control} = \frac{1}{1 + sT_s} \tag{4.7}$$

Where, $f_s = 8$ kHz represents the sampling frequency;

- the inverter block emulates the delay introduced by the inverter; its transfer function is given by (4.8) and it has the form of a first order transfer function with the time constant $T_{PWM} = 1/f_{PWM}$.

$$G_{inverter} = \frac{1}{1 + s0.5T_{PWM}} \tag{4.8}$$

Where, $f_{PWM} = 8$ kHz represents the switching frequency;

- the plant block is a simplified transfer function of the filter which only takes into account the inductance and the parasitic resistance; the transfer function of the plant is given in equation (4.9)

$$G_{plant} = \frac{1}{R + sL} \tag{4.9}$$

Where L represents the inductance of the filter and R represents the parasitic resistance; if the parasitic resistance is neglected, equation (4.9) becomes:

$$G_{plant} = \frac{1}{sL} \tag{4.10}$$

- the sampling block emulates the delay introduced for the analog to digital conversion; its transfer function is given by (4.11) and it has the form of a first order transfer function with the time constant $0.5T_s$.

$$G_{sampling} = \frac{1}{1 + s0.5T_s} \tag{4.11}$$

In order to obtain a well tuned controller, two stages were followed up. Firstly, an analytical method was used to tune the current controller, which is the optimal modulus criterion [34]. Secondly, the SISOtool package from MATLAB/Simulink was used to adjust the obtained values of the parameters of the PI controller. So, the values obtained after applying the optimal modulus criterion are used as starting values when the discrete analysis is performed in SISOtool. Thus, a fine tuning of the current controllers is achieved.

In the followings only the final transfer function of the current controller as well as the step response and the root locus of the current loop will be presented.

The expression of the PI current controller provided by SISOtool is given by:

$$C_i(z) = 8.6719\frac{z - 1}{z^{-1}} \tag{4.12}$$

From equation (4.12), identifying the parameters of the PI current controller, the next values are obtained: proportional gain $k_{pi} = 8.6719$, integration gain $k_{ii} = 32.5977$ and integration time $T_{ii} = 0.266$ [ms].

In Figure 4.7 and Figure 4.8 the plots provided by SISOtool are presented. Figure 4.7 shows the root locus of the open loop current discrete transfer function. As it can be observed, the position of the poles and zeros of the system is inside the circle, therefore the system is stable. After analyzing this graph, the damping ratio of the system ζ_i and the natural frequency ω_{ni} can be found as:

$$\zeta_i = 0.711 \tag{4.13}$$

$$\omega_{ni} = 399[Hz] \tag{4.14}$$

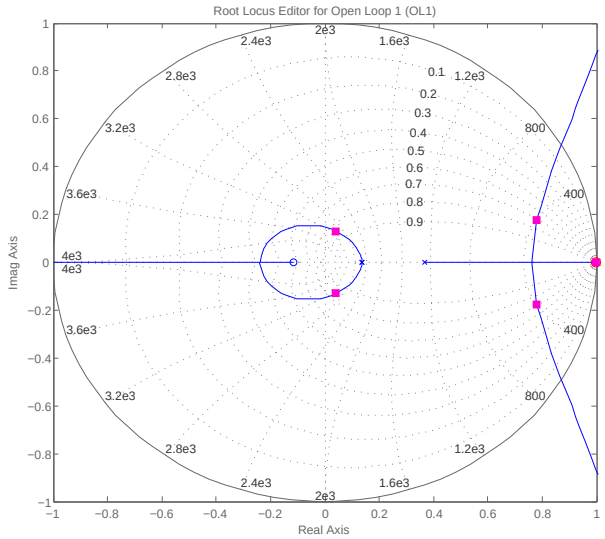

Figure 4.7: *Root locus plot of the current control loop*

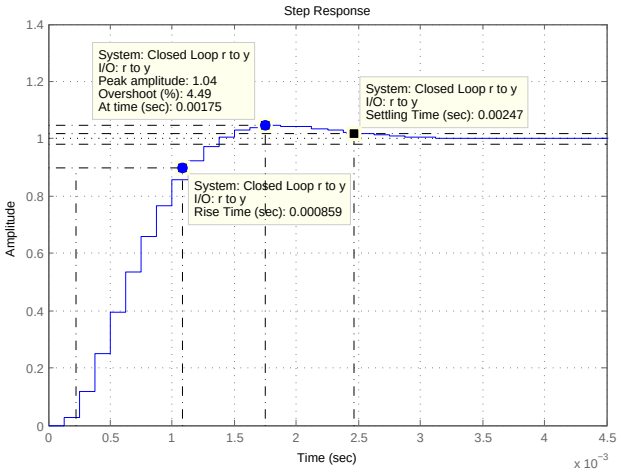

Figure 4.8: *Current step response in discrete domain*

In Figure 4.8 the current step response of the system, in discrete domain, is shown. Analyzing the above presented plot, the overshoot of the system M_{pi}, the settling time τ_{si} and the rise time τ_{ri} can be found as:

$$M_{pi} = 4.49\% \tag{4.15}$$

$$\tau_{si} = 2.47[ms] \tag{4.16}$$

$$\tau_{ri} = 0.85[ms] \tag{4.17}$$

4.4 DC Voltage Controller

The goal of the DC voltage controller is to regulate the DC-link voltage to its reference value. The DC voltage controller is used only on the onshore side of the HVDC transmission and it provides at its output the reference value of the reactive current.

The block diagram of the DC voltage controller is shown in Figure 4.9.

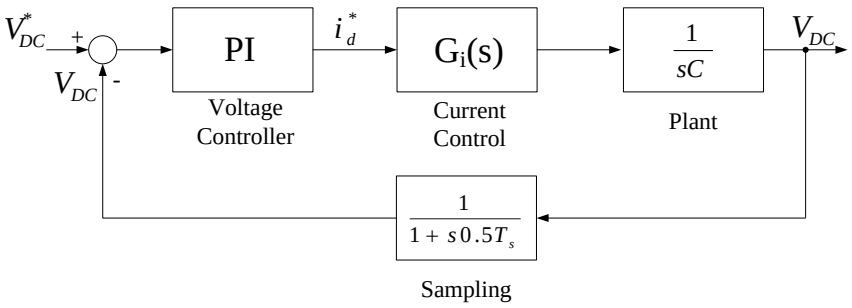

Figure 4.9: *Block diagram of the DC voltage control loop*

Tuning of DC Voltage Controller

As for the case of the inner current controller, for the tuning of the DC voltage controller the same algorithm was used. Firstly an analytical method was used to tune the DC voltage controller, which is the symmetrical optimum criterion [34], [35]. Once the starting values of the controller's parameters have been obtained using the mentioned method, the SISOtool package was used to improve these obtained values, in order to achieve the imposed design requirements.

The expression of the PI DC voltage controller provided by SISOtool is given by:

$$C_{V_{DC}}(z) = 0.15118\frac{z - 0.997}{z^{-1}} \tag{4.18}$$

From equation (4.18), identifying the parameters of the PI DC voltage controller, the next values are obtained: proportional gain $k_{pvdc} = 0.15118$, integration gain $k_{ivdc} = 3.1895$ and integration time $T_{ivdc} = 0.0474$ [s].

In Figure 4.10 and Figure 4.11 the plots provided by SISOtool are presented. Figure 4.10 shows the root locus of the open loop DC voltage discrete transfer function. As it can be observed, the position of the poles and zeros of the system is inside the circle, therefore the system is stable. After analyzing this graph, the damping ratio of the system ζ_{vdc} and the natural frequency ω_{nvdc} can be found as:

$$\zeta_{vdc} = 0.720 \tag{4.19}$$

$$\omega_{nvdc} = 228[Hz] \tag{4.20}$$

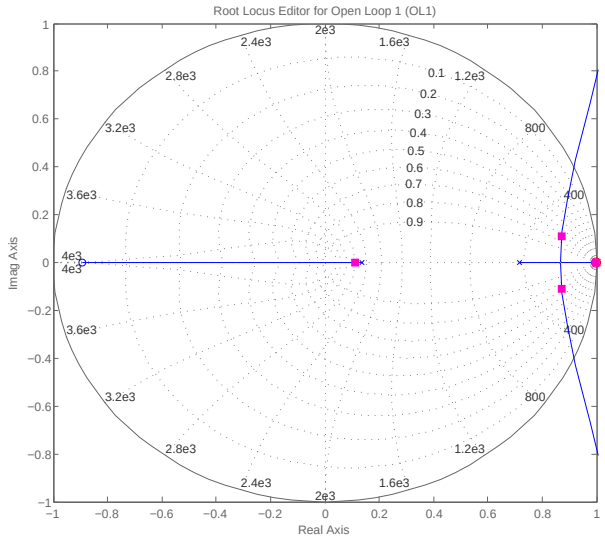

Figure 4.10: *Root locus plot of the DC voltage control loop*

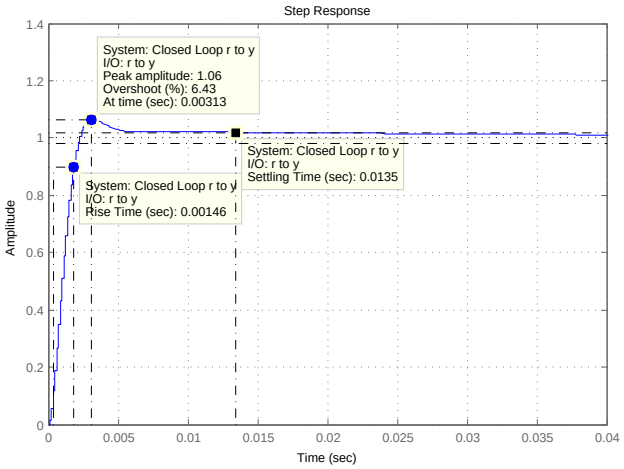

Figure 4.11: *DC voltage step response in discrete domain*

In Figure 4.11 the DC voltage step response of the system, in discrete domain, is shown. Analyzing the above presented plot, the overshoot of the system M_{pvdc}, the settling time τ_{svdc} and the rise time τ_{rvdc} can be found:

$$M_{pvdc} = 6.43\% \tag{4.21}$$

$$\tau_{svdc} = 13.5[ms] \tag{4.22}$$

$$\tau_{rvdc} = 1.46[ms] \tag{4.23}$$

One of the requirements which must be fulfilled when tuning the outer controllers is that in order to ensure stability, the outer controller (in this case, the DC voltage controller) must be slower than the inner controller (in this case, the current controller) [29]. By comparing the relations (4.16) and (4.22), it can be observed that this requirement is fulfilled.

4.5 Active Power Control Loop

For simplicity, the active power controller can be modeled as a simple P (proportional) controller. The reference of the active current is obtained using the equations of the instantaneous active power and reactive power [8], given by:

$$P = u_d i_d + u_q i_q \tag{4.24}$$

$$Q = u_q i_d - u_d i_q \tag{4.25}$$

Starting from these equations and decoupling the active and reactive currents, the reference of the active current is obtained:

$$i_d^* = \frac{P^* u_d - Q^* u_q}{u_d^2 + u_q^2} \tag{4.26}$$

Where P^* is the reference value of the active power and Q^* is the reference value of the reactive power.

If a more accurate control of active power is requested, a PI controller can be used [8], [36]. For this approach the block diagram of the active power controller is presented in Figure 4.12.

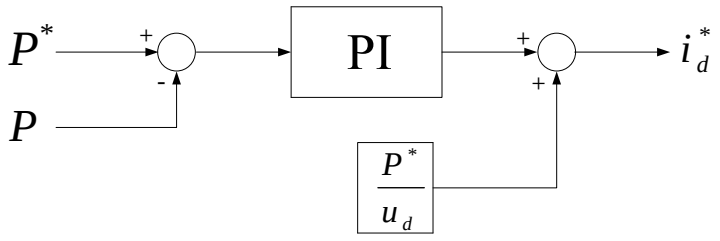

Figure 4.12: *Active power controller with PI (based on [8])*

4.6 Reactive Power Control Loop

The implemented reactive power controller is similar to the active power controller that was previously presented.

In this case, the reference value of the reactive current is also obtained starting from equations (4.24) and (4.25), yielding:

$$i_q^* = \frac{P^* u_q + Q^* u_d}{u_d^2 + u_q^2} \tag{4.27}$$

If a more accurate control of reactive power is desired, the structure presented in Figure 4.13 should be implemented [8].

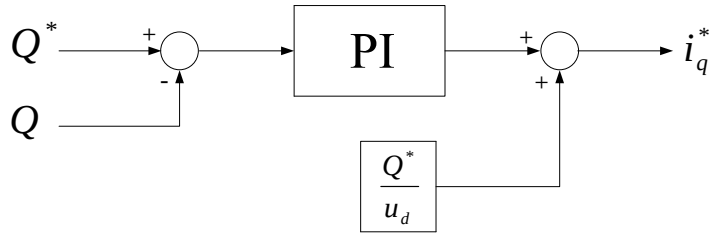

Figure 4.13: *Reactive power controller with PI (based on [8])*

4.7 AC Voltage Controller

In the VSC-based HVDC transmission systems, another variable which can be subject to control is the AC voltage. In the literature to main strategies to control the AC voltage are described. In the first strategy, the AC voltage control is realized by controlling the voltage drop over the phase reactor of the VSC, as described in [8] and [29].

The second strategy which can be used in order to control the AC voltage is described in detail in [25], [37]. and [38]. In this strategy, the AC voltage control is realized by controlling the voltage droop over the filter's capacitor C_f.

In this project, the control of the AC voltage will be implemented using the second presented strategy. Like in the case of the inner current control loop (see Section 4.3), the AC voltage control is developed in the *dq* synchronous reference frame.

As explained in [25] and [37], the control of e_d and e_q is not a straightforward task. The control scheme presented in Figure 4.14 will be implemented in order to regulate e_d and e_q.

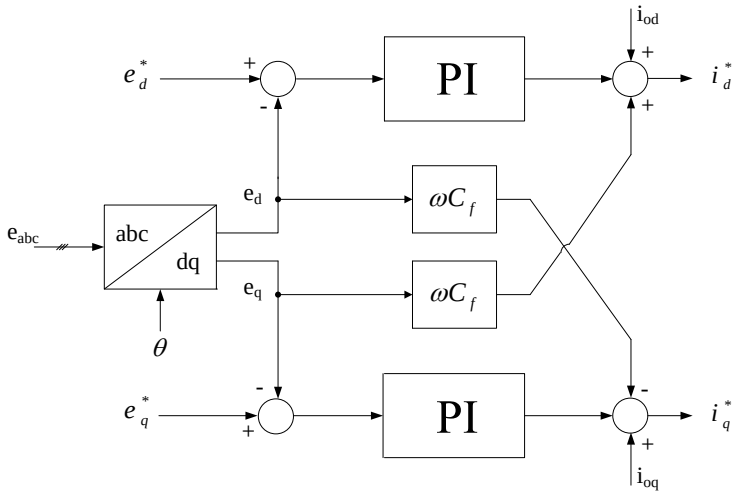

Figure 4.14: *The structure of the AC voltage controller implemented in synchronous reference frame*

Figure 4.14 illustrates that the coupling between e_d and e_q (see equations (3.13) and (3.14)) is eliminated by means of a decoupling feed-forward compensation. This feed-forward compensation mechanism is identical with the one used to decouple the i_d and i_q currents presented in Figure 4.5. Moreover, the control structure presented in Figure 4.14 makes possible to independently control e_d and e_q by i_d^* and i_q^* respectively [25] and [37].

The outer AC voltage control loops for both d and q components of the voltage have the same dynamics. Therefore, the tuning of the AC voltage controllers is realized only for the d-axis while, the parameters of the q-axis voltage controller are considered the same with the ones for the d-axis.

The AC voltage control diagram is presented in Figure 4.15.

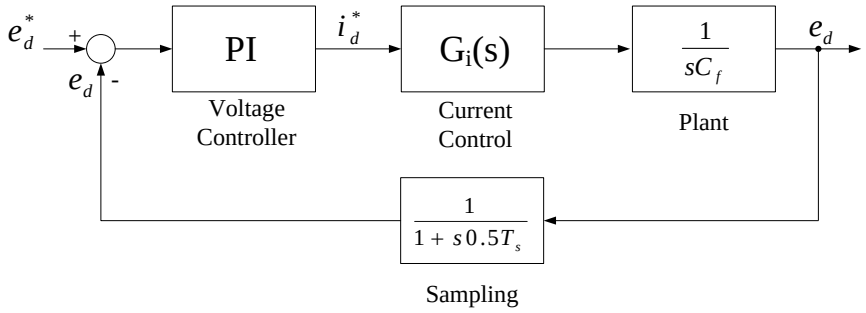

Figure 4.15: *Block diagram of the AC voltage control loop*

Tuning of AC Voltage Controller

For the tuning of the PI AC voltage controller, the same algorithm which was used for the tuning of the DC voltage controller was followed. After complying all the previously presented steps (see Section 4.4), the expression of the PI AC voltage controller provided by SISOtool was found and is given by:

$$C_{V_{AC}}(z) = 0.15475\frac{z - 0.994}{z^{-1}} \tag{4.28}$$

From equation (4.28), identifying the parameters of the PI current controller, the next values are obtained: proportional gain $k_{pvac} = 0.15475$, integration gain $k_{ivac} = 8.018$ and integration time $T_{ivac} = 0.0193$ [s].

In Figure 4.16 and Figure 4.17 the plots provided by SISOtool are presented. Figure 4.16 shows the root locus of the open loop AC voltage discrete transfer function. As it can be observed, the position of the poles and zeros of the system is inside the circle, therefore the system is stable. After analyzing this graph, the damping ratio of the system ζ_{vac} and the natural frequency ω_{nvac} can be found as:

$$\zeta_{vac} = 0.712 \tag{4.29}$$

$$\omega_{nvac} = 226[Hz] \tag{4.30}$$

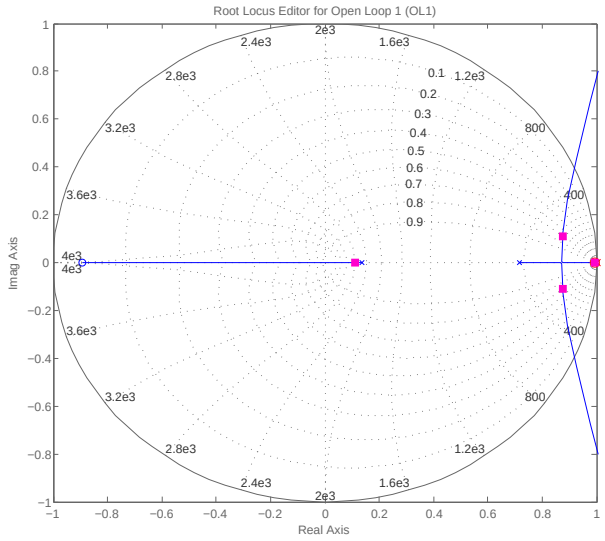

Figure 4.16: *Root locus plot of the AC voltage control*

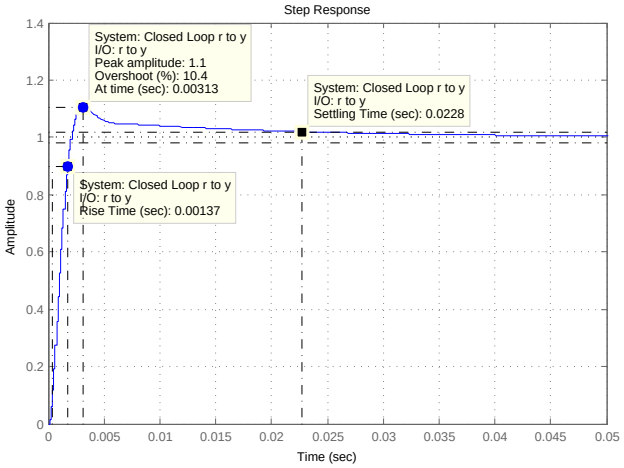

Figure 4.17: *AC voltage step response in discrete domain*

In Figure 4.17 the AC voltage step response of the system, in discrete domain, is shown. Analyzing the above presented plot, the overshoot of the system M_{pvac}, the settling time τ_{svac} and the rise time τ_{rvac} can be found as:

$$M_{pvac} = 10.4\% \tag{4.31}$$

$$\tau_{svac} = 22.8[ms] \tag{4.32}$$

$$\tau_{rvac} = 1.37[ms] \tag{4.33}$$

4.8 Summary

In this chapter the overall control structure of a VSC-based HVDC transmission system was presented.

In the first part of the chapter a brief overview of the control strategies applicable for such a system was realized. In the following, the inner current control loop was discussed and the tuning procedure for current controller was presented. Also, all the outer control loops that can be used in controlling the VSC-based HVDC transmission were discussed and the tuning of the controllers was realized.

For the inner current control loop and for the outer DC and AC voltage control loops, PI regulators have been used. The tuning was realized using analytical methods and computational methods (SISOtool package provided by MATLAB/Simulink).

For controlling the active and reactive power, simple P (proportional) controllers have been used.

The grid synchronization was realized by means of a PLL.

The controllers that were designed throughout this chapter will be tested in the following chapter, where the dynamic and steady state behavior of the VSC-based HVDC transmission system will be analyzed in detail.

Chapter 5

Simulation and Analysis

In this chapter the behavior of the VSC-based HVDC transmission system will be analyzed. Thus, in order to test the controllers which were developed in the previous chapter and to test the behavior of the system in different conditions, several study cases will be carried out throughout this chapter.

5.1 Introduction

In the previous chapter, all the controllers that can be implemented in a VSC-based HVDC transmission system have been discussed and analyzed. In the followings, two controls strategies which will be implemented and simulated in MATLAB/Simulink will be presented.

As it was stated in Chapter 4, the implementation of the outer controllers will depend on the application and requirements, respectively.

In this project, two different control strategies will be implemented in order to analyze the performances and the behavior of the VSC-based HVDC transmission system. These two strategies are presented below:

Strategy 1

- the offshore converter controls the active power and the reactive power;
- the onshore converter controls the DC voltage and the reactive power;

Strategy 2

- the offshore converter controls the AC voltage;
- the onshore converter controls the DC voltage and the reactive power.

The control structures of the offshore converter when Strategy 1 or Strategy 2 is implemented are illustrated in Figure 5.1 and Figure 5.2 respectively.

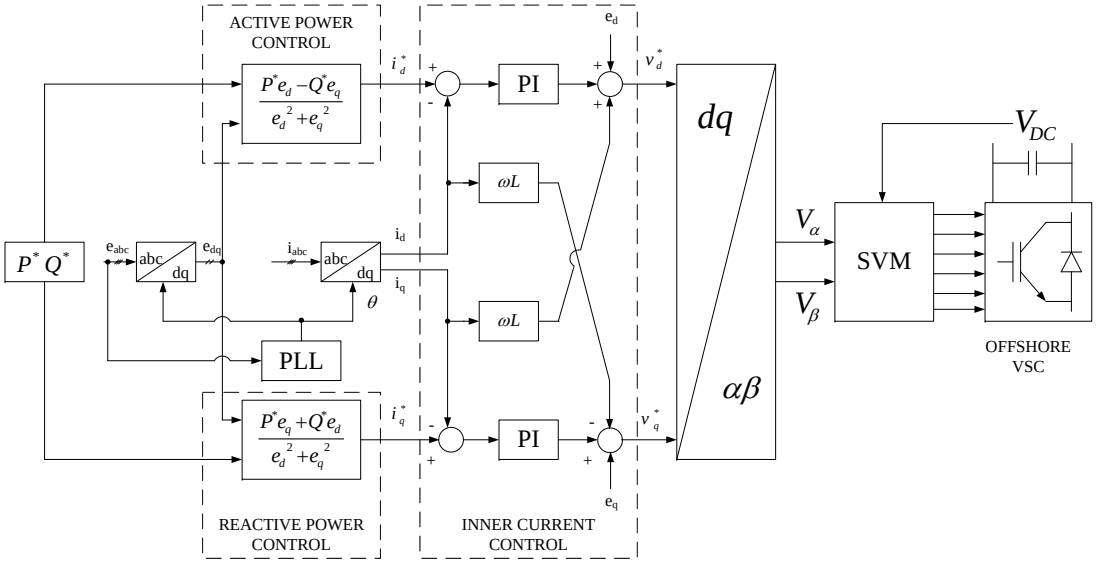

Figure 5.1: *Control structure of the offshore converter - Strategy 1*

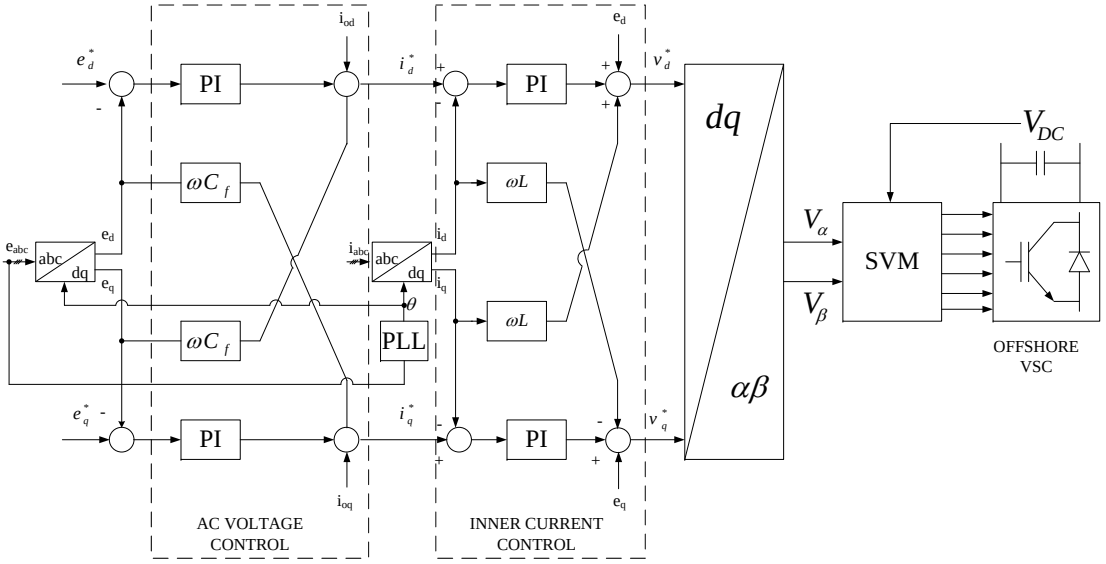

Figure 5.2: *Control structure of the offshore converter - Strategy 2*

The control structure of the onshore converter which is similar for both strategies is illustrated in Figure 5.3.

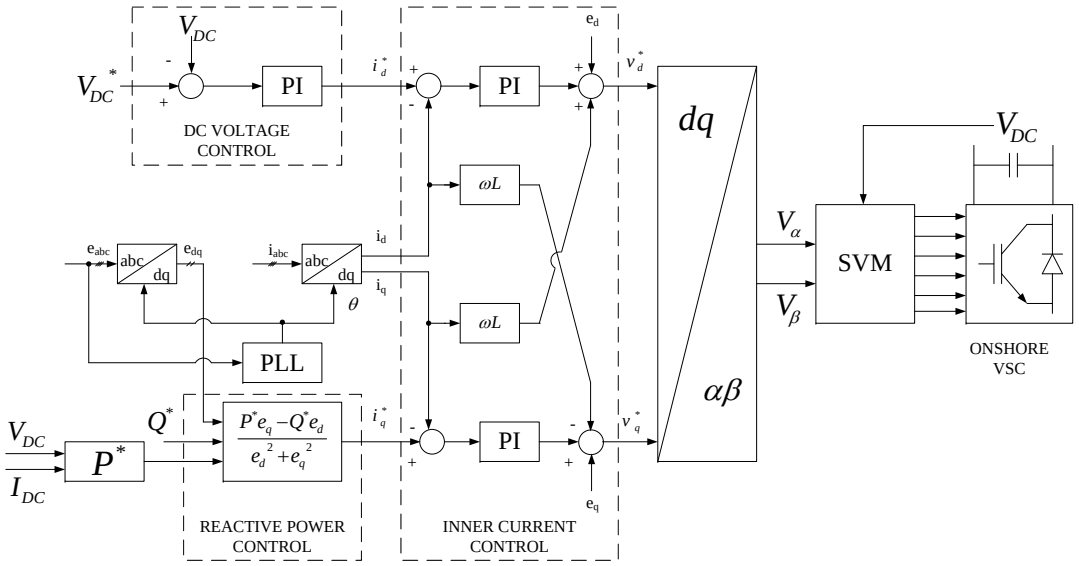

Figure 5.3: *Control structure of the onshore converter*

In order to analyze the designed control system, previously presented, the VSC-based HVDC system shown in Figure 5.4 is simulated using MATLAB/Simulink.

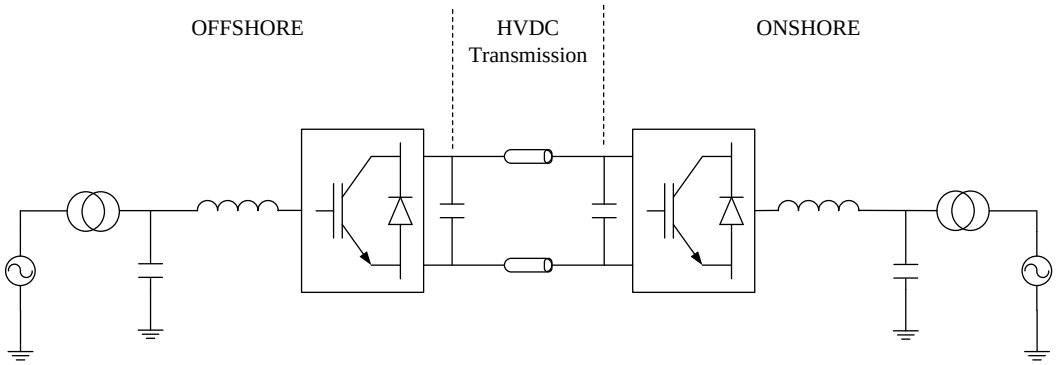

Figure 5.4: *VSC-based HVDC transmission system*

5.2 VSC-based HVDC power transmission between two terminals operating at 50 Hz - Strategy 1

The first study case aims to investigate the steady-state behavior of the VSC-based HVDC transmission system. As discussed in the previous chapter, the outer controllers which are implemented depend on the application. Thus, in this study case the following control loops are considered:

- the offshore converter (which emulates the WPP) controls the active power and the reactive power;

- the onshore converter (which emulates the AC grid) controls the DC voltage and the reactive power.

Before starting the analysis of the behavior of the developed VSC-based HVDC transmission system (plant and control) a convention of signs should be imposed. Therefore, in all the upcoming results, for both the onshore and offshore terminals the sign "-" indicates that the respective terminal is sending power, while the sign "+" indicates that the respective terminal is receiving power.

In order to analyze the behavior of the developed system, changes in the active and reactive power flow are produced at the offshore terminal and a change of the reference value of the DC voltage is also considered:

- At $t = 1$ s, a 0.3 p.u. step is applied to the reference active power (increase from -0.2 p.u. to -0.5 p.u.) at the offshore terminal;
- At $t = 1.5$ s, a 0.3 p.u. step is applied to the reference reactive power (increase from 0 to -0.3 p.u.) at the offshore terminal;
- At $t = 2$ s, a 0.05 p.u. step is applied to the reference DC voltage (decrease from 1 p.u. to 0.95 p.u.) at the onshore terminal.

The reference values of the active power, reactive power and DC voltage are shown in Figure 5.5.

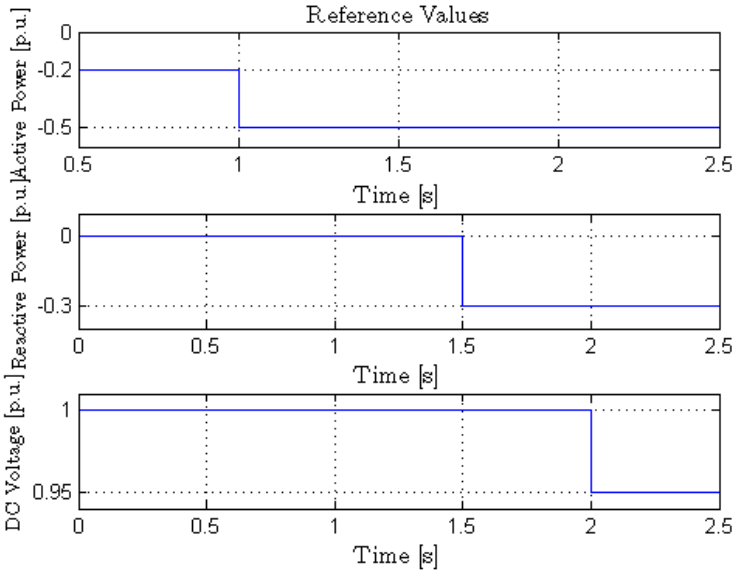

Figure 5.5: *Reference values*

The active power reference which is imposed at the offshore terminal as well as the measured active power on both onshore and offshore terminals is shown in Figure 5.6.

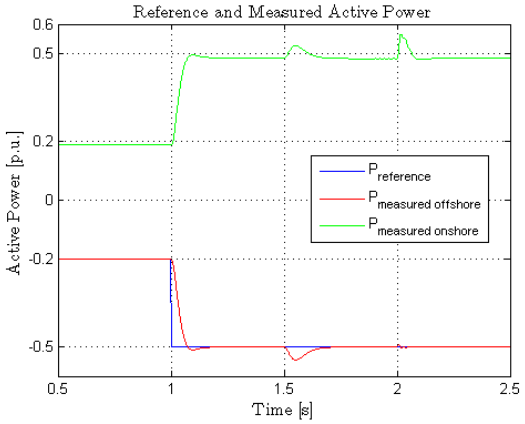

Figure 5.6: *Reference and measured active power*

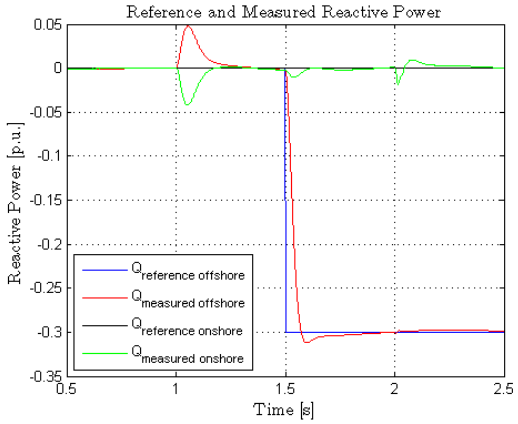

Figure 5.7: *Reference and measured reactive power*

At the instant $t = 1$ s the value of the active power flow is changed at the offshore terminal from -0.2 p.u. to -0.5 p.u. As it can be observed, the measured active power follows its reference, stabilizing fast after the transient, while the overshoot is less than 1%. At the instant $t = 1.5$ s, when a change in the reactive power takes place, a 10% overshoot in the measured active power may be observed. This overshoot is due to the cross-coupling between the active current and the reactive current.

Furthermore as it can be observed from Figure 5.6, the waveforms of the measured active power at both sides are nearly identical; the amount of power which is delivered by the offshore terminal (WPP) is the same with the amount of active power which is received by the onshore terminal (AC grid), while the difference of signs is coming from the fact that one terminal is considered sending terminal and the other one is considered receiving terminal.

The reference reactive powers and the measured reactive powers at both terminals are presented in Figure 5.7. At the offshore side, a negative step in the reactive power is considered at $t = 1.5$ s, while on the onshore side the reference reactive power is kept constant at zero. As it can be observed, the measured offshore reactive power tracks with accuracy its reference, stabilizing fast after the transient and having an acceptable overshoot value. At the same instant of $t = 1.5$ s, the onshore reactive power remains unchanged due to the fact that no reactive power exchanged is realized in case of HVDC transmission. From these presented facts it can be concluded that the onshore and the offshore VSCs are controlling their reactive power independently.

Due to the fact that the power control is connected to the inner current control, the effect of the cross-coupling between the active current and reactive current can be easily observed in both Figure 5.6 and Figure 5.7. Thus, each change in the value of the active current will be sense by the reactive current and vice-versa and consequently each change in the active power flow will be sense by the reactive power and vice-versa.

Therefore, the transient in the measured reactive powers which may be observed at the time instant of 1 s is caused by the boost in the active power flow, while the transient in the measured active powers which may be observed at the time instant of 1.5 s is caused by the change of the reactive power reference value.

One of the purposes of the onshore VSC terminal is to keep the DC voltage constant whatever changes in the active power occur. Figure 5.9 shows the reference and measured

DC voltages on the onshore side.

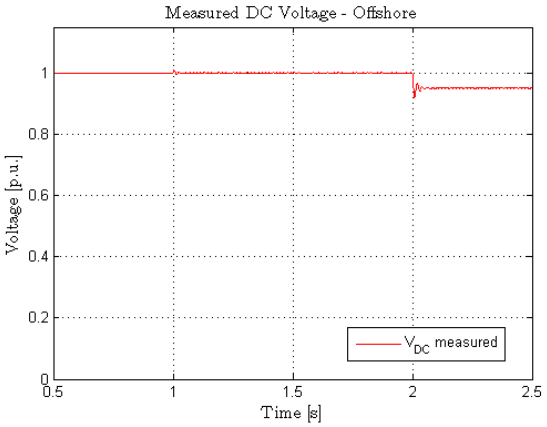

Figure 5.8: *Measured DC voltage - offshore terminal*

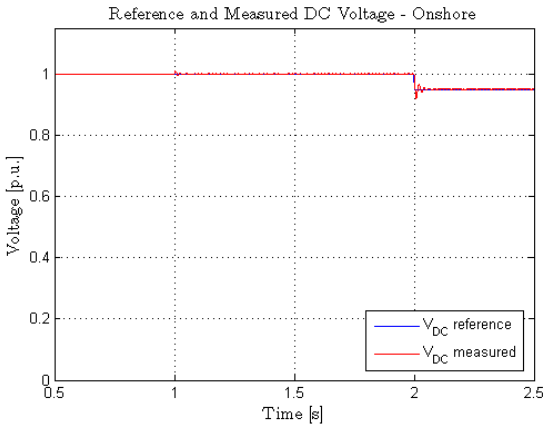

Figure 5.9: *Reference and measured DC voltage - onshore terminal*

As it can be observed from this plot, the measured DC voltage tracks accurately its reference. It can be noticed, at the time instant of 1 s, a transient occurs on the DC voltage which is due to the increase active power from -0.2 p.u. to -0.5 p.u., but the DC voltage stabilizes fast at its operating point. The second transient which can be observed (at time, $t = 1.5$ s) is due to the increase of the onshore reactive power. This transient is smaller than the previous one and the operating point is again fast reached. At $t = 2$ s, the value of the DC voltage reference is decreased from 1 p.u. to 0.95 p.u. and the measured DC voltage tracks fast the new imposed value.

In order to improve the performance of the outer DC voltage controller two methods were tested: decreasing of the control response and adding a reference pre-filter. The first method offered good results with a simple implementation and it was finally used.

The d and q components of the measured offshore and onshore currents are plotted in Figure 5.10 and Figure 5.11, respectively. From these plots it can be noticed that the measured signals are tracking well the reference signals; the overshoot caused by the transients have an acceptable value, while the measured signals are settling fast after the transient ends.

Due to the fact that i_d determines the active power, it can be observed that its reference is changing proportionally with the reference of the active power (see Figure 5.5). On the other hand, because i_q is directly related with the reactive power, its reference is changing according to the changes in the reactive power flow.

Moreover, because the d and q components of the current are cross-coupled (see equations (3.8) and (3.7)), each change in the waveform of a component will cause a small transient in the waveform of other component.

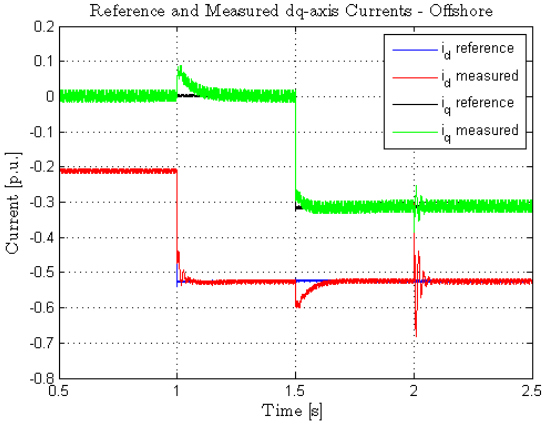

Figure 5.10: *Reference and measured dq-axis currents - offshore terminal*

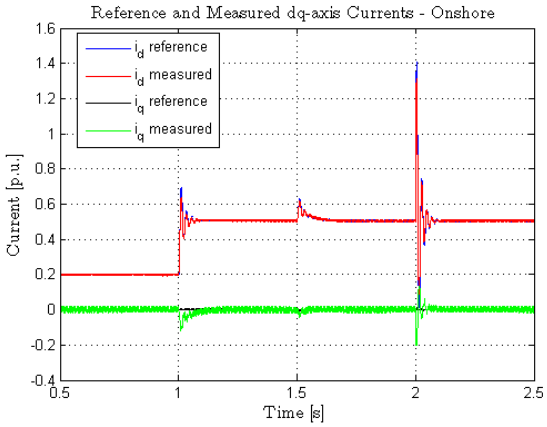

Figure 5.11: *Reference and measured dq-axis currents - onshore terminal*

The three-phase currents measured at the output of the offshore side VSC and at the output of the onshore side VSC are presented in Figure 5.12 and Figure 5.13 respectively.

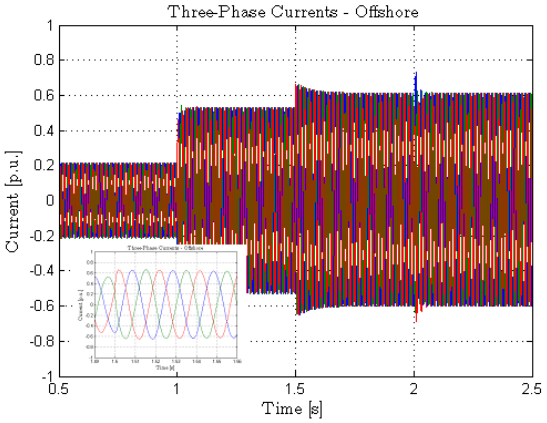

Figure 5.12: *Measured three phase currents - offshore terminal*

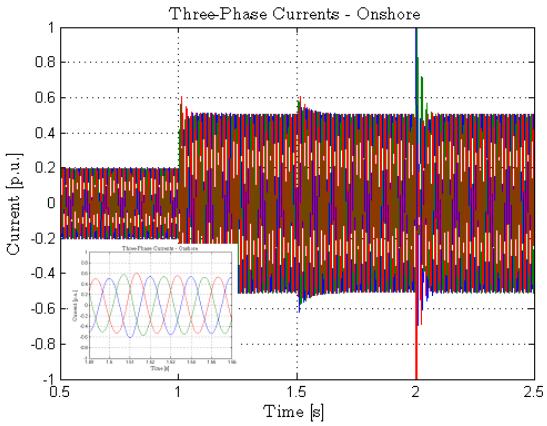

Figure 5.13: *Measured three phase currents - onshore terminal*

The operational principles of VSC-based HVDC transmission system were studied in this test case. The results presented throughout this section had shown a good behavior of the developed VSC-based HVDC transmission system. The active power flow between the offshore terminal and the onshore terminal was successfully achieved. Moreover, through this study case the independent control of reactive power at each terminal was verified. The DC voltage controller had shown a good behavior, regulating the DC-link voltage to its reference value, whatever changes in the active power flow were considered.

5.3 VSC-based HVDC power transmission between two terminals operating at 50 Hz and 60 Hz - Strategy 1

The second study case investigates the connection of the offshore WPP, which is delivering power at 60 Hz through a VSC-based HVDC transmission system to a 50 Hz AC network.

The simulated system (plant and control) is nearly identical with the one used in previously treated study case.

The first difference is coming from the frequency value of the offshore grid voltage, which in this case is set at 60 Hz. The second change is made in PLL block, which was modified in order to successfully synchronize the VSC-HVDC system to the 60 Hz working WPP.

In order to analyze the behavior of the modeled VSC-based HVDC system when the transmission of power is realized between a 60 Hz terminal and a 50 Hz terminal, the test conditions presented in Figure 5.5 are considered.

The use of the same test conditions as in the previous study case makes possible the comparison of the results obtained in these two test cases (i.e. power transmission between two terminals working at 50 Hz and power transmission between two terminal working at different frequencies).

The results will be presented in parallel, for the offshore and onshore terminals.

In Figure 5.14 and Figure 5.15 the phase voltages at the two terminals are presented and as it can be observed their frequency is different.

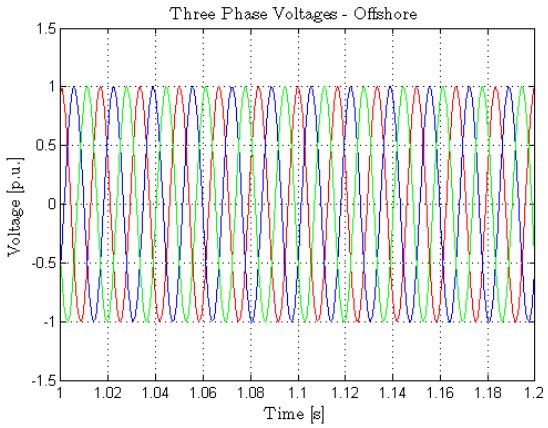

Figure 5.14: *Measured three phase voltages at the offshore terminal (60Hz)*

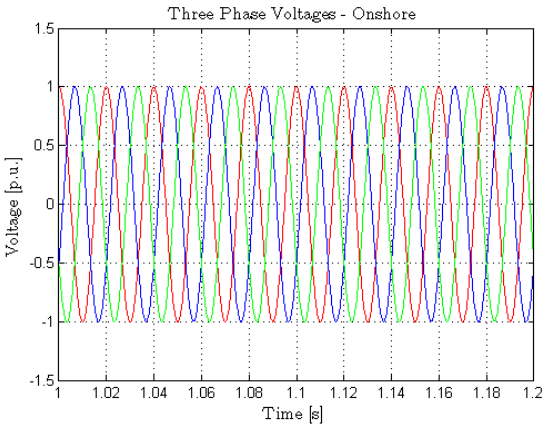

Figure 5.15: *Measured three phase voltages at the onshore terminal (50Hz)*

In the following, the same plots as the ones presented in the first study case will be shown and the same comments are also valid for this study case.

Figure 5.16 and Figure 5.17 present the reference and measured active and reactive powers at the offshore and onshore terminal respectively.

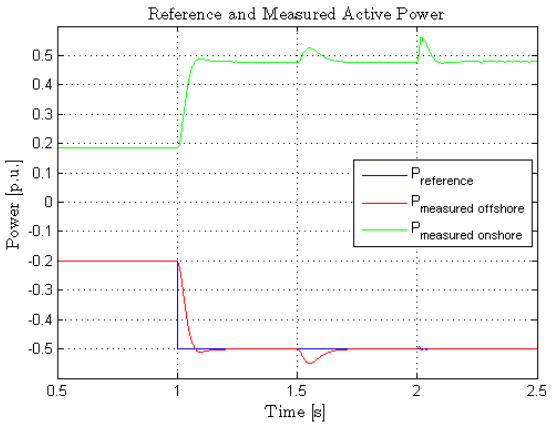

Figure 5.16: *Reference and measured active power*

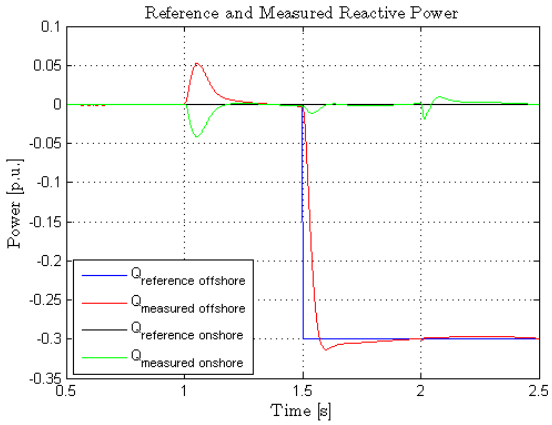

Figure 5.17: *Reference and measured reactive power*

The reference DC voltage and the measured DC voltage at the onshore terminal are presented in Figure 5.19 while, the measured DC voltage at the offshore terminal, which is not subject to control, is shown in Figure 5.18.

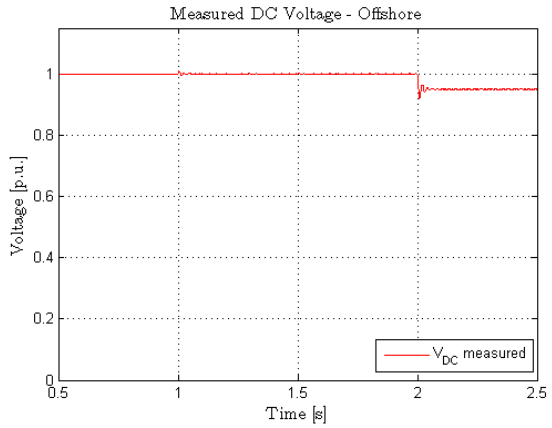

Figure 5.18: *Measured DC voltage - offshore terminal*

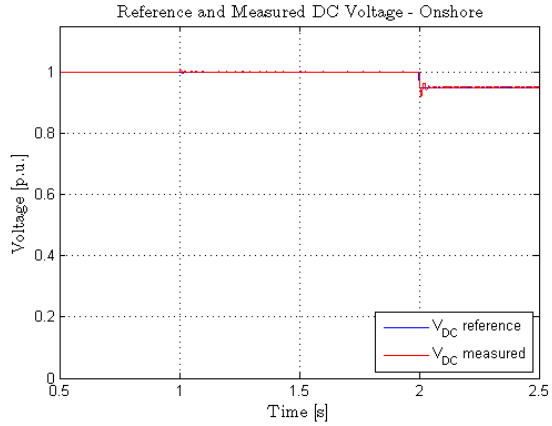

Figure 5.19: *Reference and measured DC voltage - onshore terminal*

The i_d and i_q currents which are controlled in the inner control loop are shown in Figure 5.20 and Figure 5.21.

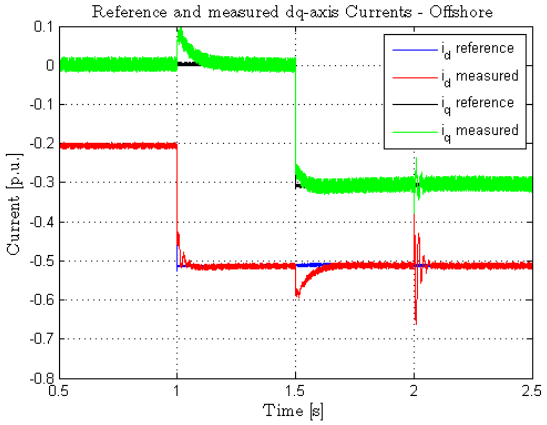

Figure 5.20: *Reference and measured dq-axis currents - offshore terminal*

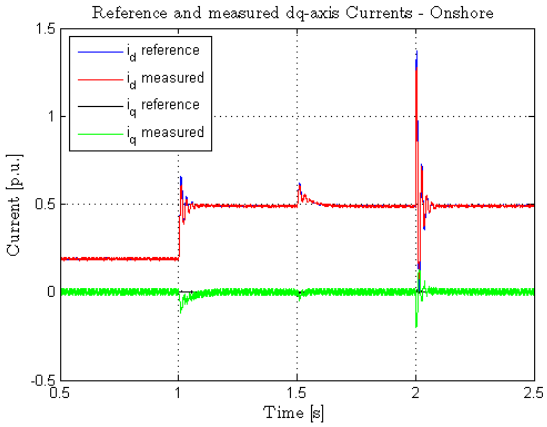

Figure 5.21: *Reference and measured dq-axis currents - onshore terminal*

The three-phase currents measured at the offshore and onshore terminal respectively are plotted in Figure 5.22 and Figure 5.23 respectively. As in the case of the phase voltages presented in Figure 5.14 and Figure 5.15 respectively, the three-phase currents measured at the offshore terminal have a 60 Hz frequency while the three-phase currents measured at the onshore terminal have a 50 Hz frequency.

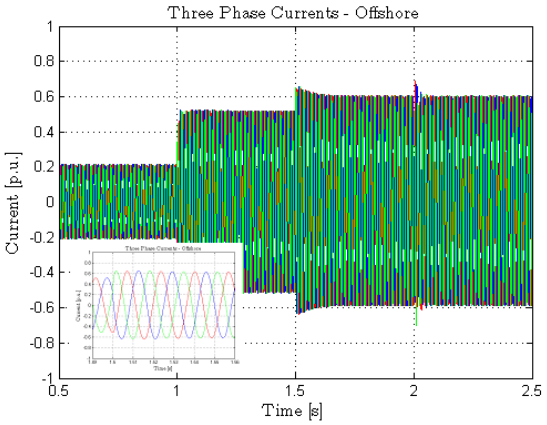

Figure 5.22: *Measured three phase currents - offshore terminal*

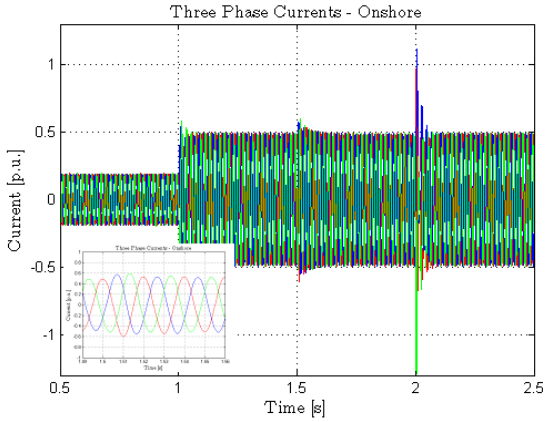

Figure 5.23: *Measured three phase currents - onshore terminal*

By comparing the plots of the parameters which are measured offshore, when working at 60 Hz, with the plots of the same parameters measured offshore, when working at 50 Hz (see Section 5.2), no difference in the dynamics of the systems can be observed. Therefore, if the synchronization with the grid is well realized no differences in sending power between areas working at different frequencies shall occur.

5.4 VSC-based HVDC power transmission between two terminals operating at 50 Hz - Strategy 2

This study case aims to investigate the behavior of the VSC-based HVDC transmission system when control Strategy 2 is used.

In order to simulate a situation close to the real applications (when the WPP acts like a current source), a third VSC is added in the configuration. This VSC emulates the grid-side converter from the back-to-back converter system of each wind turbine. The control of this new considered VSC is identical with the one considered for the onshore VSC (DC voltage and reactive power controllers, plus inner current controller).

For this study case the test condition is the following: through the DC-link of the third converter the power produced by the WPP is injected into the VSC-HVDC system.

At the offshore VSC terminal, the AC voltage control is achieved by applying the desired reference voltage along the d-axis (in the simulated test case, 325 V), while setting the q-axis voltage at 0 [28]. At the onshore VSC terminal, the DC voltage should be kept constant at its reference value (650 V) independently from the changes in the active power flow. Moreover, the onshore VSC ensures reactive power assistance by consuming or injecting reactive power from or to the AC grid respectively.

In order to analyze the behavior of the system when Strategy 2 is used, at the input of the grid-side converter from the back-to-back converter system of the turbine, a change in the power flow is considered - Figure 5.24.

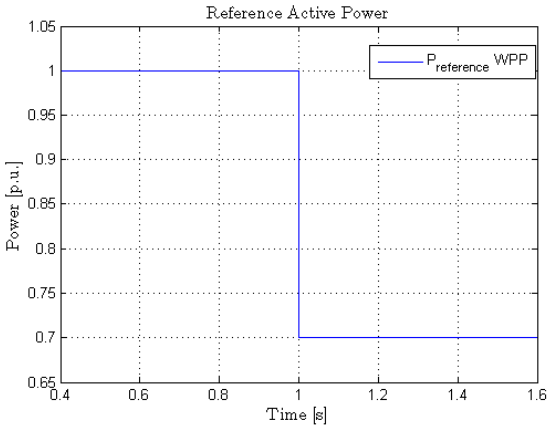

Figure 5.24: *Reference active power from WPP*

In Figure 5.25, the measured active power at both terminals and the power delivered by the WPP are plotted. As it can be observed, the value of the measured active power at the onshore terminal is equal with the value of the reference power given by the WPP. This is due to the fact that in the simulated VSC-HVDC system no losses have been considered.

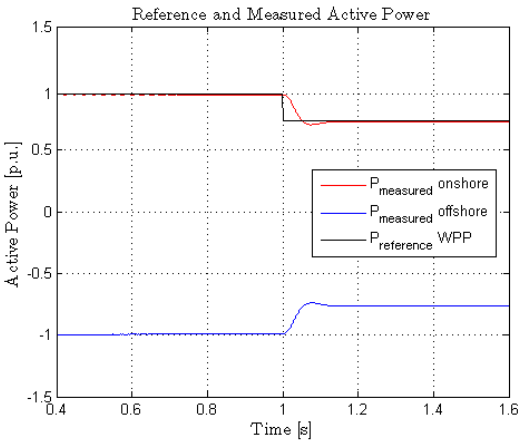

Figure 5.25: *Reference and measured active power*

In Figure 5.26 and Figure 5.27 the measured DC voltages at both terminals are shown.

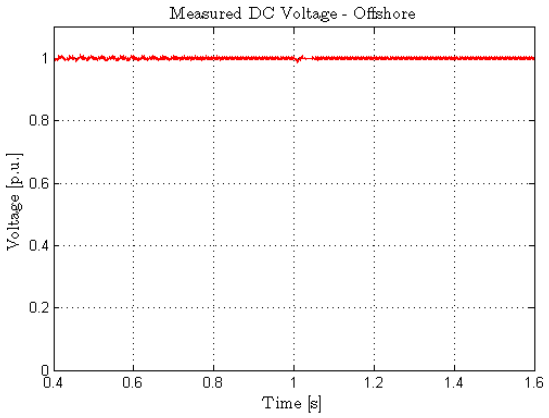

Figure 5.26: *Measured DC voltage - offshore terminal*

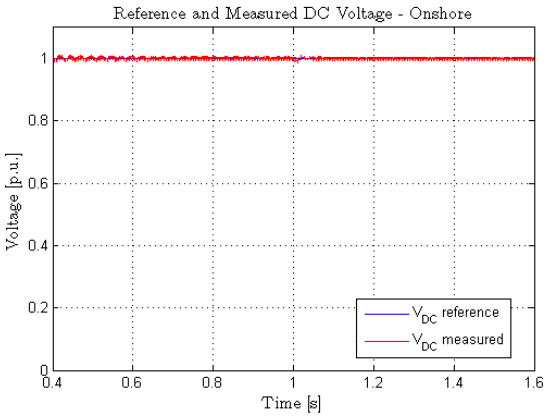

Figure 5.27: *Reference and measured DC voltage - onshore terminal*

As it is illustrated in Figure 5.27 the DC voltage controller behaves well, tracking the reference with accuracy, whatever changes in the active power flow are considered.

The reference and measured dq-axis voltages at the offshore terminal, which are subject to control, are shown in Figure 5.28. At the time instant $t = 1$ s, when a negative step change in the value of the transmitted active power is considered, a transient in the measured e_d and e_q can be observed. However, these signals are stabilizing fast once the transient in the active power is finished.

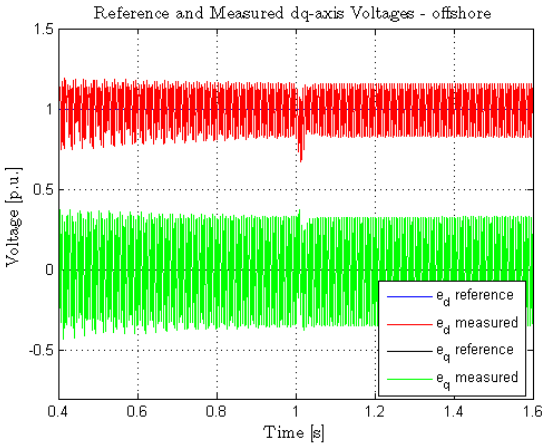

Figure 5.28: *Reference and measured dq-axis voltages -PCC offshore*

In Figure 5.29 and Figure 5.30 the three-phase currents measured at both terminals are plotted. Analyzing Figure 5.29, Figure 5.30 and Figure 5.24 it can be observed that the phase currents are proportional with the active power.

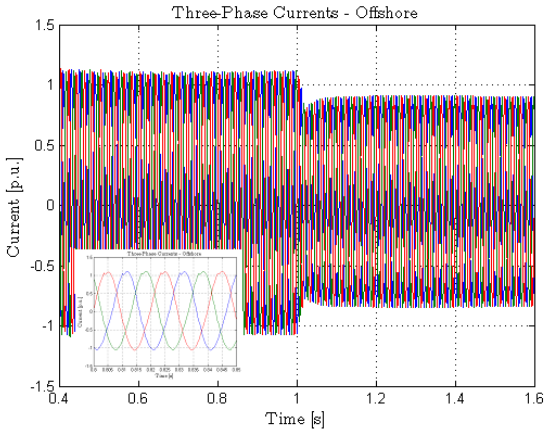

Figure 5.29: *Measured three phase currents - offshore terminal*

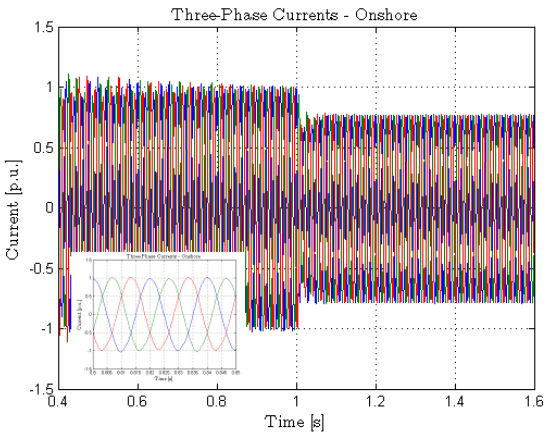

Figure 5.30: *Measured three phase currents - onshore terminal*

Figure 5.31 and Figure 5.32 are showing the phase voltages measured at the PCC of each terminal respectively.

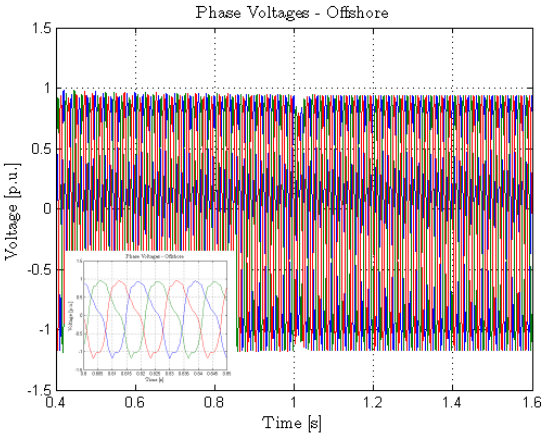

Figure 5.31: *Measured three phase voltages - offshore terminal*

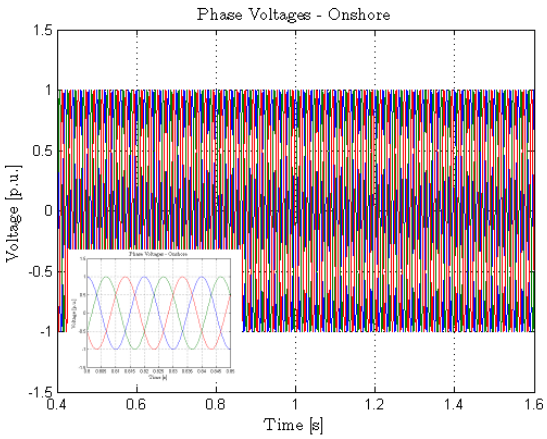

Figure 5.32: *Measured three phase voltages - onshore terminal*

The results obtained in this study case are showing a good behavior of the VSC-based HVDC transmission system. The results obtained throughout this test case are close to the results obtained when Strategy 1 (see Section 5.2) was used to control the HVDC system. Therefore, the control Strategy 1 can be seen as a good alternative to the control Strategy 2 which is more close to the control strategies used in the real wind power applications.

5.5 Summary

The behavior of the VSC-based HVDC transmission system was analyzed in this chapter by means of simulations. For this analysis the two control strategies that have been introduced at the beginning of the chapter were considered.

In the first part of the chapter (see Section 5.2 and Section 5.3), the behavior of the system was analyzed for the case when Strategy 1 (offshore VSC is controlling the active and reactive power, while the onshore VSC is controlling the DC voltage and the reactive power) was implemented.

In the second part of the chapter (see Section 5.4), the behavior of the system was analyzed for the case when Strategy 2 (offshore VSC is controlling the AC voltage, while the onshore VSC is controlling the DC voltage and the reactive power/AC voltage) was implemented.

In all the considered test cases the developed VSC-based HVDC system had shown a good behavior, which however should be validated by means of laboratory experiments.

The results obtained in this chapter will be used as reference for the laboratory implementation of the VSC-based HVDC power transmission system which will be presented in the next chapter.

Chapter 6

Laboratory Validation of the System Using dSPACE Platform

Throught out this chapter the laboratory implementation of the VSC-based HVDC transmission system is presented. In the beginning, a description of the system configuration is presented. The control has been implemented on dSPACE platform. Finally, the laboratory results,that confirm the results obtained from simulation, are presented and discussed.

6.1 Set-up Description

The experimental setup used in the laboratory to carry out the study cases is presented in Figure 6.1. The circuit of the experimental test setup is shown in Figure 6.2.

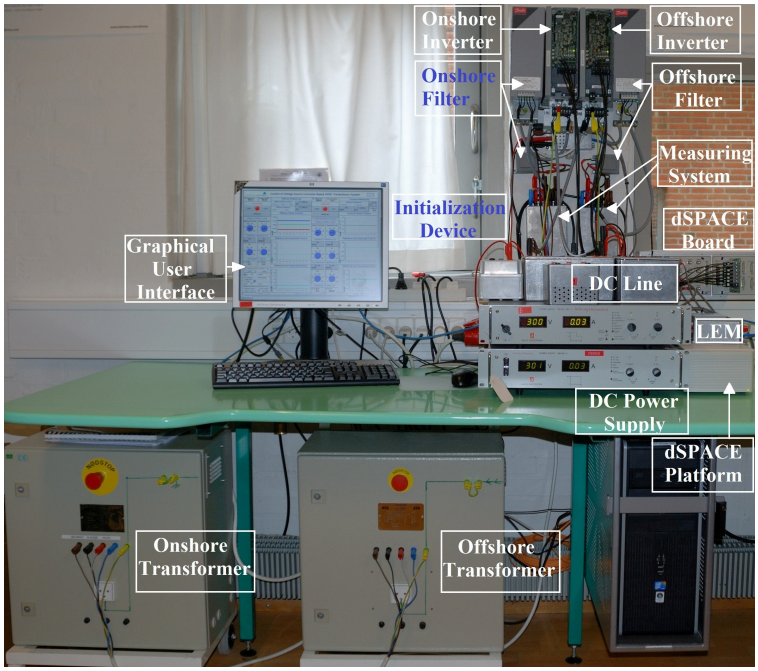

Figure 6.1: *Experimental setup*

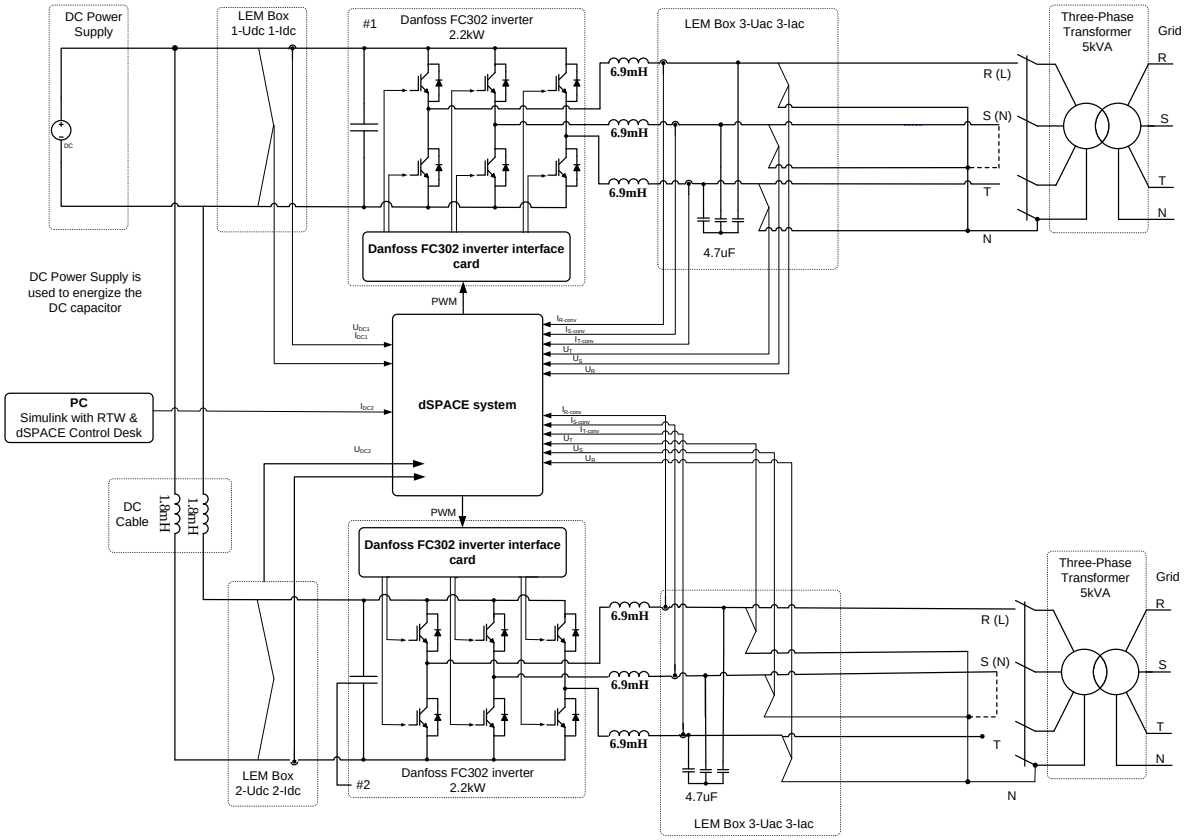

Figure 6.2: *Block diagram of the experimental setup*

The main components of the system setup are:

- 2 Danfoss Inverters FC-302
  - Rated power: 2.2 kW
  - Rated input voltage: $3 \times 380V_{rms} - 500V_{DC}$
  - Rated input current: 5.0/4.3 A
  - Rated input frequency: $50 - 60$ Hz
  - Rated output voltage: $3 \times 0 - V_{in}$
  - Rated output current: 5.6/4.8 A
  - Rated output frequency: $0 - 1000$ Hz
  - Rated output current: 4.6/4.8 A
- 2 Danfoss Sine Wave Filter
  - Rated power: 3 kW
  - Rated voltage: 500 V
  - Rated current: 8 A

  - Maxim switching frequency: 8 kHz
- 2 series connected Delta Elektronika DC power supplies
  - Type: $SM300-5$
  - Rated current: 5 A
  - Rated voltage: 300 V
  - Type: $SM400-AR-8$
  - Rated current: 8 A
  - Rated voltage: 400 V
- 4 measurement systems including
  - 2 LEM box for measurement of DC Voltages and Currents
  - 2 LEM box for measurement of AC Voltages and AC Currents
- 2 Three phase transformers
- dSPACE system
- California Instruments 4500 Lx

In order to implement the control, the DC voltage, the DC current, the three phase currents and voltages of the inverter have been measured. These measurements were done by means of LEM boxes.

The California Instruments is connected to the presented set-up in order to validate the study case where the terminals are working at different frequencies. The California Instruments represent in that case the offshore terminal which is going to be set at 60 Hz.

The converter is controlled through the DS1103 PPC digital controller.

6.2 dSPACE Implementation

The control system needs to be tested using a real time application in order to check its performances. Therefore, the control was implemented in dSPACE platform, in the Green Power Laboratory of Aalborg University.

The real time interface has been develloped using MATLAB/Simulink and the processes of compiling and downloading are carried out in the background. Due to the performances of the Control Desk software a control was developed in MATLAB/Simulink and then automatically processed and run by the DS1103 PPC card.

A Graphical User Interface (GUI) has been built using the Control Desk software of dSPACE, in order to facilitate the control of the system. The Control Desk interface is presented in Figure 6.3.

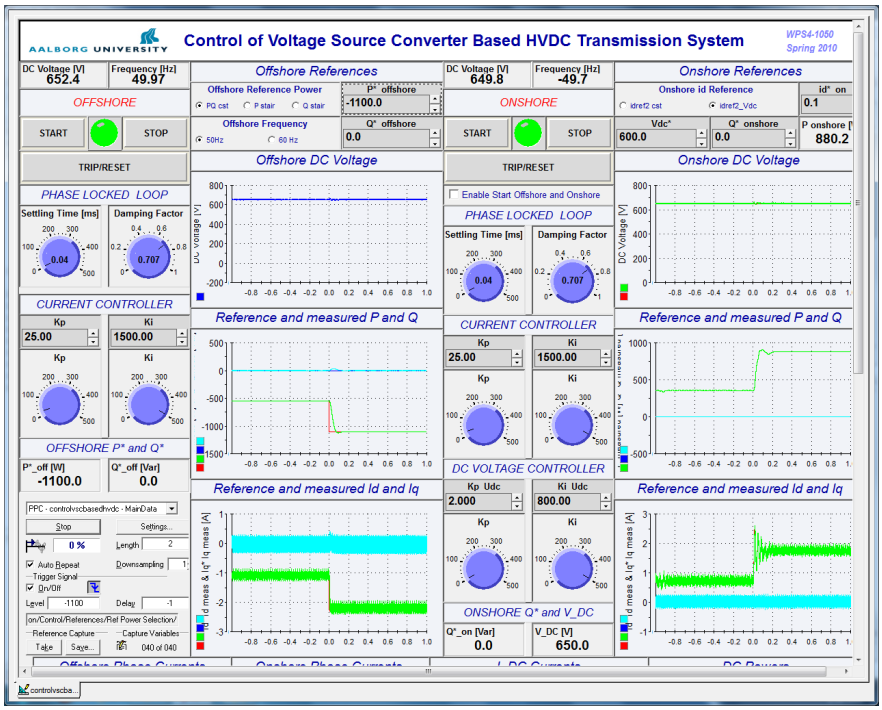

Figure 6.3: *Control Desk Graphical User Interface*

The interface can be used to provide inputs like:

- Active power reference for offshore terminal
- Reactive power reference for both terminals
- DC-link voltage reference
- Set the frequency for offshore terminal

Also, it can be used to vizualize different outputs like:

- Measured DC-link Voltage for offshore terminal
- Reference and measured DC-link Voltage for onshore terminal
- Reference and measured active and reactive power for both terminals
- Measured DC current and power for both terminals
- Reference and measured *dq*-axis currents for both terminals
- Measured three phase currents and voltages for both terminals
- Grid synchronization(theta provided by the PLL)

6.3 Start-up of VSC-based HVDC Transmission

In this study case the startup of the VSC-based HVDC was analyzed. For this study case no power transmission has been considered. When the power transmission should start-up both terminals, the offshore and the onshore terminal respectively, can be energized separately. The DC busses are energized by DC power suply through the antiparallel diodes in the bridge. When the gates are charged the converters in both terminals can be connected by the switches on the DC side. The onshore converter which is deblocked will control the DC voltage then, the offshore converter will be deblocked and the transmission of the active power can start.

The result of this study case will be presented in parallel, for the offshore and onshore terminals respectively.

Figure 6.4 presents the measured DC voltage at the offshore terminal. In Figure 6.5 the reference and measured DC voltage at the onshore terminal are presented. The DC voltage rises slowly until 650 V (1 p.u.). In this time, when the DC voltage rises, the DC capacitor is charging.

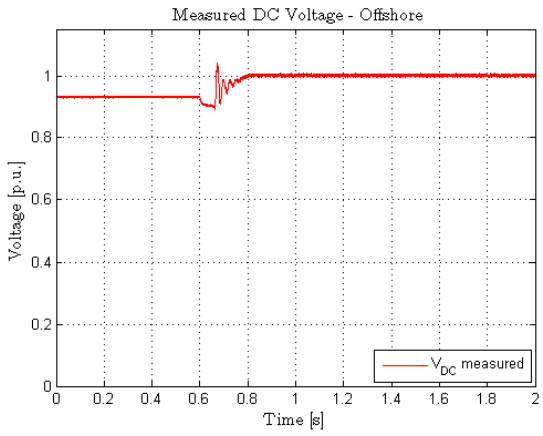

Figure 6.4: *Measured offshore DC voltage at the start-up of the system*

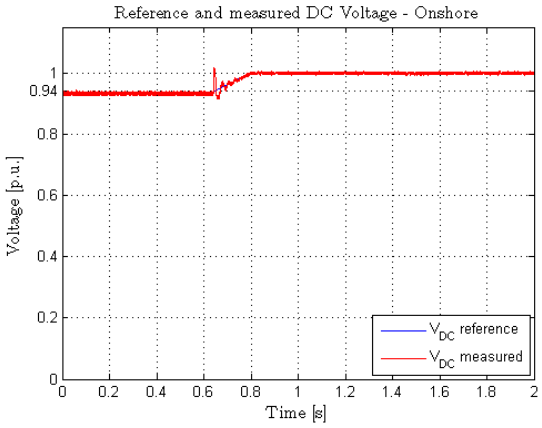

Figure 6.5: *Reference and measured onshore DC voltage at the start-up of the system*

The active and the reactive power are shown in Figure 6.6 and Figure 6.7 respectively.

The measured active and reactive powers at the offshore terminal are maintained constant at zero, as it was expected. The reactive power measured at the onshore terminal is kept constant, at zero, excepte the transient period.

As it can be observed from Figure 6.6, the active power measured at the onshore terminal is kept constant arround 0.03 p.u until the transient. The transient which can be observed (around 0.65 s) is due to the increase of the DC voltage. After transient, the active power is stabilized at -0.1 p.u.. The active power which is measured at the onshore terminal (even when no power is transmitted) is caused by the losses of the system.

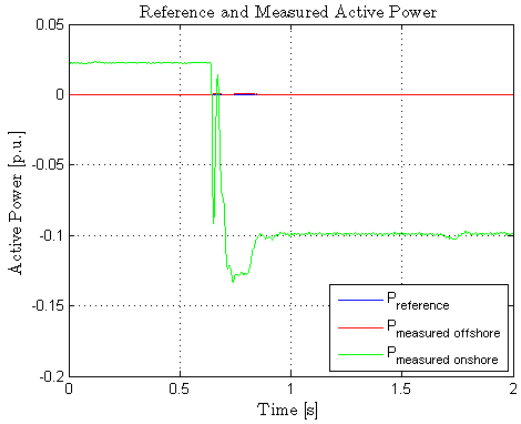

Figure 6.6: *Reference and measured active power at the start-up of the system*

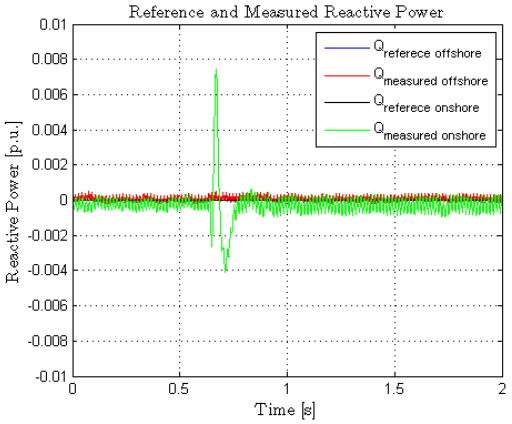

Figure 6.7: *Reference and measured reactive power at the start-up of the system*

The d and q components of the measured offshore and onshore currents are plotted in Figure 6.8 and Figure 6.9, respectively.

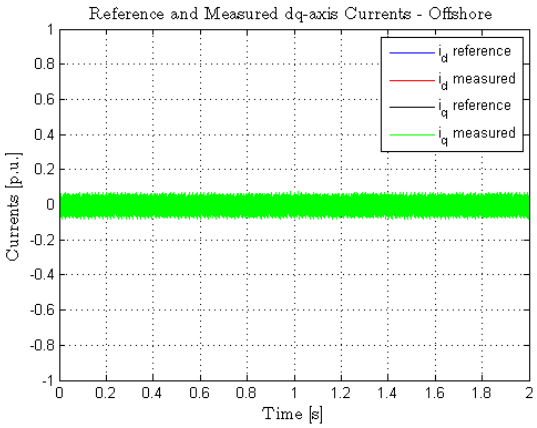

Figure 6.8: *Reference and measured offshore dq-axis currents at start-up of the system*

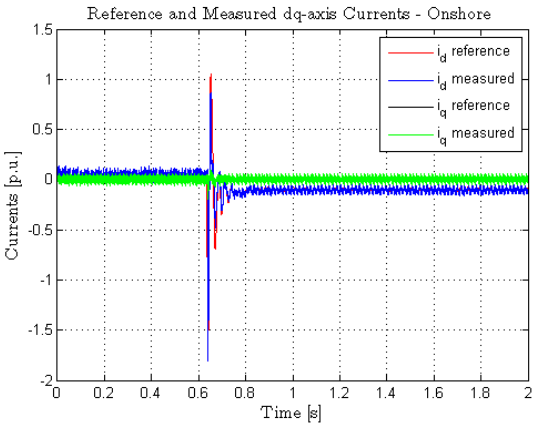

Figure 6.9: *Reference and measured onshore dq-axis currents at start-up of the system*

As expected, the dq-axis currents measured at the offshore terminal are not affected at the start-up of the system (see Figure 6.8) while, at the onshore terminal the dq-axis currents are modified during the transient (see Figure 6.9).

The i_d reference at the onshore terminal is proportionally with the active power at the onshore terminal, because the active power is determined by i_d. The measured i_d current at the onshore terminal follows its reference. After the transient, the currents are stabilizing fast.

The three phase currents measured at the output of the offshore converter and the three phase currents measured at the output of the onshore converter are shown in Figure 6.10 and Figure 6.11.

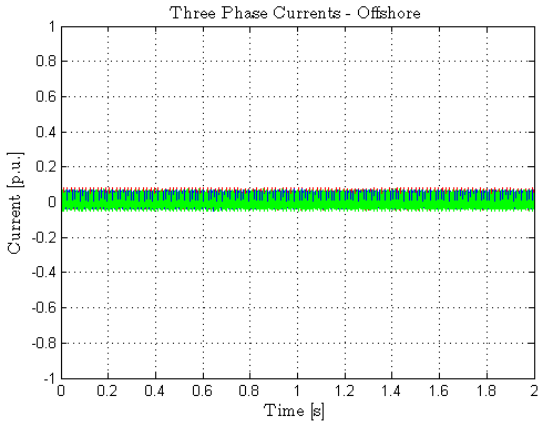

Figure 6.10: *Measured three phase offshore currents at the start-up of the system*

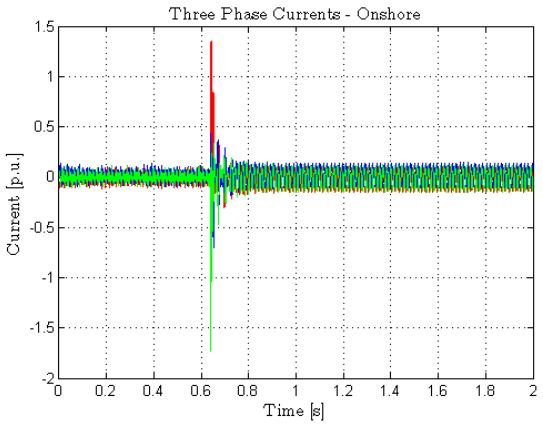

Figure 6.11: *Measured three phase onshore currents at the start-up of the system*

6.4 VSC-based HVDC power transmission between two terminals operating at 50 Hz - Strategy 1

The aim of this test case which was implemented on the laboratory setup was to validate the results which were obtained from the simulations presented in Section 5.2.

The test conditions which were considered in laboratory are the same with the ones used in simulation: the offshore-side VSC was controlling the active and reactive power flow while, the onshore-side VSC is controlling the DC voltage and the onshore reactive power flow. Furthermore, the references given at the input of the controllers, which are shown in Figure 6.12, were the same with the ones used in simulation.

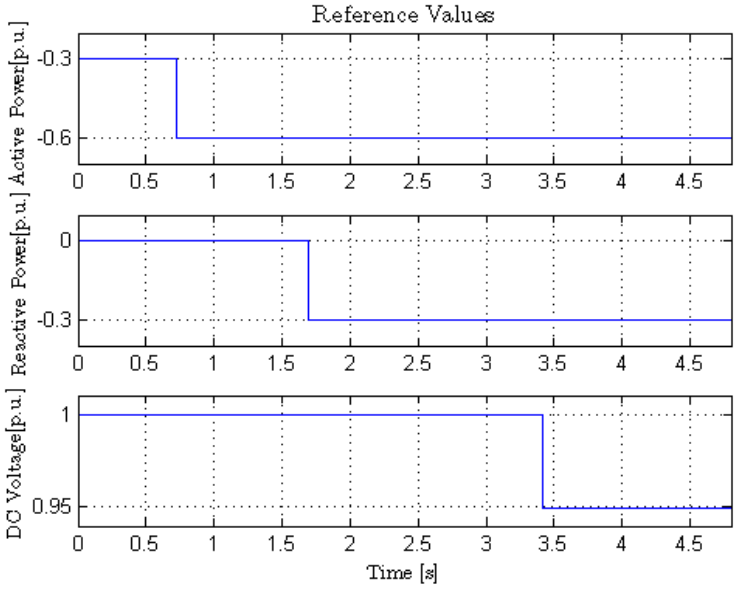

Figure 6.12: *Reference values*

Through Figure 6.13 and Figure 6.14 the validation of the designed PLL system as well as the proving of the synchronization with the grid voltages is achieved.

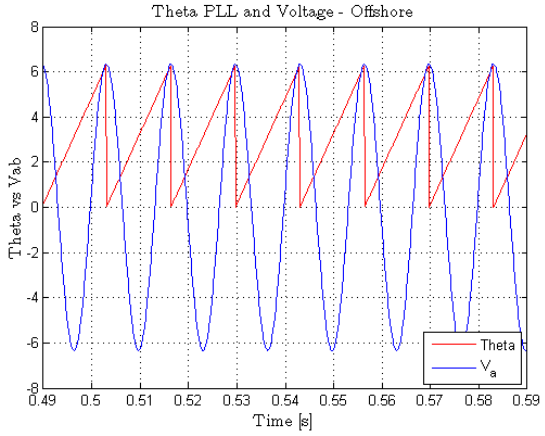

Figure 6.13: *The estimated grid voltage Θ - offshore terminal*

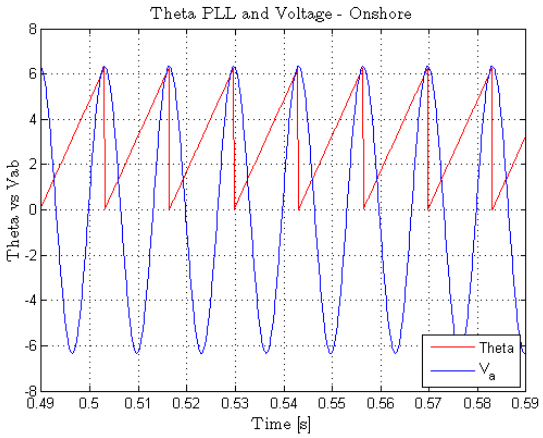

Figure 6.14: *The estimated grid voltage Θ - onshore terminal*

The reference and measured active power at both terminals are shown in Figure 6.15. From this plot, it can be observed that the active power measured at the offshore terminal tracks with accuracy the reference.

As it can be observed from Figure 6.15, the onshore terminal receives the amount of power that is delivered by the offshore terminal minus the losses from the system. These losses are mainly caused by the transmission line and by the filter of the onshore VSC.

The reference and measured reactive power at the offshore and onshore terminal respectively are presented in Figure 6.16. At the offshore terminal, at the time instant $t = 1.7$ s, the reactive power reference is changed, while at the onshore terminal the reactive power reference is kept constant at zero during the entire transmission.

As it can be noticed from Figure 6.16, the two terminals are controlling independently the reactive power. At the moment when the amount of active power which is transmitted between the terminals is changed, a small positive transient in the reactive power occurs. The transient in the reactive power is positive or negative depending if the active power is absorbed or delivered respectively.

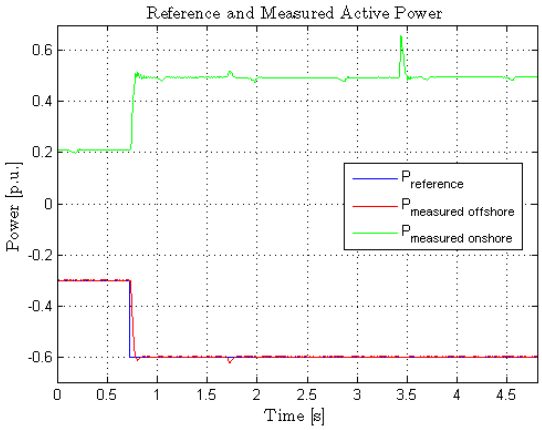

Figure 6.15: *Reference and measured active power*

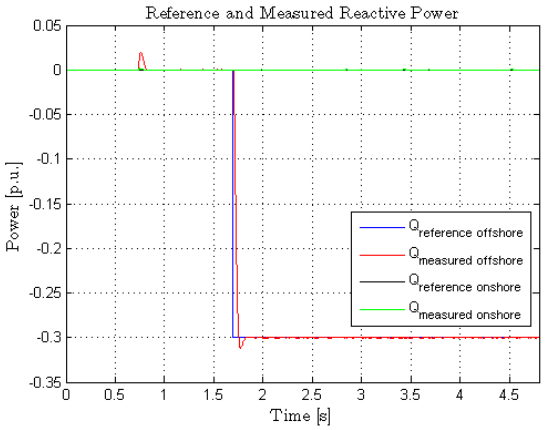

Figure 6.16: *Reference and measured reactive power*

The response of the DC voltage controller at the different applied transients is presented in Figure 6.18. The waveform of the measured DC voltage at the onshore terminal, shows only minor oscillations when the transient in the active power occurs. Furthermore, the measured DC voltage tracks with accuracy its reference when the negative step is applied.

Figure 6.17 shows the DC voltage measured at the offshore terminal which is not subject to control.

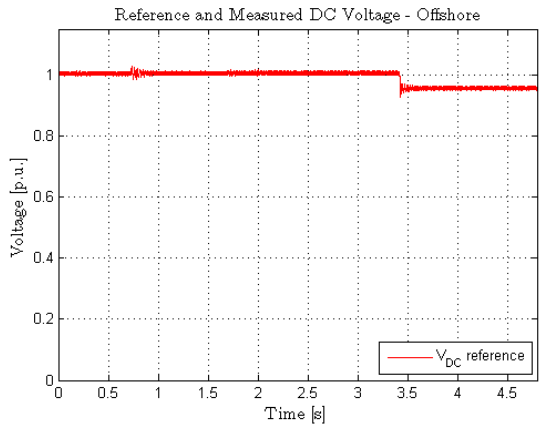

Figure 6.17: *Measured DC voltage - offshore terminal*

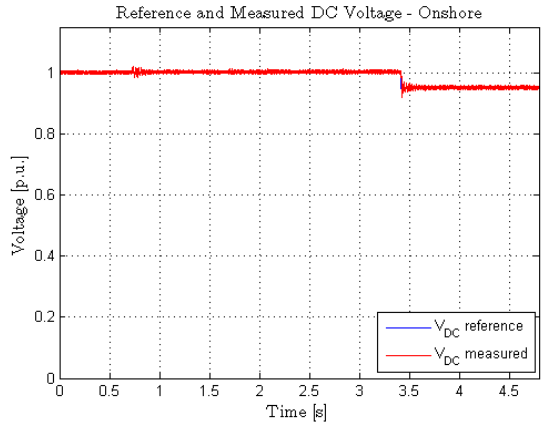

Figure 6.18: *Reference and measured DC voltage - onshore terminal*

The dq components of the currents at both terminals are presented in Figure 6.19 and Figure 6.20. The dependence between the active power and i_d, respectively between the reactive power and i_q is very clear suggested by the two figures.

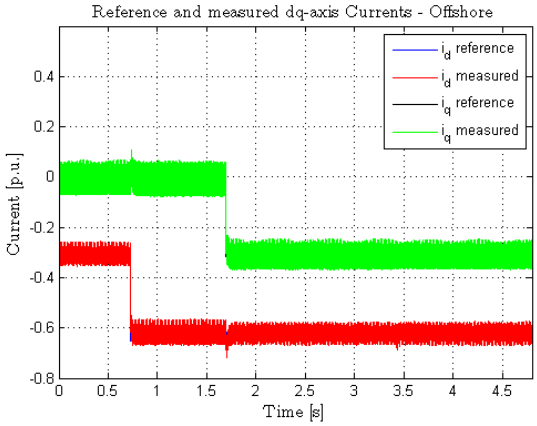

Figure 6.19: *Reference and measured dq-axis currents - offshore terminal*

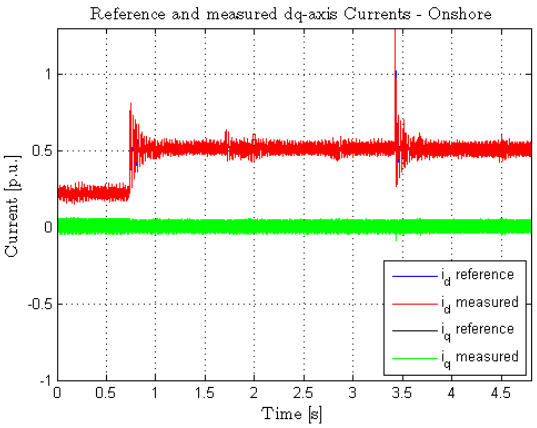

Figure 6.20: *Reference and measured dq-axis currents - onshore terminal*

Figure 6.21 and Figure 6.22 are presenting the three phase currents measured at both terminals.

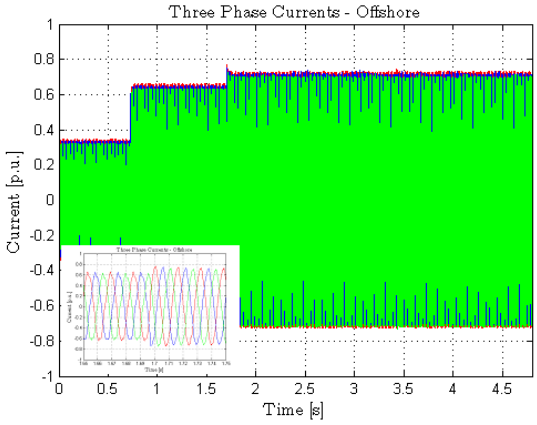

Figure 6.21: *Measured three phase currents - offshore terminal*

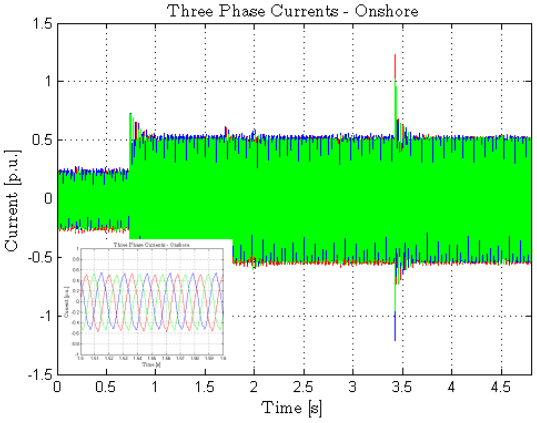

Figure 6.22: *Measured three phase currents - onshore terminal*

Through this test case which was implemented on the small-scale laboratory setup, the behavior of the VSC-based HVDC transmission system (when using control Strategy 1) was validated.

Until now, in this section all the presented results had referred to one of the terminals being offshore and the other one onshore. In this case the active power flow is unidirectional, from the offshore terminal to the onshore terminal. However the control structure which was tested in this study case (Strategy 1) is also applicable for the application when both terminals are onshore and the active power flow is bidirectional.

In Appendix A, the study case for a VSC-HVDC transmission system between two onshore terminals is carried out in simulations and validated in laboratory. For this study case, the active power flow is considered from the onshore terminal to the offshore terminal, since the case when the active power flow is considered from offshore to onshore has been validated.

6.5 VSC-based HVDC power transmission between two terminals operating at 50 Hz and 60 Hz - Strategy 1

In order to validate the second study case case which was analyzed in simulation, the setup of the laboratory was change.

To emulate a WPP working at 60 Hz, the programmable AC power supply from California Instruments was connected at the offshore terminal.

The laboratory test conditions are the same with the test conditions used in simulation (see Section 5.3): the offshore WPP working at 60 Hz is delivering power to a 50 Hz AC network.

The considered step changes in the references are the same as in the previous study case implemented in the laboratory. This fact makes possible the comparison between an offshore terminal working at 50 Hz and an offshore terminal working at 60 Hz.

The results, like in previous study case, are presented in parallel for both terminals.

In Figure 6.23 and Figure 6.24 the phase voltages at the two terminals are presented and as it can be observed their frequency is different.

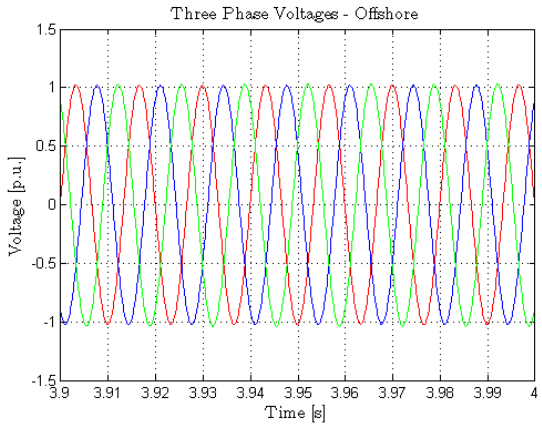

Figure 6.23: *Measured three phase voltages at the offshore terminal (60Hz)*

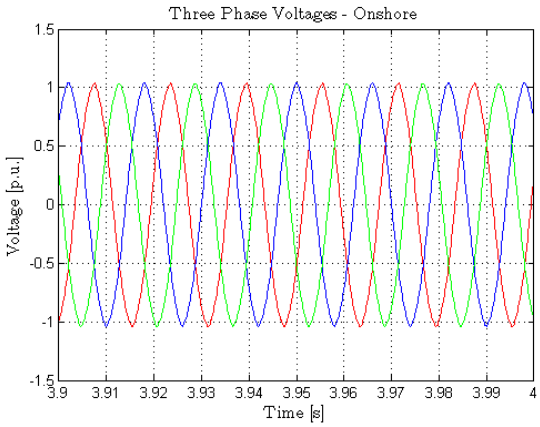

Figure 6.24: *Measured three phase voltages at the onshore terminal (50Hz)*

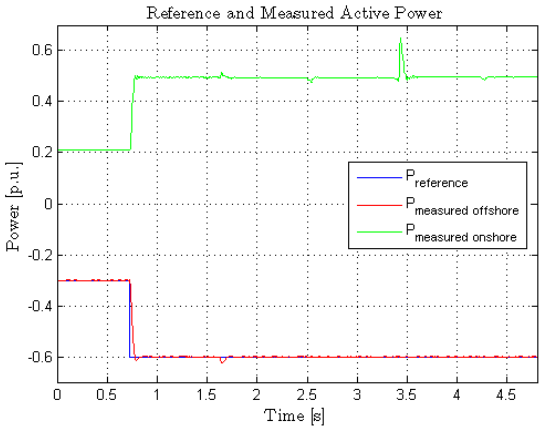

Figure 6.25: *Reference and measured active power*

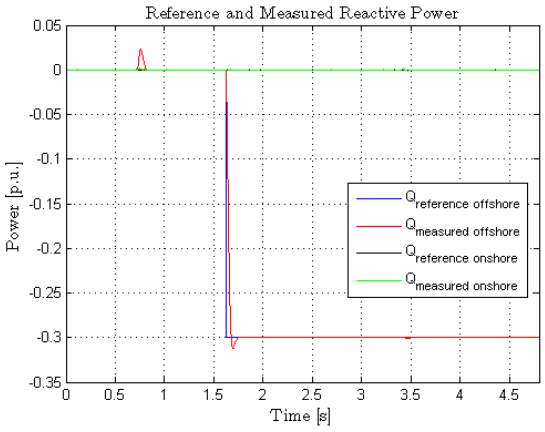

Figure 6.26: *Reference and measured reactive power*

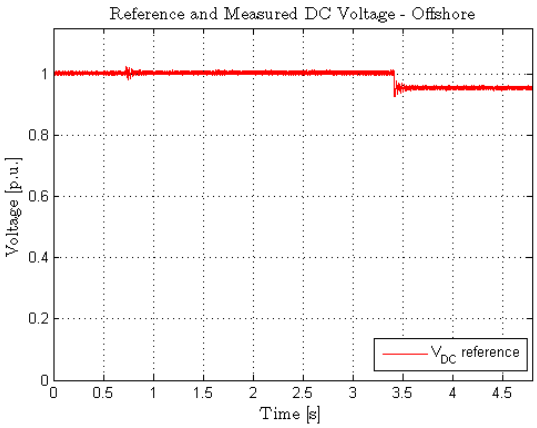

Figure 6.27: *Measured DC voltage - offshore terminal*

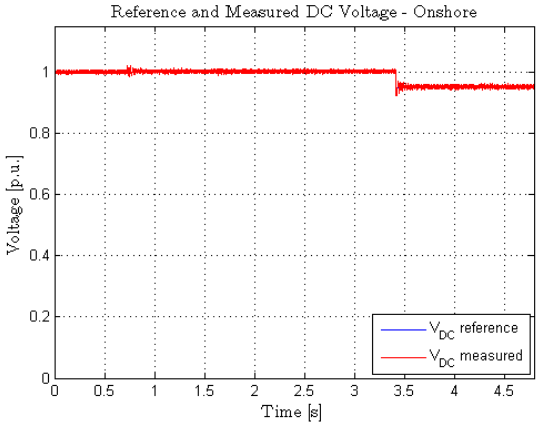

Figure 6.28: *Reference and measured DC voltage - onshore terminal*

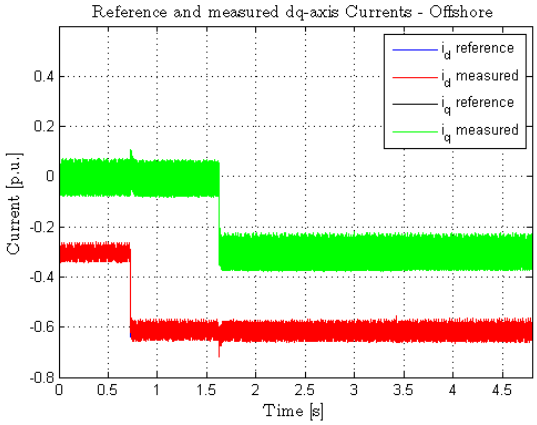

Figure 6.29: *Reference and measured dq-axis currents - offshore terminal*

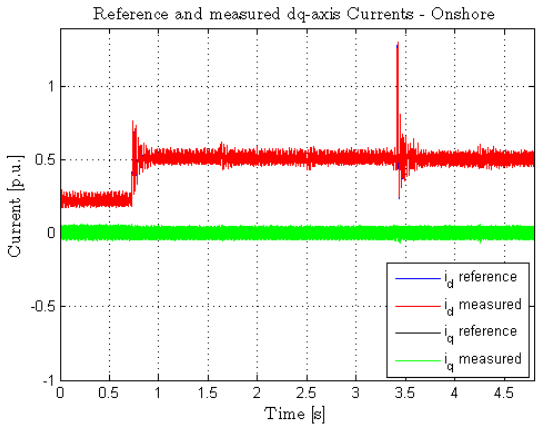

Figure 6.30: *Reference and measured dq-axis currents - onshore terminal*

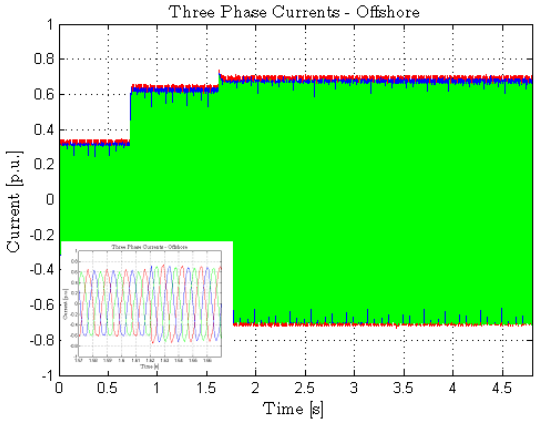

Figure 6.31: *Measured three phase currents - offshore terminal*

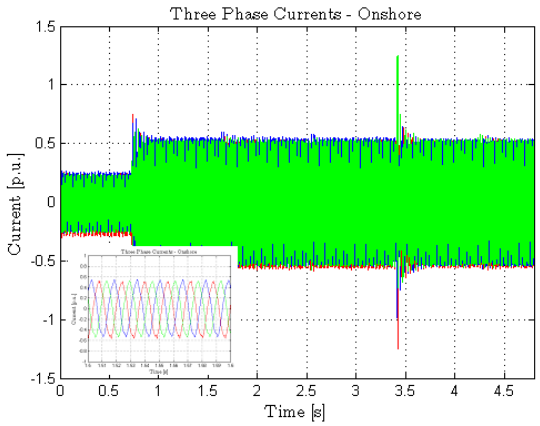

Figure 6.32: *Measured three phase currents - onshore terminal*

By comparing the results obtained in the laboratory for the first study case with the results obtained in the laboratory for the second study case it can be stated that no notable differences in the power transmission were observed. Therefore, if the synchronization with the grid is well realized, and the control structure is working well, no difference shall occur when the power is transmitted between two terminals working at different frequencies.

6.6 Influence of the configuration of the DC cable in a VSC-based HVDC transmission system

The aim of the third study case which has been tested in the laboratory was to investigate the influence of the configuration of the DC line (cable) in the case of a VSC-based HVDC transmission system.

For this study case, four sets of measurements were acquired. In the first case, no line was considered between the two VSCs (see Figure 6.33(a)). In the second case, the configuration of the DC line is the one presented in Figure 6.33(b). In the case of the third and fourth sets of measurements the DC line has the same configuration (see Figure 6.33(c) and Figure 6.33(d)), only the rating of the inductance being different.

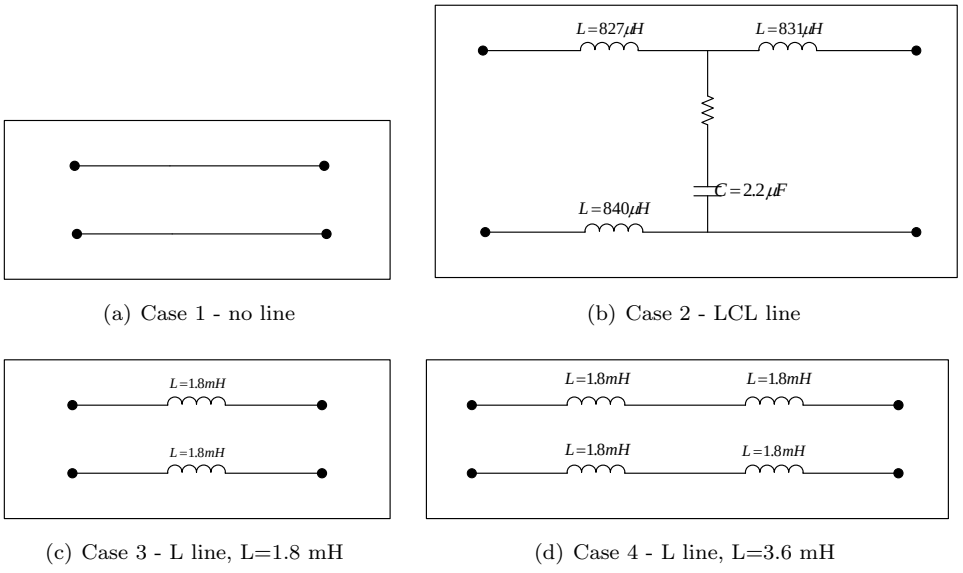

(a) Case 1 - no line

(b) Case 2 - LCL line

(c) Case 3 - L line, L=1.8 mH

(d) Case 4 - L line, L=3.6 mH

Figure 6.33: *Configuration of the DC line*

The control structure of the HVDC system, for the present study case, is similar with the control structure which was used in the previous study case, being detailed present in Figure 5.1 and Figure 5.3.

In order to perform this test case and to analyze the response of the VSC-based HVDC system at power flow changes, a positive change in the active power was considered at the input of the offshore terminal, as shown in Figure 6.34.

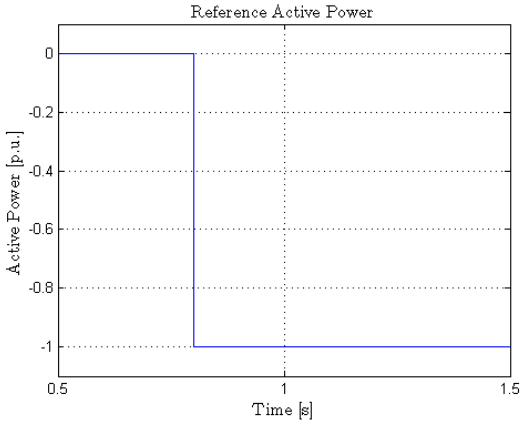

Figure 6.34: *Active power reference at the offshore terminal*

For an easier analysis and comparison of the results acquired from the laboratory measurements, the plots for the four study cases will be presented in parallel.

In Figure 6.35, the measured active power (at both terminals) is plotted for all the four cases respectively.

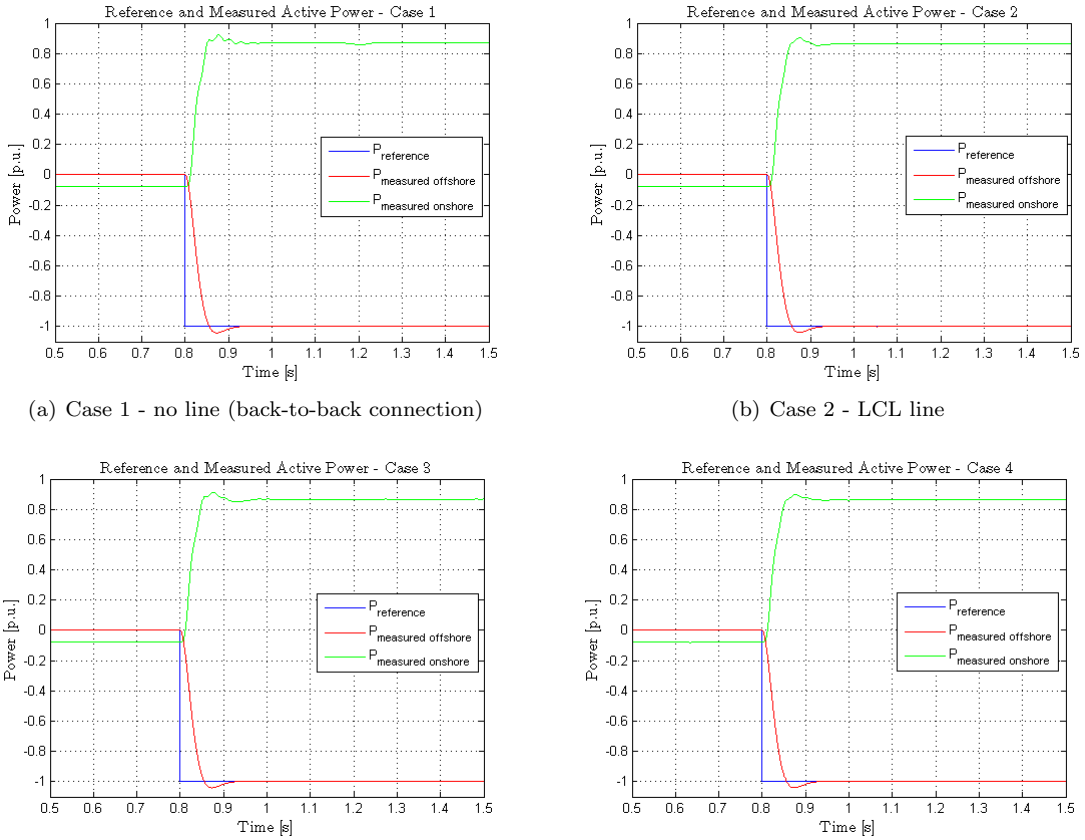

(a) Case 1 - no line (back-to-back connection)

(b) Case 2 - LCL line

(c) Case 3 - L line, L=1.8 mH

(d) Case 4 - L line, L=3.6 mH

Figure 6.35: *Reference and measured active power at both terminals*

Analyzing the above presented plots, it can be noticed that the active power responses, at the step change, have nearly identical dynamics during the transient. While, the worst response of the system is obtained in the case of the back-to-back connection between the inverters (Case 1), the best behavior of the system is obtained when the LCL filter emulates the DC cable (Case 2). The damped response of the system in Case 2 is given by the presence of the capacitor in the configuration of the line. Furthermore, since the rating of the inductance used is Case 4 is bigger than in the other cases, the losses in the active power are more pronounced in this test. However, these losses are no more than 0.01 pu (approximately 20 W) when comparing the best scenario (Case 1) with the worst (Case 4).

In Figure 6.36, the reference and measured DC voltage at the onshore terminal are presented for all the four measured cases respectively.

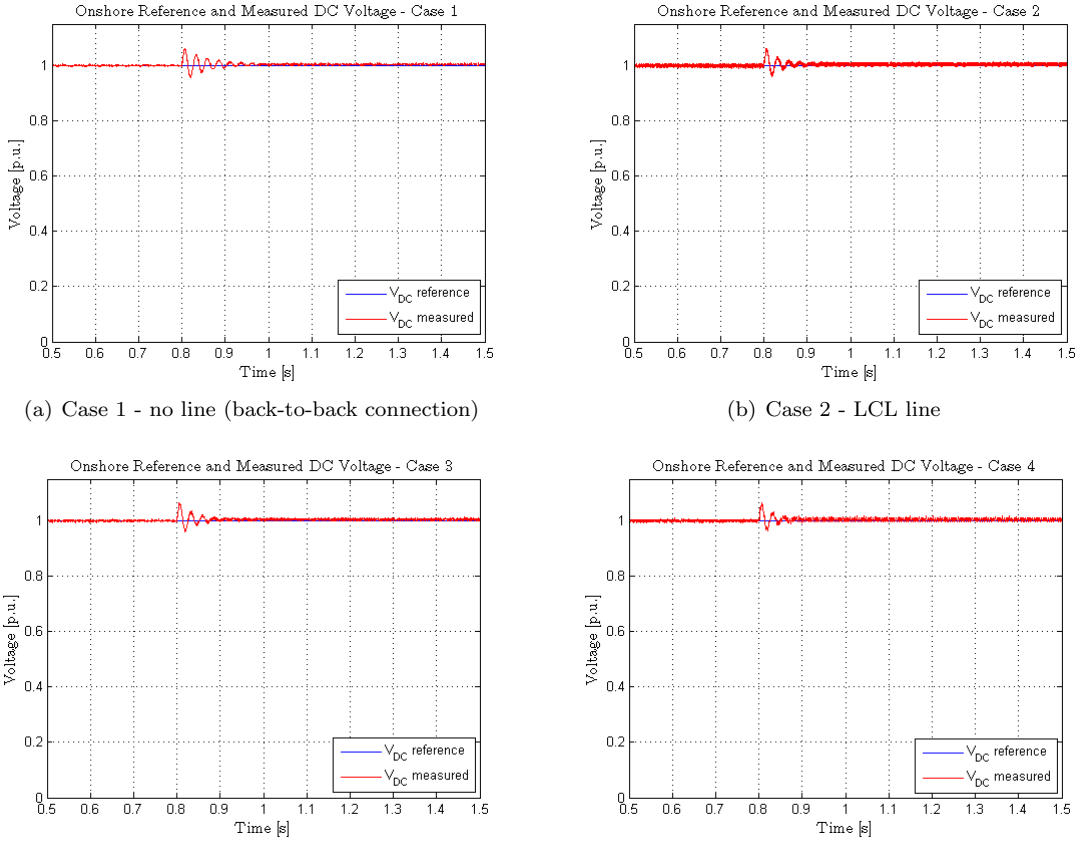

(a) Case 1 - no line (back-to-back connection)

(b) Case 2 - LCL line

(c) Case 3 - L line, L=1.8 mH

(d) Case 4 - L line, L=3.6 mH

Figure 6.36: *Reference and measured DC Voltage at the onshore terminal*

By comparing the results presented in Figure 6.36 , it can be observed that the oscillations in the measured DC voltage which are caused by the transient in the active power can be reduced by using DC lines with bigger inductance (Case 4).

The last variables which are analyzed in this study case are the three phase currents measured after the phase reactor of the onshore VSC.

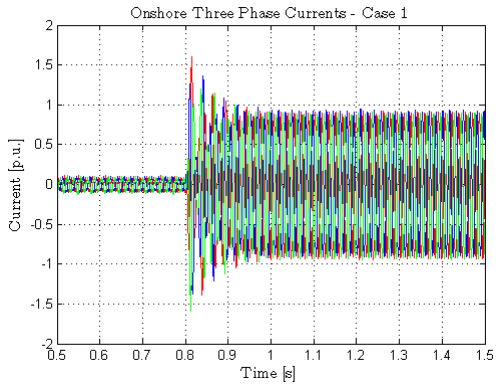

(a) Case 1 - no line (back-to-back connection)

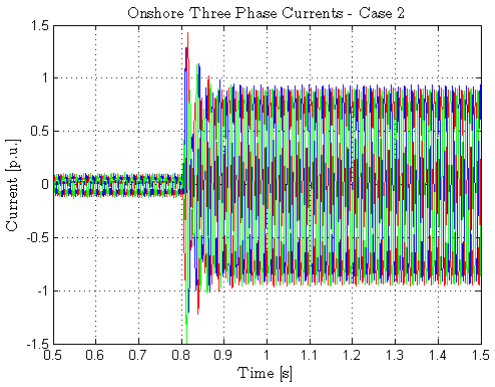

(b) Case 2 - LCL line

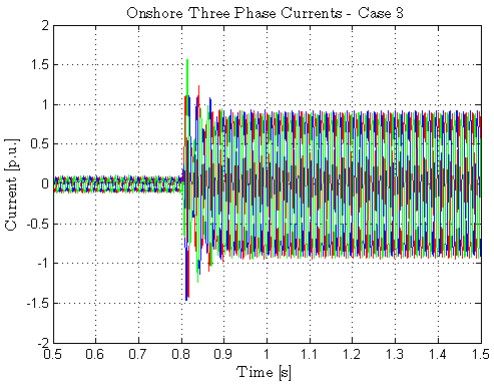

(c) Case 3 - L line, L=1.8 mH

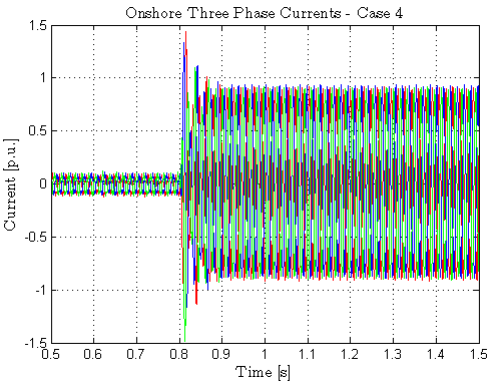

(d) Case 4 - L line, L=3.6 mH

Figure 6.37: *Measured three-phase currents at the onshore terminal*

Analyzing the above presented plots, it can be noticed that the phase currents measured in the four cases have nearly similar behavior. Moreover, like in the case of the measured active power, the same losses are to be found in the values of the measured phase currents when Case 4 is considered.

Summarizing the above presented facts, it can be concluded that the configuration of the DC cable is a very important topic in the case of the VSC-based HVDC transmission systems. As it was shown in this study case, the components of the DC cable and their ratings have influence on the dynamics of the system and also on the system's losses. Therefore, a trade-off solution has to be found when the type of the DC cable used for HVDC transmissions is chosen.

However, for a better analysis of the influence of the DC cable's configuration in the VSC-HVDC systems, a test case using data from real applications should be also considered and it can be subject to a future work.

6.7 Summary

In this chapter the laboratory implementation of the VSC-based HVDC transmission system was presented.

In the debut of the chapter a description of the laboratory setup was realized. In order to test the laboratory VSC-HVDC system the control was implemented on a dSPACE platform. Thus, the results obtained in the simulations could be validated using a real setup.

Due to the limitations encountered in the laboratory, only the control Strategy 1 could be verified. For this control strategy several study cases were carried out with success.

As it can be observed from the plots presented throughout Chapter 5 and 6 respectively, the results obtained in the laboratory are very similar with the ones obtained in simulations. Therefore, the performance of the VSC-based HVDC transmission system could be validated.

Chapter 7

Conclusions and Future Work

7.1 Conclusions

The main topic of this project was to investigate and to analyze the behavior of the VSC-based HVDC transmission system. The current project was structured into seven chapters which will be briefly presented in the followings.

The first chapter represents an introduction to the project. This chapter contains a short background, the problem formulation and also the objectives of this project are stated in this section. Moreover, the limitations encountered during the development of this project are also presented in Chapter 1.

The second chapter could be seen as an overview of the VSC-based HVDC transmission systems. In the first section of this chapter several valuable advantages of the HVDC transmissions over the HVAC transmissions are presented. These advantages make the HVDC transmission systems more suitable for specific applications, such as: long distance power transmissions, asynchronous connections of AC power systems, offshore transmissions etc. The second section of this chapter dealt with the presentation of the four basic VSC-HVDC configurations: monopolar, bipolar, back-to-back and multi-terminal respectively. Furthermore, the advantages of the studied topology (VSC-HVDC) over the classical HVDC topologies were presented and their areas of application were also enumerated (e.g. power supply to insular loads, offshore applications etc).

The third chapter of the project dealt with the modeling of a simple VSC-based HVDC transmission systems. Here, the mathematical models of the main components (VSC, filter and grid) were presented. Since the control was implemented in the dq synchronous reference frame, the model of the VSC and filter were also developed in the same reference frame.

The next chapter was focused on the design of the control system of the VSC-based HVDC transmission system. In the beginning, an overview of the applicable control loops was realized. As it was shown, all the control strategies have at their bottom level a fast inner current control loop. The slower outer control loops can regulate various parameters, such as: DC voltage, AC voltage, active power, reactive power and/or frequency. Depending on the application and on the imposed requirements, one or more of this control loops can be used to control the converter. Investigating all this applicable controllers, two control strategies were developed in order to control the offshore and onshore terminals of the VSC-HVDC system. In the first control strategy ("Strategy 1") the offshore VSC is controlling the active power and the reactive power in the outer loops, while the onshore VSC is controlling the DC

voltage and the reactive power. In the second control strategy ("Strategy 2"), the offshore VSC is controlling the AC voltage in the outer loop, while the control system of the onshore VSC is the same with the one used in Strategy 1. The two control strategies were developed in the dq synchronous reference frame and PI controllers have been used to regulate the desired parameters. For the tuning of the controllers an analytical method was used and the obtained results were verified and, if necessary, adjusted using the SISOtool package provided by MATLAB. Moreover, in this chapter the PLL technique used for synchronization with the grid was presented.

The fifth chapter was dedicated to the analysis of the steady-state behavior of the VSC-HVDC system. For this analysis the two developed control strategies were considered. In the first part of this chapter, the behavior of the VSC-HVDC system was analyzed for the case when Strategy 1 has been implemented. The analysis was performed by applying positive and/or negative step changes (of different amplitudes) in the controlled parameters. In the second part of this chapter the behavior of the system was analyzed for the case when Strategy 2 has been implemented. For both developed control strategies, the VSC-based HVDC transmission system performed well, being able to realize the active power transmission between the offshore and onshore terminals. Moreover, the independently control of reactive at both terminals was proved. The results obtained in this chapter were validated in the laboratory using a small-scale setup (2.2 kW).

In Chapter 6, the experimental results are presented. Firstly, the laboratory setup was described and the graphical user interface which was built in Control Desk was presented. The second part of this chapter is dedicated to the explanation of the tests which were performed in the laboratory. Due to the encountered limitations, only the control method Strategy 1 could be validated using the laboratory setup. The tests carried out using the small-scale laboratory setup are identical with the ones carried out simulations. In order to obtain a well functional VSC-HVDC transmission system, the laboratory implementation of the control structure was realized step-by-step. Thus, firstly the inner current controllers were tested individually for both onshore and offshore converters respectively. Secondly, the outer controllers (DC voltage, active power and reactive power controllers) were implemented and tested.

The results obtained in the laboratory had confirmed the ones obtained in the simulations and thus the developed control strategy was validated.

7.2 Future Work

In order to improve the current project, other topics related to the project can be also investigated. The below presented items are suggested as future work for this project:

- simulation of the VSC-HVDC transmission systems using real-life values for the system's parameters; decreasing of the switching frequency in the simulation and in the laboratory implementation in order to emulate better the real life condition;
- implementation and testing in the laboratory of the developed AC voltage controller;
- testing and analysis of the dynamic performances of the VSC-based HVDC system during disturbances, balanced and unbalanced grid faults;
- implementation of the developed control strategies in the $\alpha\beta$ stationary reference frame using PI or PR controllers; comparison of the results with the results obtained using dq synchronous reference frame.

Bibliography

[1] EWEA, "Wind energy - the facts," March 2009.

[2] EWEA, "Wind in power - 2009 european statistics," February 2010.

[3] EWEA, "Wind directions," February2010.

[4] EWEA, "Pure power - wind energy targets for 2020 and 2030," tech. rep., EWEA, 2009.

[5] S. Meier, *Novel Voltage Source Converter based HVDC Transmission System for Offshore Wind Farms*. PhD thesis, Royal Institute of Technology, Departament of Electrical Engineering Electrical Machines and Power Electronics, Stockholm, Sweden, 2005.

[6] EWEA, "Oceans of opportunity - harnessing europe's largest domestic energy resource offshore," tech. rep., EWEA, September 2009.

[7] V. Sood, *HVDC and Facts Controllers - Applications of Static Converters in Power Systems*. Kluwer Academic Publishers, 2004. ISBN 1-4020-7891-9.

[8] C. Du, *The control of VSC-HVDC and its use for large industrial power systems*. PhD thesis, Departament of Electric Power Engineering, Chalmers University of Technology, Goteborg, Sweden, 2003.

[9] M. P. Bahrman, "Overview of hvdc transmission," *PSCE*, pp. 18–23, 2006.

[10] M. P. Bahrman, "Hvdc transmission overview," *IEEE*, pp. 1–7, 2008.

[11] N. Flourentzou, V. G. Agelidis, and G. D. Demetriades, "Vsc-based hvdc power transmission systems: An overview," *IEEE Transactions on Power Electronics*, vol. 24, pp. 592–602, March 2009.

[12] K. R. Padiyar, *HVDC Power Transmission Systems*. John Wiley & Sons, 1990. ISBN 0-470-20267-X.

[13] R. Rudervall, J. Charpentier, and R. Sharma, "High voltage direct current (hvdc) transmission systems technology review paper,"

[14] ABB, *Its time to connect - Technical description of HVDC Light® technology*.

[15] F. Schettler, H. Huang, and N. Christl, "Hvdc transmission systems using voltage sourced converters - design and applications," *IEEE*, pp. 715–720, 2000.

[16] C. Du, M. H. J. Bollen, E. Agneholm, and A. Sannino, "A new control strategy of a vsc-hvdc system for high-quality supply of industrial plants," *IEEE Transactions on Power Delivery*, vol. 22, pp. 2386–2394, October 2007.

[17] L. Weimers, "New markets need new technology," *Powercon 2000 Conference*, pp. 873–877, 2000.

[18] K. Johannesson, A. Gustafsson, J. Karlstrand, and M. Jeroense, "Hvdc light cables for long distance grid connection," *Europe Offshore Wind Conference 2009, Stockholm, Sweden*, Sept 14-16, 2009.

[19] ABB, "Abb goes offshore - innovative integration of offshore wind energy into the grid," tech. rep.

[20] ABB, "Grid connection of offshore wind farm cluster borkum 2," tech. rep.

[21] E. System and Eltra, *Wind Turbines Connected to Grids with Voltages above 100kV - Technical regulation for the properties and the regulation of wind turbines*, December 2004.

[22] "Iec 61000-3-7: Electromagnetic compatibility (emc)," tech. rep.

[23] R. Wu, S. Dewan, and G. Slemon, "A pwm ac to dc converter with fixed switching frequency," *IEEE*, 1988.

[24] V. Blasko and V. Kaura, "A new mathematical model and control of a three-phase ac-dc voltage source converter," *IEEE Transaction on Power Electronics*, vol. 12, pp. 116–123, January 1997.

[25] A.Yazdani and R.Iravani, *Voltage Source Converters in Power Systems*. John Wiley & Sons, March 2010. ISBN: 978-0-470-52156-4.

[26] F. Iov, A. Hansen, P. Sorensen, and F. Blaabjerg, "Wind turbine blockset in matlab/simulink," tech. rep., Aalborg University and RISO, March 2004.

[27] G. A. Raducu, "Control of grid side inverter in a b2b configuration for wt applications," Master's thesis, Aalborg University, 2008.

[28] S. Chandhary, R. Teodorescu, P. Rodriguez, P. Kjaer, and P. Christensen, "Modelling and simulation of vsc-based hvdc connection for offshore wind power plants," *Ph.D. Seminar on detailed Modelling and Validation of Electrical Components and Systems*, pp. 53–57, 2010.

[29] C. Du, A. Sanino, and M. Bollen, "Analysis of the control algorithms of voltage source converter hvdc," *Power Tech, IEEE Rusia*, pp. 1–7, 2005.

[30] A. Timbus, *Grid Monitoring and Andvanced Control of Distributed Power Generation Systems*. PhD thesis, Aalborg University, Institute of Energy Technology, Denmark, May 2007.

[31] M. Kazmierkowski, R. Krishnan, and F.Blaabjerg, *Control in Power Electronics - Selected Problems*. Academic Pres, 2002.

[32] F. Blaabjerg, R. Teodorescu, M. Liserre, and A. Timbus, "Overview of control and grid synchronization for distributed power generation systems," *IEEE Transactions on Industrial Electronics*, vol. 53, pp. 1398 – 1409, 2006.

[33] R. Song, C. Zheng, R. Li, and X. Zhou, "Vscs based hvdc and its control strategy," *IEEE/PES Transmission and Distribution*, pp. 1–6, 2005.

[34] E. Ceanga, C. Nichita, L. Protin, and N. Cutululis, *Theorie de la Commande des Systemes*. Ed. Tehnica, Bucuresti, 2001.

[35] W. Leonhard, *Control of Electrical Drives, Third Edition*. Springer, 2001. ISBN 3-540-41820-2.

[36] A. Lindberg, *PWM and Control of Two and Three Level High Power Voltage Source Converters*. PhD thesis, Royal Institute of Technology, Stockholm, Sweden, 1995.

[37] M. Delghavi and A.Yazdani, "A control strategy for islanded operation of a distributed resource (dr) unit," *Power and Energy Society General Meeting, PES '09. IEEE*, pp. 1–8, 2009.

[38] L.Xu, B.W.Williams, and L.Yao, "Multi-terminal dc transmission systems for connecting large offshore wind farms," *Power and Energy Society General Meeting - Conversion and Delivery of Electrical Energy in the 21st Century, IEEE*, pp. 1–7, 2008.

Acronyms

AC	Alternating Current
CSC	Current Source Converter
DC	Direct Current
EU	European Union
EWEA	European Wind Energy Association
HVAC	High Voltage Alternative Current
HVDC	High Voltage Direct Current
IGBT	Insulated Gate Bipolar Transistor
LCC	Line Commuted Converter
P	Proportional
PCC	Point of Common Coupling
PI	Proportional Integral
PLL	Phase Locked Loop
PWM	Pulse Width Modulation
RoW	Right-of-Way
THD	Total Harmonic Distortion
TIF	Telephone Influence Factor
TSO	Transmission System Operator
VSC	Voltage Source Converter
WF	Wind Farm
WPP	Wind Power Plant
XLPE	Cross Linked Poly-Ethylene
ZOH	Zero Order Hold

Nomenclature

C	DC capacitance	$[F]$
C_f	Filter capacitance	$[F]$
d_k	Duty cycles	
e_k	Phase voltages	$[V]$
f_s	Sampling frequency	$[Hz]$
f_{PWM}	Switching frequency	$[Hz]$
G_{plant}	Transfer function of the plant	$-$
G_{PIc}	Transfer function for current control loop	$-$
H	PLL transfer function	$-$
k_p	Proportional gain	$-$
k_i	Integrator gain	$-$
I	Amplitude of the phase current	$[A]$
I_a, I_b, I_c	Three phase currents	$[A]$
i_{c_k}	Current flowing in the capacitor	$[A]$
i_d, i_q	dq-axis currents	$[A]$
I_{DC}	DC - current	$[A]$
I_g	Grid side current	$[A]$
i_k	Phase currents	$[A]$
i_{PCC_k}	Phase current at PCC	$[A]$
k	Index for the three phase	$-$
L	Phase reactor inductance	$[H]$
L_g	Grid side inductance	$[H]$
M_p	Overshoot	$[\%]$
P	Active power	$[W]$
Q	Reactive power	$[Var]$
r	Resistance of the switches	$[\Omega]$
r_f	Internal resistance of the capacitor	$[\Omega]$
R	Phase reactor resistance	$[\Omega]$
R_g	Grid side parasitic resistance	$[\Omega]$
s	Continuous operator	$-$
t	Time	$[s]$
T_i	Integrator time	$[s]$
T_{PWM}	Period of the switching frequency of the PWM	$[s]$
T_s	Sampling time	$[s]$
T_{set}	Settling time	$[s]$
V	Amplitude of the phase voltage	$[V]$
V_a, V_b, V_c	Three phase voltages	$[V]$
v_{an}, v_{bn}, v_{cn}	Inverter leg voltages	$[V]$
v_d, v_q	dq-axis voltages	$[V]$
V_{DC}	DC - voltage	$[V]$
V_g	Grid voltage	$[V]$
V_{PCC}	Voltage at PCC	$[V]$
z	Discrete operator	$-$

θ	PLL output angle	$[rad]$
ω	Angular frequency	$[Hz]$
ω_n	Natural frequency	$[Hz]$
τ_r	Rise time	$[s]$
τ_s	Settling time	$[s]$
ζ	Damping factor	$-$
*	References	$-$

Appendix A

VSC-based HVDC transmission system between two onshore terminals working at 50 Hz

As it was mentioned in Section 6.4, with the developed VSC-HVDC system (plant + control) a bidirectional active power flow can be achieved.

From the start it should be stated that this study case is not related with the case of an HVDC transmission system, which has at one teerminal a wind farm and at the other terminal the AC grid. This study case refers at the application when the VSC-HVDC transmission is used to transmit power between onshore substantions.

Section 6.4 had presented the active power flow in one direction (offshore - onshore) while, in the following "the power flow from the onshore terminal to the offshore terminal" is consider.

The upcomming results are obtained from simulations and the validation of this study case was performed using the laboratory setup.

Simulation Results

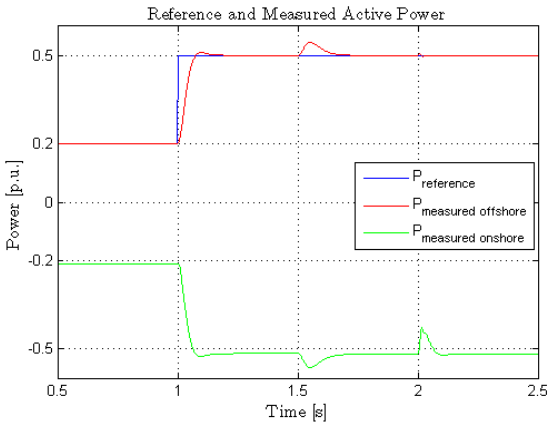

Figure A.1: *Reference and measured active power*

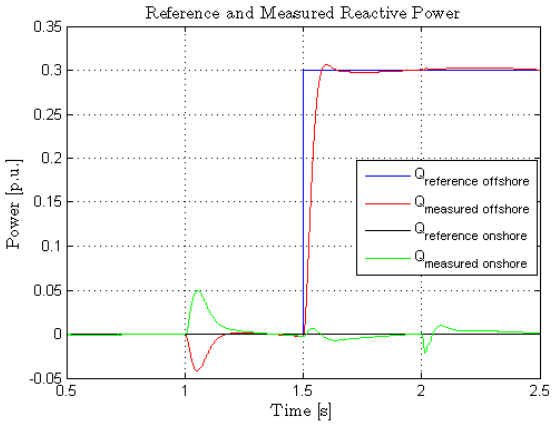

Figure A.2: *Reference and measured reactive power*

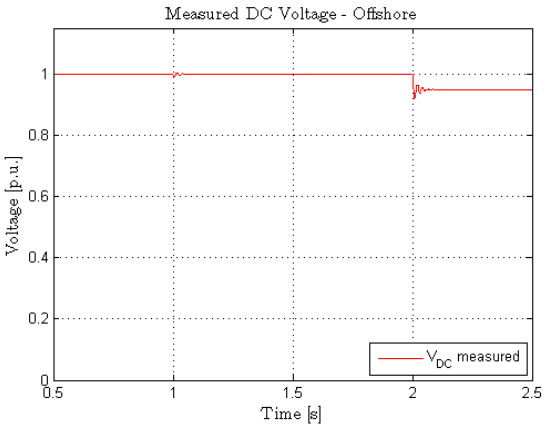

Figure A.3: *Measured DC voltage - offshore terminal*

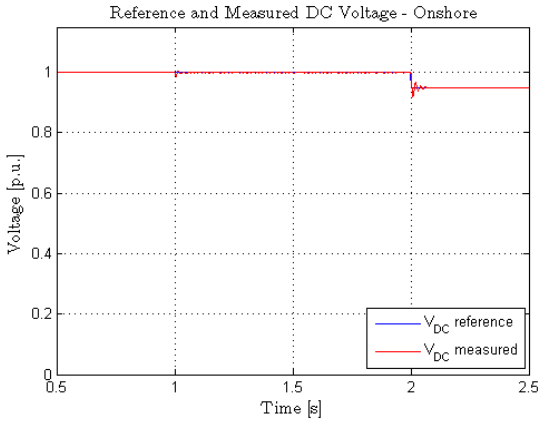

Figure A.4: *Reference and measured DC voltage - onshore terminal*

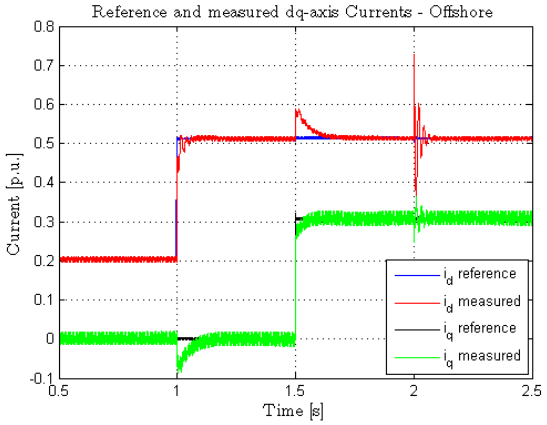

Figure A.5: *Reference and measured dq-axis currents - offshore terminal*

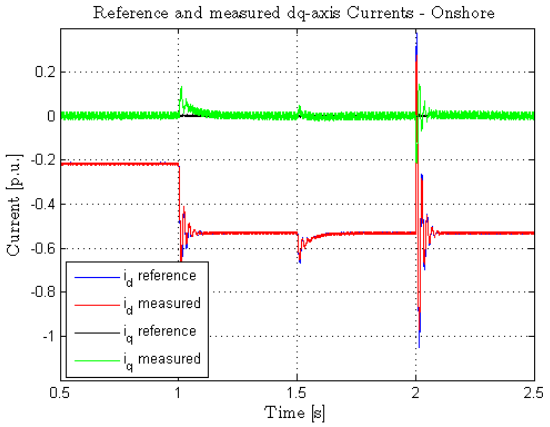

Figure A.6: *Reference and measured dq-axis currents - onshore terminal*

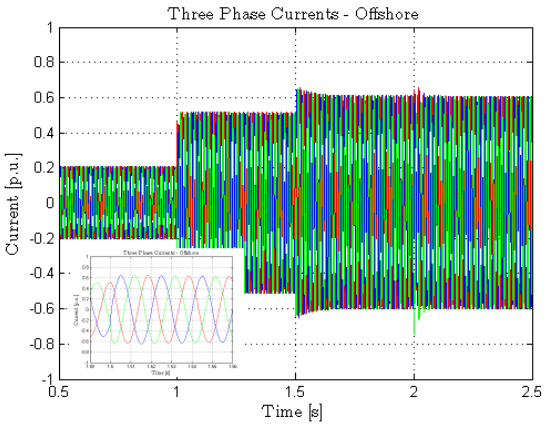

Figure A.7: *Measured three phase currents - offshore terminal*

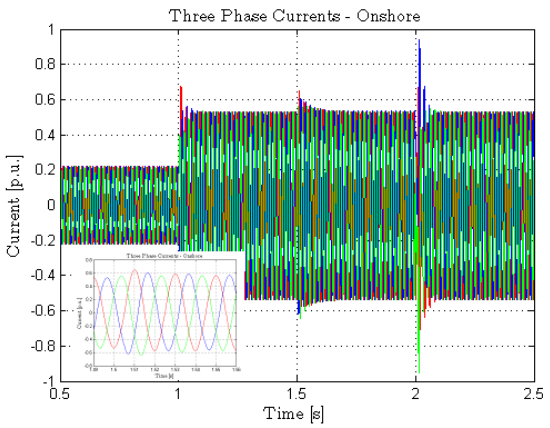

Figure A.8: *Measured three phase currents - onshore terminal*

Laboratory Results

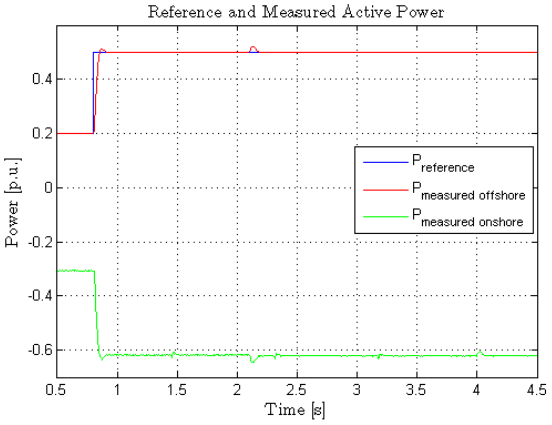

Figure A.9: *Reference and measured active power*

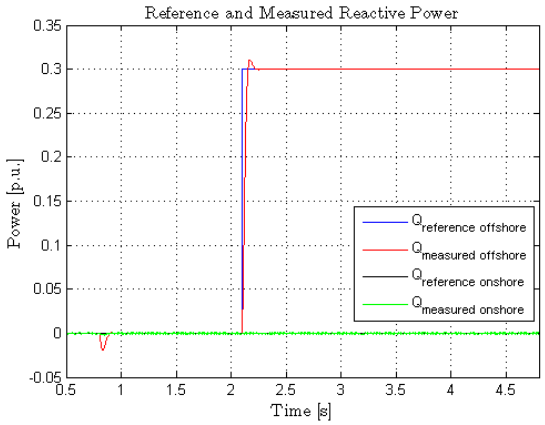

Figure A.10: *Reference and measured reactive power*

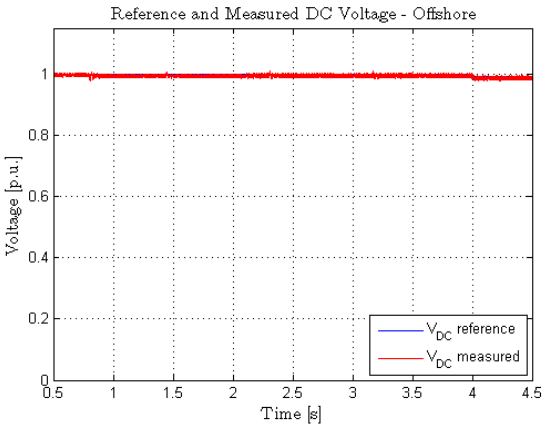

Figure A.11: *Measured DC voltage - offshore terminal*

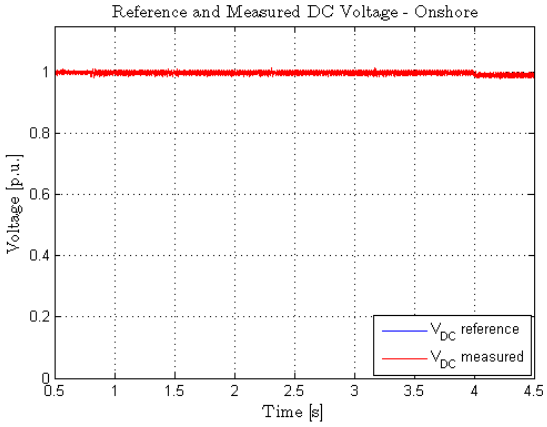

Figure A.12: *Reference and measured DC voltage - onshore terminal*

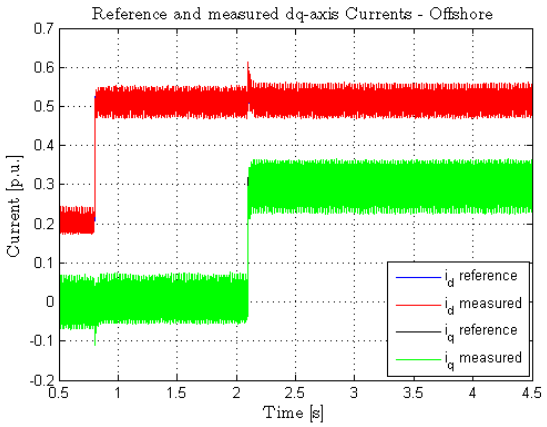

Figure A.13: *Reference and measured dq-axis currents - offshore terminal*

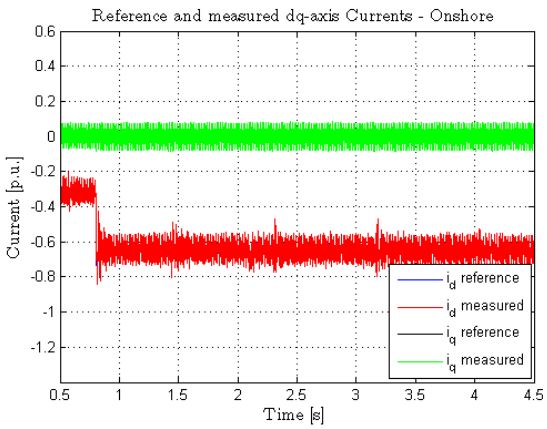

Figure A.14: *Reference and measured dq-axis currents - onshore terminal*

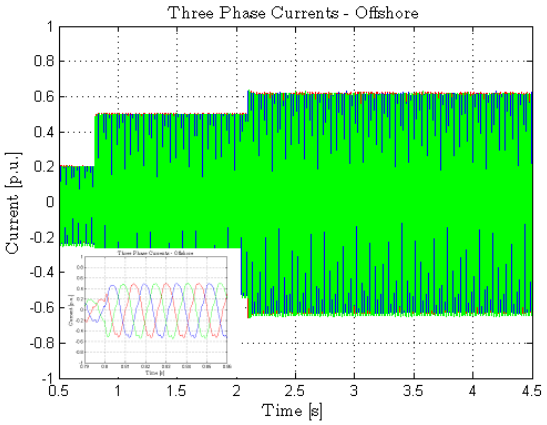

Figure A.15: *Measured three phase currents - offshore terminal*

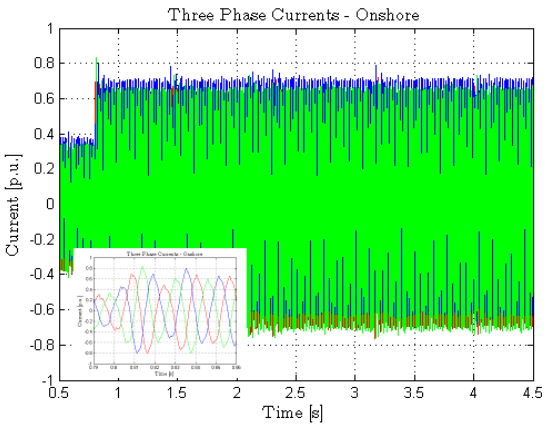

Figure A.16: *Measured three phase currents - onshore terminal*

Appendix B

Contents of CD-ROM

- **Articles:**
  - This folder contains all articles used as references in the project.
- **Report files:**
  - This folder contains all source files in the LATEX project file structure.
- **MATLAB/Simulink files**
  - This folder contains the Matlab/Simulink models used for the simulations.
- **Laboratory files**
  - This folder contains the files from the laboratory implementation.